UNIVERSITY OF CANTERBURY

DEPARTMENT OF MECHANICAL ENGINEERING

Upper-Limb Active Exoskeleton BITERS

STRATHAN MCKENZIE

A thesis submitted in fulfilment of the requirements for the Degree of Masters in Mechanical Engineering

Enrolment Date: March 1, 2019

Abstract

Stroke can result in injury and death, with impairments such as loss of somatosensation, loss of fractionated movement, impaired motor speed, and paresis being common post-stroke. The upper-limb is important to many activities of daily living (ADLs), with these impairments often limiting the execution of basic tasks. Rehabilitation works to develop motor movements and develop neuroplasticity, which can be approached in many different ways and forms. Stroke rehabilitation robotics and exoskeletons have many benefits over traditional methods and other technology. This field has a range of approaches in terms of actuation, sensing, and control systems. Exoskeletons are wearable devices that directly interact with the human body, exerting force onto the wearer to excite movement.

The BITERS exoskeleton is a 5-degree of freedom (DOF) active upper-limb exoskeleton, which features two active joints and three passive joints. The kinematic model of the exoskeleton has been modeled as an open-loop chain encompassing from the centre of the torso out to the upper arm (humerus). Two passive DOFs accommodate the translation of the glenohumeral (GH) joint in the frontal plane. The rotational joint at the centre of the torso allows for 40° of shoulder elevation from active human movement. The prismatic joint is a linear slider bearing in series with a 40mm compression spring. The inclusion of this prismatic joint is a novel feature of the exoskeleton, allowing for the displacement of the GH joint along the direction of scapula sliding, and accommodating for a large range of discrete shoulder movements. This DOF can translate the device's work-space anteriorly (against a restorative force) or posterally while encouraging correct shoulder posture. The GH joint allows the rotation of the humeral head in the shoulder girdle and is approximated by three rotational DOFs which form a spherical assembly whose axis intercept with the centre of the humerus head. The first and third of these DOFs (parallel to the coronal and sagittal planes respectively) are actuated by a DC motor driven bidirectional Bowden cable system, allowing for actuated abduction/adduction and flexion/extension. The remaining DOF in the spherical assembly allows the passive free movement of the other DOFs, internal/external rotation is theorised to occur autonomously given the freedom to passively move at this joint.

Portability was a focus area during development. The exoskeleton is lightweight with its arm unit weighing 500g and back unit weighing 3500g. The 3D polycarbonate (PC) build of the exoskeleton arm provides high tensile strength while

reducing weight, a 50% infill is used in these links to improve flexibility. All larger loads are positioned distally on the backplate, whose force is distributed across the user's shoulders via padded yoke straps. Compliance is desired in systems for safety and comfort. Soft actuation, the shift of weight away from the actuation points, compliant exoskeleton-body attachment (cuffs), and flexible filament material, are all used to increase the compliance of the system.

A Teensy 3.5 microcontroller is used to read sensor feedback, implement control, and provide a user interface. This system is powered by a 14.8V 4000mAh battery and has an operating life of 25 to 45 minutes. The exoskeleton's proportional control system uses joint angle feedback and EMG to provide real-time adjusted assistance based on the effort outputted by the user. The posterior deltoid was determined to be a suitable EMG control input, due to its significant response to shoulder flexion, extension, and abduction, and its low response to passive movements such as internal/external rotation.

BITERS successfully modelled the human shoulder motion and allowed for active actuation of the shoulder with DC motor actuation and Bowden cable power transmission. Both manual proportional control and EMG assist-as-need based control were implemented by software. Validation of the exoskeletons range of motion (ROM) was successfully performed through the use of CAD simulation, modelled work-space analysis, and 3D motion tracking technology. The developed exoskeleton allows for 157° flexion, 30° extension and 177° abduction, with a work-space volume of $0.00446m^3$. The peak torque achieved was 7.71Nm at the actuated joints, enabling assisted shoulder motion in flexion/extension and adduction/abduction.

Contents

List of Figures

List of Tables

1 List of Acronyms

ABS Acrylonitrile Butadiene Styrene

AC Acromioclavicular

AC Alternating Current

ADC Analogue to Digital Converter

AD Anterior Deltoid

ADL Activities of Daily Living

AM Additive Manufacturing

BITERS Biomedical Interactive Therapy Exoskeleton, for Rehabilitation subsequent to Stroke

BT Bilateral Training

CAD Computer Aided Design

CMRR Common Mode Rejection Ratio

COM Centre of Mass

DC Direct Current

DH Denavit–Hartenberg

DOF Degrees of Freedom

ECG Electrocardiogram

EMI Electronic Magnetic Interference

EMG Electromyography

FEA Finite Element Analysis

FES Functional Electrical Stimulation

GH Glenohumeral

IDE Integrated Development Environment

IMU Inertial Measurement Unit

IC integrated circuits

ISP Infraspinatus

LiPo Lithium Polymer

LLD Lower latissimus Dorsi

LPM Lower Pectoralis Major

LT Lower Trapezius

MD Middle Deltoid

MCU Microcontroller

MT Middle Trapezius

MVC Maximum Voluntary Contraction

NMES Neuromuscular Electrical Stimulation

P Proportional

PC Polycarbonate

PD Posterior Deltoid

PI Proportional Integral

PLA. Plastic or Polylactic Acid

RHOM Rhomboid Major

RMS Root Mean Squared

ROM Range of Motion

SA Serratus anterior

SC Sternoclavicular

SEA Series Elastic Element

sEMG Surface Electromyography

SNR Signal to Noise Ratio

SSP Supraspinatus

ST Scapulothoracic

SUBS Subscapularis

TIA Transient Ischemic Attacks

TM Teres Major

ULD Upper Latissimus Dorsi

UPM Upper Pectoralis Major

URES Resulting Displacement

UT Upper Trapezius

UT Unilateral Training

VR Virtual Reality

3D Three Dimentional

2 Introduction

2.1 Thesis Statement

The objective of this research is to develop an inexpensive, active, assist-as-need exoskeleton for the shoulder, allowing a full range of motion. This will facilitate post-stroke shoulder rehabilitation, using a combination of robotic actuation, passive actuation, and electromyography (EMG). The exoskeleton will be controlled with user inputs in the form of muscle activation energy and/or analog joystick position. This will account for patient effort and current position by applying assist-as-needed control. The exoskeleton will be developed for the functional movements of shoulder flexion/extension and adduction/abduction. Key design requirements are that the device will be lightweight, portable, compliant, and relatively inexpensive.

2.2 Motivation

A stroke occurs when the supply of blood to the brain is either interrupted or reduced, limiting the quantity of oxygen delivered resulting in damage to cells. Stroke can result in injury and death, with impairments such as loss of somatosensation, loss of fractionated movement, impaired speed, paresis etc. being common post-stroke. As well as physical effects, mental and social effects may also be experienced.

The greater part of recovery during rehabilitation occurs within three months of the stroke, with a delay of treatment often resulting in medical complications. Rehabilitation works to develop motor movements, such as activities of daily living (ADL), and develop neuroplasticity. Many stroke rehabilitation methods exist and are practiced. However, the introduction of alternative rehabilitation methods such as robotic exoskeletons and electrical stimulation offer a large range of potential non-invasive therapies. The use of robotic exoskeletons are increasingly popular as an alternative stroke rehabilitation method due to potential benefits such as cost, and home-based care.

Robotic rehabilitation has many economic, social, and endurance related benefits

when compared to traditional techniques. With robotic rehabilitation, patients can complete rehabilitation in a home environment, while providing feedback to clinical staff on the quality and quantity of therapy. This is less time consuming than traditional techniques, which is beneficial to the financial provider as it reduces the required time with physiotherapists and clinical professionals. Robotic exoskeletons enable longer sessions by assisting the patient with movement while still requiring them to apply active muscle input. Development in EMG signal processing and sensory control systems enable similar integration of assist-as-needed control into these exoskeletons. Developments also in wireless technologies such as BLE/WIFI communications and the continuously reducing size of components (motors, batteries, sensors, controllers etc.) further increase the capability and availability of portable rehabilitation therapy. ADLs and their physical motions can have a significant effect on the success of rehabilitation. These are easier to simulate in a home environment, thelack of reliance on trained professionals or healthcare environments creates an opportunity for more user-driven therapy.

The focus of this thesis will be to develop an active, actuated, assist-as-need robotic shoulder exoskeleton, with EMG functionality. The developed exoskeleton is called BITERS for Biomedical Interactive Therapy Exoskeleton, for Rehabilitation subsequent to Stroke. It is called this for two reasons; because it is an accurate description of its functionality and purpose as a rehabilitation exoskeleton, and to address the issue of mental health in the rehabilitation field, hence the name resembles the word "bitters". Rehabilitation is a painful, slow, and often an unwelcome task for many. The idea that some may be “bitter” about their current situation and impairment is often ignored or viewed negatively. It is my hope that by naming my project after these negative emotions some awareness can be given to the mental health side of rehabilitation.

Supervisory Team

Senior Supervisor: Chris Pretty

Co-Supervisor:

3 Literature Review

3.1 Types, Causes Physical Effects of Stroke

A stroke is a cerebrovascular event that occurs when the flow of blood to the brain is interrupted, starving the brain of oxygen, resulting in brain cell death. This can cause significant disability or death. Stroke is the third highest cause of death in New Zealand, accounting for 8.2% of total deaths and 4.2% of premature deaths [1].

Ischemic and haemorrhagic strokes are the two major classes of stroke. Ischemic strokes are caused by blood clots lodging in arteries or blood vessels and stopping blood flow, this can be classed as either embolic or thrombotic. Embolic strokes are a result of blood clots forming in the body and moving with the blood flow, eventually blocking small blood vessels in the brain, resulting in a stroke. Thrombotic strokes occur when there is a blockage to an artery supplying blood to the brain, restricting the blood flow [2]. In addition, Transient Ischemic Attacks (TIA) occur when the blood flow to the brain is momentarily restricted, then restored [3]. These have almost identical symptoms, an ischemic stroke and can last from a few minutes to 24 hours, often indicating that the individual experiencing a TIA is at risk of a stroke. These forms of blood clot strokes often occur due to blood vessels building up cholesterol and fat, causing obstructions. When this occurs, the body identifies these build-ups as small injuries to the blood vessel walls and responds by generating blood clots [2].

Haemorrhagic strokes are a result of a breakage of a blood vessel in the brain. These can be caused by conditions such as chronic high blood pressure and cerebral aneurysms. Aneurysms are thin weakened patches on blood vessel walls, these exist at birth and develop over time. Haemorrhagic strokes can be classed as either subarachnoid or intracerebral. Subarachnoid haemorrhages result from aneurysms, that burst in an artery near the membrane encompassing the brain, causing blood to mix with the cerebrospinal fluid around the brain. Intracerebral haemorrhages are largely caused by high blood pressure (hypertension), and bleeding occurs within the blood vessels of the brain [2].

3.1.1 Paresis and Loss of Fractionated Movement

Paresis is the decrease or lack of ability to voluntarily activate individual muscles. Paresis is common after stroke and is a result of damage to the corticospinal system causing inability to activate spinal neurons. This lack of voluntary motion means that movements involving multiple sets of muscles may be uncoordinated and have decreased force in contrast to neurologically-intact individuals. Paresis is very common after stroke, and the effects can range from a slight decrease in muscle coordination to not being able to activate muscles at all. Hemiparesis, which is paresis limited to one side of the body, is particularly common. Similarly, plegia is the paralysis of the muscles rather than just weakness, hemiplegia is also common post-stroke.

Fractionated movement is the ability to selectively and voluntarily activate muscles independently. Fractionated movement defects leave the individual unable to selectively activate muscles [4]. Fractionated movement defects may occur due to paresis, spasticity, and muscle weakness. Both paresis and loss of fractionated movement make ADLs difficult to achieve.

3.1.2 Muscular Atrophy

Muscle atrophy is the reduction or "wasting away" of muscles. This atrophy is often caused by hemiparesis and stroke induced damage, and results in muscles unable to sufficiently activate and perform physical activity [5]. Aerobic and motor stimulation exercise rehabilitation for paretic limbs has been shown to help prevent or reduce negative muscle changes which result from inactivity. This rehabilitation dominantly effects skeletal muscle changes and mass [6]. For rehabilitation to be effective, the patient's muscles have to be self-activated during rehabilitation, as the therapist cannot do the movements for them. Therefore, assist-as-need rehabilitation is useful as it facilitates both voluntary and assisted movement, prolonging beneficial rehabilitation.

3.1.3 Abnormal Muscle Tone

Muscle tone refers to the resistance of muscles to elongation and stretching. A change of this resistance is called abnormal muscle tone and can be separated into two classes, hypotonicity, and hypertonicity. Hypotonicity is a reduction in the muscle's resistance to passive movement and decreased stretch reflex response due to a reduced neural drive to the muscle. These effects are usually due to damage to the corticospinal neurons. Hypertonicity (spasticity) is an increase in the muscle's resistance to passive movement and increased stretch reflex response due to a loss of inhibition to the spinal cord. Hypertonicity is usually due to damage to the corticospinal tract. Acute Hypotonicity is usually present immediately after a stroke, with hypertonicity developing over time [4].

3.1.4 Loss of Somatosensation

The somatosensory system contains all the parts of the central and peripheral nervous systems for transmission and processing information on stimuli from around the body such as pain, warmth etc [7]. Damage to the somatosensory system reduces the ability to monitor, transmit, and correct movements and information. This loss of sensory feedback means that stroke patients often may not be able to feel pain or monitor their limb positions correctly, which could be deemed a hazard. Motor impairment and weakness often occur together with loss of somatosensation, these are often associated with sensory impairment [8]. This loss generally affects an entire side of the body and is a result of damage to the ascending somatosensory pathways or the somatosensory cortical areas [4].

3.1.5 Shoulder Subluxation

Glenohumeral (GH) subluxation is a frequent complication in patients with post-stroke hemiplegia and is the partial dislocation of the shoulder joint [9]. This condition is often due to weakness or reduced muscle mass in the surrounding muscles. GH sublaxation can be treated with basic support structures to reduce ligament strain and restrict movement, while still allowing enough range of motion (ROM) to

complete ADLs and allow access to the surrounding muscles for electrical stimulation [10].

3.2 Activities of Daily Living

Activities of daily living (ADLs) define fundamental skills and motions that are essential to independently care for oneself. They are used extensively in rehabilitation research and practice and can be used as a metric to indicate a patient's functional status and progress. ADLs typically require developed cognitive, motor (movement and coordination), and perceptual (sensory) abilities [11]. ADLs can be described as:

- Basic: the ability to physically care for oneself, such as dressing, eating, and cleaning.
- Instrumental: more complex activities essential for independent living, such as housekeeping, exercising, and driving.

Stroke rehabilitation tends to focus on basic ADLs with a dependency on the motor and peripheral skills. The inability to accomplish basic ADLs may lead to unsafe conditions and a poor quality of life [12].

For upper-limb post-stroke rehabilitation, determining the motions required to complete ADLs is difficult as the upper-limb is complex, with a wide ROM and containing several degrees of freedom (DOF) and interacting joints. Many discrete movements and muscle patterns are needed to complete even basic ADLs. The complexity of the shoulder makes it difficult to determine which muscles, movements and joint trajectories are required to complete ADLs and to gauge performance. [13].

3.3 Rehabilitation Devices and Techniques

Stoke can have a significant impact on an individual's motor functions and ability to achieve ADLs. The process of rehabilitation can restore movement and functionality, which can also significantly impact the individual's mental health [14]. The aim

of therapy and rehabilitation is to recover lost motor function, learn new motions using different muscle groups, improve coordination, induce neural plasticity and recovery, and prevent secondary injuries and complications [15]. The development of neural plasticity is important in the recovery of motor function after stroke, where task-specific training, along with aerobic exercise, is considered a highly effective and practiced treatment for post-stroke rehabilitation [16].

Delay between the stroke event and rehabilitation increases the chance of the individual developing medical complications and having further degraded motor skills. Shoulder pain, shoulder subluxation, and spastic limb are the main complications developed [17]. Stroke patients who begin rehabilitation within 30 days of the stroke have a high rate of recovery while stroke patients who begin rehabilitation after this recover at a reduced rate. The neurological recovery of the patient over time has non-linear and logarithmic traits [9] which can be seen in Figure 3.3.1, where recovery largely takes place in the first three months. However, recovery is not limited to this time-frame and can begin at any point post-stroke and still produce results.

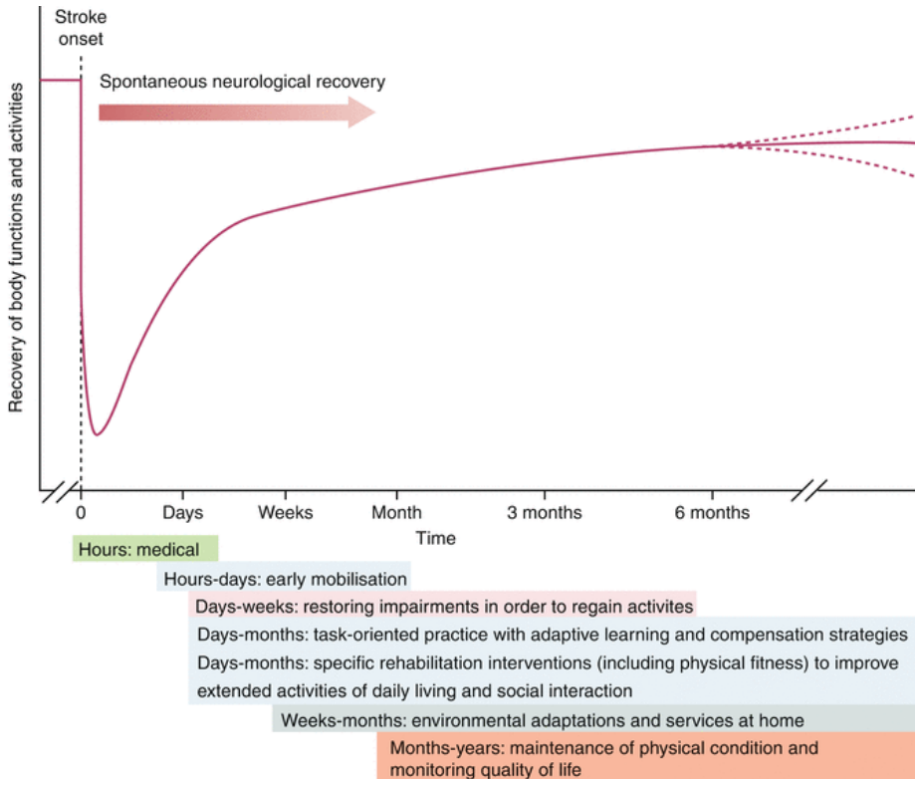

Figure 3.3.1: Predicted timeline of recovery post-stroke [9]

There is a large range of non-invasive, upper extremity devices and techniques which can be used to treat patients post-stroke. Examples of these are robotic tools, electrical stimulation, bilateral training, mirror theory, virtual reality, and motor imagery.

3.3.1 Electrical Stimulation

Neuromuscular Electrical Stimulation (NMES) is the forceful activation of paretic muscles by stimulation of intact lower motor neurons, using electrical impulses through skin electrodes to elicit muscle contractions. The common operational stimulation frequency of NMES is 10-50Hz, where muscle contractions will occur in this range. Functional electrical stimulation (FES) is the use of NMES to achieve functional tasks, such as ADL's, activating inactive muscles to achieve movement [18]. Varying the NMES frequencies used can elicit a range of muscle reactions; frequencies lower than 30Hz result in muscle tremors and twitching, frequencies between 30-50Hz result in tetany (continuous and selective muscle contractions), and frequencies up to 100Hz produce continuous contractions at a proportionally increasing level. Care must be taken at higher frequencies, as fast-twitch muscle fibres are recruited, resulting in fatigue and pain.

The pulse width of the supplied stimulation used in NMES/FES rehabilitation is typically between 200-250us. However, longer pulse widths of 350-450us can be used to activate paretic muscle fibres. Short pulse intervals result in less fatigue but the length of the pulse width limits the applied power to the muscle. Following the depolarisation of a nerve's membrane potential, there must be a recovery/repolarisation sage where no impulses may occur. The duty cycle must consider the patient's muscle endurance and be adjusted accordingly to mimic the muscle's normalised movement. The parameters required to stimulate muscle contractions will vary per patient, this is often dependent on muscle size, the severity of stroke damage, and skin-electrode impedance [19].

FES for rehabilitation can be triggered by sensor inputs, such as EMG, joint position, joint angle [16], or manually. Electrical stimulation rehabilitation is effective but may induce fatigue. Fatigue is the impaired performance of muscles resulting from high intensities of rehabilitation. [20].

3.3.2 Bilateral and Unilateral Training

Bilateral coordination is essential to achieve normal movement and basic ADLs, which require the use of both sides of the body often simultaneously. Due to the effects of stroke, patients are likely to experience a loss of motor function making coordination difficult. The basis of bilateral training (BT) is that by using the healthy limb to perform movements, the damaged arm can be promoted to re-learn basic movement and coordination [21].

BT is the act of training both arms identically and simultaneously, or independently but performing the same movements [22]. The impaired arm can copy the non-effected arm's movements through visual inspection and repetitive action. Unilateral training (UT) is the act of only training the affected arm at high intervals/repetitions [23]. BT has been found effective for stroke recovery and is suggested to be superior to unilateral training over long term rehabilitation [24].

3.3.3 Motor Imagery

Motor imagery is a cognitive rehabilitation technique that involves the act of imagining a specific movement, without actually doing it physically. The act of imagining the act often involves thinking of the muscles required, the feeling of it, and sometimes scent (e.g. imagining reaching for coffee and thinking of the smell). This method is a repetitive task where the patient keeps picturing the same movement. Imagery training helps increase motor function in patients with neurologically related conditions [25]. The efficacy of motor imagery varies significantly per patient as the patient's mental state and extent or location of stroke-induced damage [26].

3.3.4 Virtual Reality

Virtual reality (VR) rehabilitation is an interactive computer-based technique which is often coupled with interactive robotic devices. Repetitive task-orientated training is typically the focus of VR rehabilitation, which involves the patient interacting in a two-dimentional (2D) or three-dimensional (3D) environment [16]. VR provides an alternative rehabilitation environment that encourages higher numbers of repeated

tasks and longer sessions as it provides a more interesting environment compared to traditional rehabilitation [27]. Studies have shown that when used in collaboration with traditional or other alternative rehabilitation techniques, VR is highly effective at improving motor functions and the completion of ADLs. [28].

3.3.5 Mirror Theory

Paralysis of limbs on a single side (hemiplegia) is a very common effect of stroke, which makes achieving ADLs difficult. Mirror therapy involves placing a mirror between the affected limbs (between arms or legs) where the non-affected limb gives the illusion through the mirror that the affected limb is moving identically. This illusion causes the brain to register stimulations that don't exist such as feeling and movement, aiding neuroplasticity. This method has been found to be an effective and simple rehabilitation technique that can still provide suitable rehabilitation after 6 months post-stroke [29].

3.3.6 Orthoses and Neuro-prostheses

Orthoses are external removable devices that can be applied to limit or assist movement and reduce pain and spasticity. Orthoses are often devices such as exoskeletons and braces. Orthoses that enhance or replace input from the nervous system are called neuro-prostheses [30]. Neuro-prostheses can be used to facilitate and build muscle movement during stroke rehabilitation. Commonly, these prostheses operate based on voluntary muscle contractions through the use of EMG [31], and can be used to produce "assist-as-need" control.

3.3.7 Robotic Rehabilitation Devices

Robotic devices have become increasingly available and are being developed for alternative post-stroke rehabilitation. Task-orientated repetitive movements are used during rehabilitation to increase muscle strength, coordination, and motor unit activation. Robotic exoskeletons can provide rehabilitation for both the upper and lower extremities. Robotic aids are usually categorised as either clinical, which is for use in

a clinical environment as a shared resource between patients, or home-use systems, which are for rehabilitation focused on ADLs.

Robotic rehabilitation aids can be defined as passive, active, or interactive systems. Passive systems use mechanical components to model the patient's limbs, where no electrical actuation is required. In order to move, fix, or limit actuation, components such as bearings, springs, pulleys, and frames are utilized. Active systems use actuators, such as motors, hydraulics, and pneumatics to move the patient's limbs. Interactive systems usually include some form of actuation; However, they also include some form of interactive medium or control strategy to control the rehabilitation and ensure motivation/interaction from the patient [15].

3.4 Muscular and Skeletal System

3.4.1 Muscle Types

The muscles in the body can be classified as either smooth, cardiac, or skeletal muscle. Smooth muscles are spindle-shaped in structure and found in the walls of organs and anatomical structures. These can include blood vessels, the uterus, stomach, bladder, bronchii etc. Cardiac muscles are striated in structure, and are involuntary muscles only found in the heart. Skeletal muscles are voluntary muscles that are attached to the bone by tendons and control the direct movement of the skeletal body.

Smooth and cardiac muscle both contain one nucleus per muscle cell, where skeletal contains multiple peripherally located nuclei. Skeletal and cardiac muscles are striated, with uniform arrangements of muscle containing the sarcomere. Striated muscle types are used for regular, short interval, intense bursts, whereas non-striated muscle types (smooth) can sustain contractions for very long intervals [32].

3.4.2 Shoulder Movement and Joints

The shoulder complex includes the humorous, scapula, and clavicle skeletal bones, with four joints connecting these and facilitating movement; these are the glenohumeral (GH), acromioclavicular (AC), sternoclavicular (SC), and scapulothoracic

(ST) joints. The shoulder girdle is comprised of the clavicle and scapula, including the GH, AC, and SC joints as shown in Figure 3.4.1.

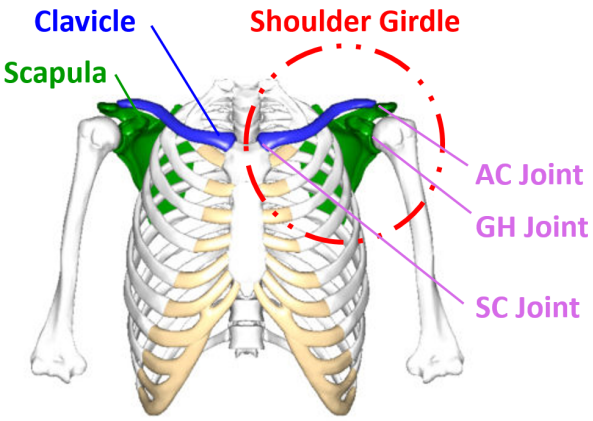

Figure 3.4.1: Shoulder girdle diagram

The GH joints head and socket are similar in structure, with only a 3mm difference in radius, making the joint kinematics rotational. Due to this structure, the GH joint is usually modelled as a ball and socket joint, equivalent to a 3-DOF spherical joint. However, this assumption does not consider the shoulder girdle, which moves linearly and introduces several more DOFs into the complex shoulder kinematics. To achieve these DOFs, muscles must be contracted and extended simultaneously. The GH's 3 revolute DOFs in terms of general movements are flexion/extension, abduction/adduction, and internal/ external (medial/lateral) rotation, which can be seen in Figure 3.4.2 [33].

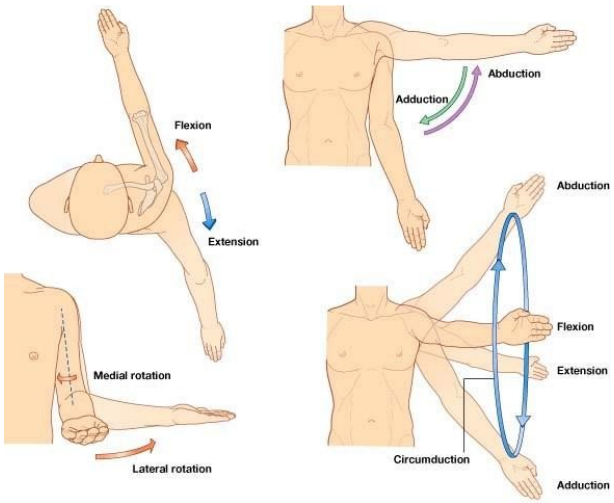

Figure 3.4.2: 3-DOF shoulder movements [33]

In terms of shoulder movement, flexion is the anterior (forward) movement of the upper arm at the GH joint, where extension is the posterior (backward). Abduction is the movement of the arm away from the midsagittal plane of the torso. This movement involves both GH joint motion and movement of the shoulder girdle. Adduction is the movement of the arm toward the midsagittal plane of the torso. External/internal rotation are both around the longitudinal axis of the humerus at the GH joint. The arm rotates towards the midsagittal plane during internal rotation and away during external.

Other key movements considered include shoulder girdle elevation/depression. Shoulder elevation is a movement where the scapula moves in an upward direction at the sternoclavicular joint. Depression is where the scapula moves in an downwards direction. [34]. These movements translate the GH joint position.

Movement at the GH joint is caused by the scapulohumeral muscles. The latissimus dorsi and the pectoralis major also attach to the humorous to facilitate movement. The summation of muscles about the GH joint cause abduction/adduction, flexion/extension, and internal/external rotation as shown in Table 3.4.1 [35]

Table 3.4.1: Activated muscles during shoulder movement

Flexion	Extension	Internal Rotation	External Rotation	Abduction	Adduction
Deltoid	Deltoid	Deltoid	Deltoid	Deltoid	Teres Major
Coracobrachialis	Latissimus Dorsi	Latissimus Dorsi	Infraspinatus	Supraspinatus	Latissimus Dorsi
Biceps Brachii	Triceps	Subscapularis	Teres Minor		Pectoralis Minor
Pectoralis Major	Teres Major	Teres Major			Pectoralis Major

3.5 Shoulder Range of Motion

Both passive and active forces can move the shoulder. Passive movement is caused by an external force acting on joints/muscles during muscular inactivity. Passive movement is used in rehabilitation and therapy to improve motor function in paretic or weakened limbs, while also preventing local tissue complications as a result of inactivity [36]. Active movement is produced by voluntary force from the patients own muscles. Therefore, an active ROM defines the shoulder's "normal" movement patterns and should allow all ADLs to be achieved within its range. Flexion/extension and abduction/adduction angles are important parameters for the description and evaluation of joint rotations, translations, and orientations in the analysis of human movement [37]. The definition of an absolute ROM is key to ensuring that all functional movement is achievable in space.

Vermeulen [38] analysed shoulder movement patterns in 3D space using electromagnetic tracking devices. The subjects of this study had "frozen shoulders" and both the affected and non-affected shoulders movements were measured before and after therapy. The non-affected shoulder ROM was used as a baseline, and was measured for both active and passive movement. Forward flexion was measured as 156° for active and 167° for passive movement. Abduction/Adduction was measured as 164° for active and 173° for passive movement. External rotation was measured as 60° for active and 69° for passive movement.

Dougherty et al. [39] makes the important distinction between the GH joints and shoulders ROM while determining the reliability of inclinometery to measure passive shoulder ROM. Total shoulder flexion and abduction were exercised to determine the ROM of the shoulder complex in its un-restrained movement space. To determine ROM of the GH joint, movement of the shoulder complex had to be re-

strained and the GH isolated. For the isolated GH movements the patient was placed in a sitting position, and a passive downwards external force was applied on the spine of the scapula to eliminate its movement from the system. The average readings across the testing set were derived for reference. The passive shoulder ROM was found to be 172° in flexion, 176° in abduction, 97° in external rotation and 97° in internal rotation. The isolated ROM of the GH joint was significantly lower with 103° in flexion and 69° in abduction, which is to be expected due to the restrictions of the humerus head/GH joint. McLauren [40] reports similar values to Dougherty et al. for exclusive GH movement, with 110° flexion, 60° extension, 120°abduction and 90° internal/external rotation. Unrestrained shoulder motion measured 180° flexion, 90° extension, 180°abduction, 30° adduction and 90° internal/external rotation.

Barnes et al. [41] analysed the passive/active ROM of the shoulder complex across several subjects to determine the effects of age, sex, and shoulder dominance on ROM of the shoulder. The subjects of this study were aged 2-69 years old and without shoulder pathology. Across the entirety of the results, the passive ROM results were 57.5°-65.4° internal rotation, 101.9°- 118° external rotation, 187.4°-195° abduction, 173.5°-176.7° flexion, and 77.4°- 84.6° extension. The active ROM results were 41.2°-51.5° internal rotation, 91.1°- 104.9° external rotation,180.1°-188.6° abduction, 173.5°-176.7° flexion, and 64.6°- 68.7° extension.

The results of these studies are tabulated in Table 3.5.1.

Table 3.5.1: Summary of the shoulders ROM from reviewed literature. All units in °.

Applied Force	Movement	Vermeulen[38]	Dougherty et al.[39]	Barnes et al.[41]	McLauren[40]
Passive	Flexion	167	172	173.5-176.7	-
	Extension	-	-	77.4- 84.6	-
	Abduction	173	176	187.4-195	-
	Adduction	-	-	-	-
	Internal Rotation	-	97	57.5-65.4	-
	External Rotation	69	97	101.9- 118	-
Active	Flexion	156	-	173.5-176.7	180
	Extension	-	-	64.6- 68.7	90
	Abduction	164	-	180.1-188.6	180
	Adduction	-	-	-	30
	Internal Rotation	-	-	41.2-51.5	90
	External Rotation	60	-	91.1- 104.9	90

For rehabilitation purposes, ADLs may define the shoulders necessary functional ROM. Murray and Johnson [42] studied the ROM required to complete ADLs, the results are tabulated in Table 3.5.2. The maximum required ROMs are significantly smaller than the shoulder ROMs from previously reviewed literature. Abduction is the most notable of these, with only 39.7° required to complete all tasks.

Table 3.5.2: Summary of the shoulder ROM required for ADLs [42]

Movement	**Max/Min**	**Angle (°)**	**SD (°)**
Shoulder flexion	Max	111.9	7.4
	Min	14.7	7.6
Shoulder abduction	Max	39.7	6.9
	Min	20.1	9.2
Shoulder internal rotation	Max	85.9	11.7
	Min	18.7	7.8

3.5.1 Exoskeleton Range of Motion

The aim of the rehabilitation exoskeleton is to assist the movement of the user. The maximum reachable ROM of the shoulder complex shall be defined from the active ROMs reported in literature in Section 3.5. Assistance above this range is outside of the natural active ROM and therefore unnecessary for ADLs. The maximum active ROM for each study were mean averaged for each movement. The active maximum movement averages are as follows; the achievable ROM is 154° in flexion, 74° in extension, 163.35° in abduction , 48° in internal rotation and 87° for external rotation. Shoulder flexion of 112° and abduction of 39.7° would be suitable for ADL exercises for rehabilitation [42].

The acceptable ROM for the modelled exoskeleton will achieve the set boundaries based on data presented in the literature. The defined ROM parameters are suitable for actuated movement and sufficient for ADLs. This ROM will be achieved through passive actuation, active electrical actuation, and user-driven active movement. A reference coordinate frame for movement at the GH joint is described in Figure 4.0.1. Flexion/Extension is about the x-axis, adduction/abduction is about the z-axis and internal/external rotation is about the y-axis. Figure 3.5.2, Figure 3.5.3 and Figure 3.5.4 illustrate flexion/extension, Adduction/abduction and internal/external rotation, respectively.

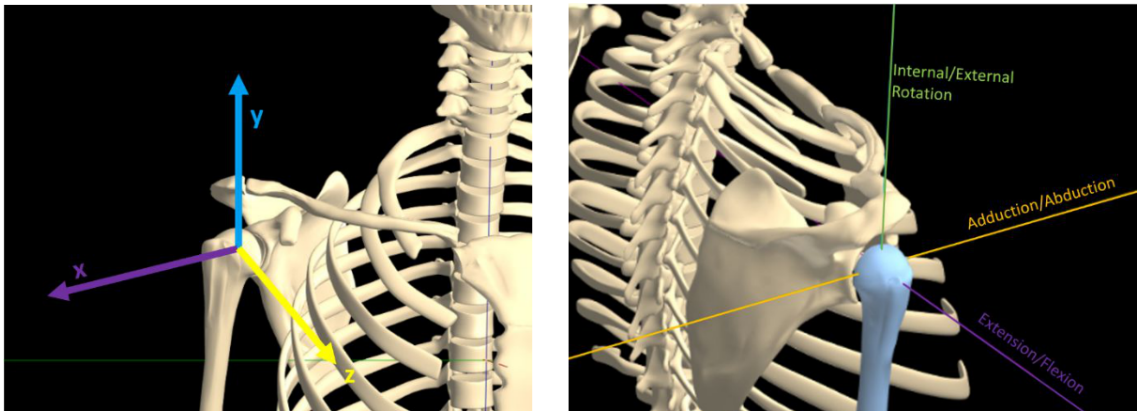

Figure 3.5.1: GH joint coordinate system showing axes of rotation

The GH joint has limited range, and can only achieve larger ROM with the addition of other bodies in the shoulder complex. Shoulder elevation and other discrete muscle movements can physically enable the humerus to nearly 180° in flexion. However, physical limitations and muscular constraints make this full movement difficult and uncomfortable. The desired flexion for the passive exoskeleton is therefore lower at 154°. Similarly, the exoskeleton will allow 74° shoulder extension.

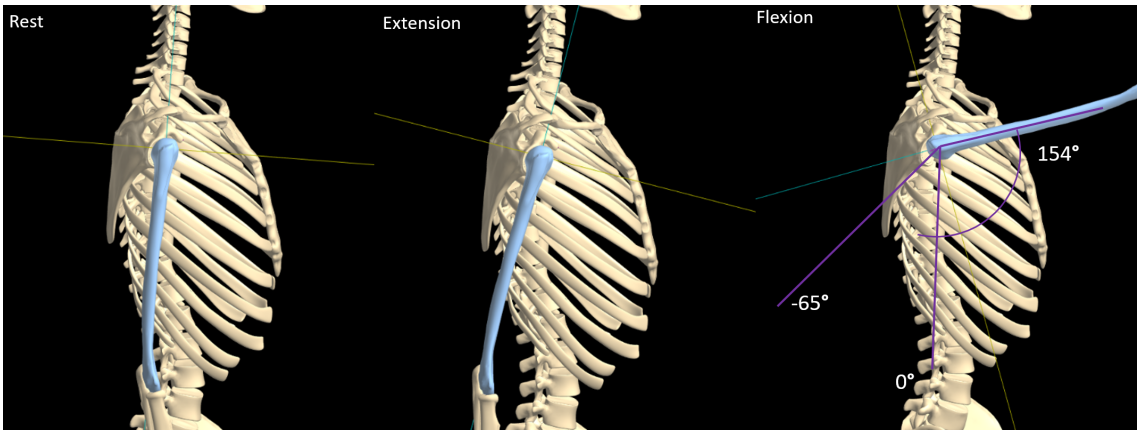

Figure 3.5.2: Flexion/Extension example and definition

Similarly, the exoskeleton should achieve 163°of shoulder abduction. An amount of actuated movement for shoulder adduction will be permitted. Adduction of 5° from rest will allow a closer workable space to the body and a more complete set of movement parameters.

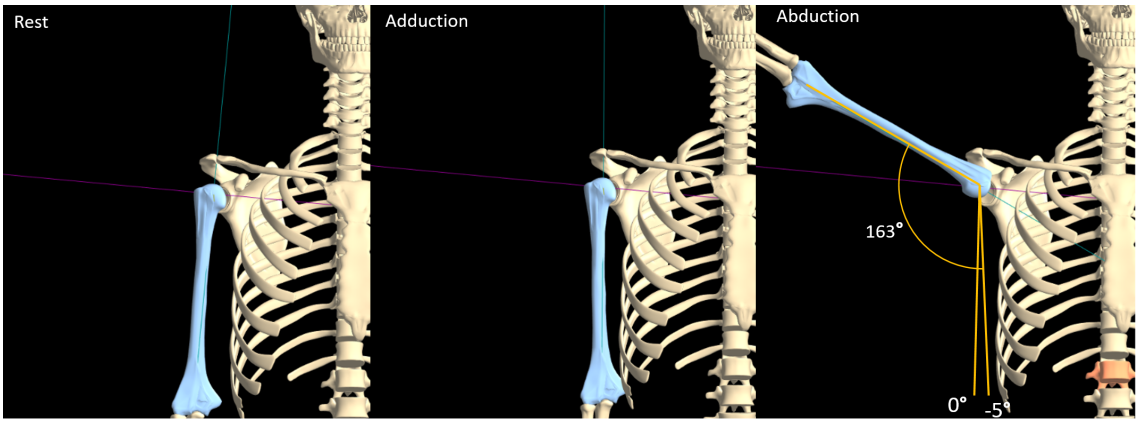

Figure 3.5.3: Adduction/Abduction example and definition

Internal/external rotation varies in research and across different exoskeleton models, with 90° either direction being the maximum reported ROM allowable by the shoulder complex. The exoskeleton will allow for a minimum of 47° and 86° for internal and external rotation respectively. However, this movement will not be electrically actuated, but passively supported. Rotation will naturally occur during other actuated movements.

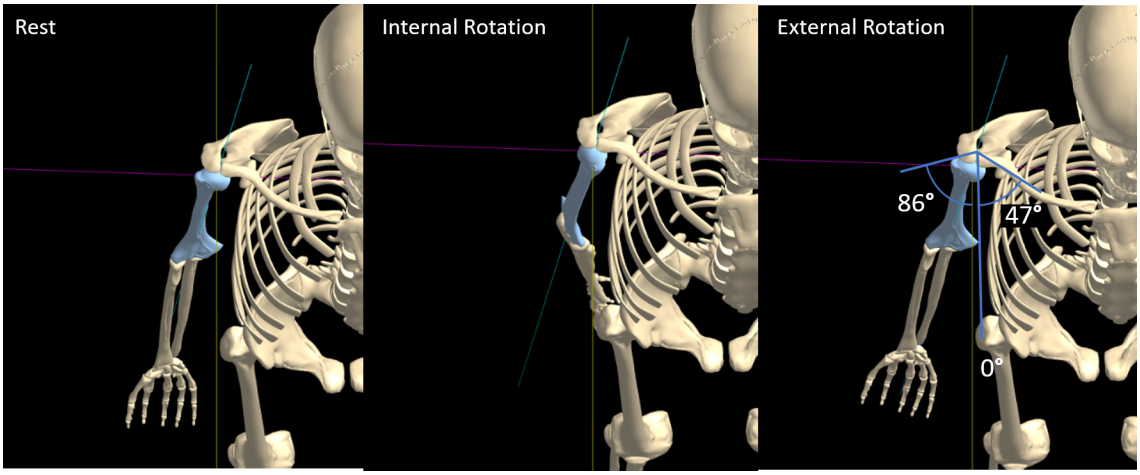

Figure 3.5.4: Internal/External rotation example and definition

The AC joint's motion encompasses the movement of the scapular, in relation to the clavicle and acromion. The scapular can rotate upwards or downwards along the coronal plane with a small angular offset. Abduction and flexion movement result in the upwards rotation of the scapula (Figure 3.5.5), and adduction/abduction

result in the downwards rotation. These rotations occur along the same axis. Internal/External rotation of the scapular occurs during protraction/retraction, and tilting of the scapular occurs during shoulder elevation/depression where the scapular tilts laterally or anteriorly.

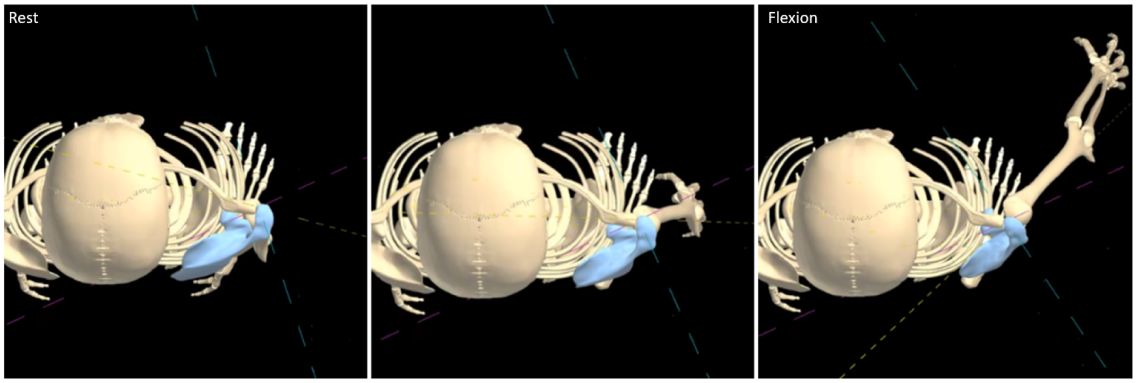

Figure 3.5.5: Scapula sliding during shoulder flexion

The human shoulder complex has many discrete movements. However, the DOFs and ROM of the proposed exoskeleton do not have to actuate all of these movements. Actuating flexion/extension and adduction/abduction only offers the minimum necessary movements for stroke recovery and ADLs. By allowing free motion (passive joints) in parts of the shoulder complex, fluid human motion can be achieved. The AC features similar DOF to the GH joint. The sliding of the scapula during AC movement can be simplified and modelled by a prismatic joint along the axis of scapula sliding (Figure 3.5.6). This motion will allow scapular movement for flexion/extension and adduction/abduction. The movement of the scapular during elevation/depression is negligible. [43]

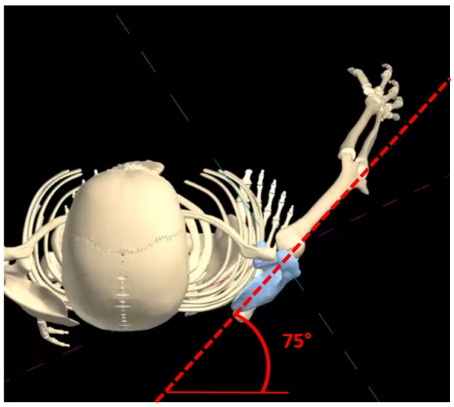

Figure 3.5.6: AC scapular sliding during flexion

The sternoclavicular joint facilitates retraction/protraction and elevation/depression. Retraction/protraction (Figure 3.5.7) motion is facilitated by both SC and AC joint movement, where the generalised motion to cover both of these can be simplified as one linear DOF. Retraction/protraction and elevation/depression (Figure 3.5.8) both translate the centre of the GH joint, which is essential to allow a wide ROM of the shoulder joint. This translation increases the ROM by allowing the shoulder to girdle the freedom to move during shoulder movements above the natural height of the GH centre. [44]

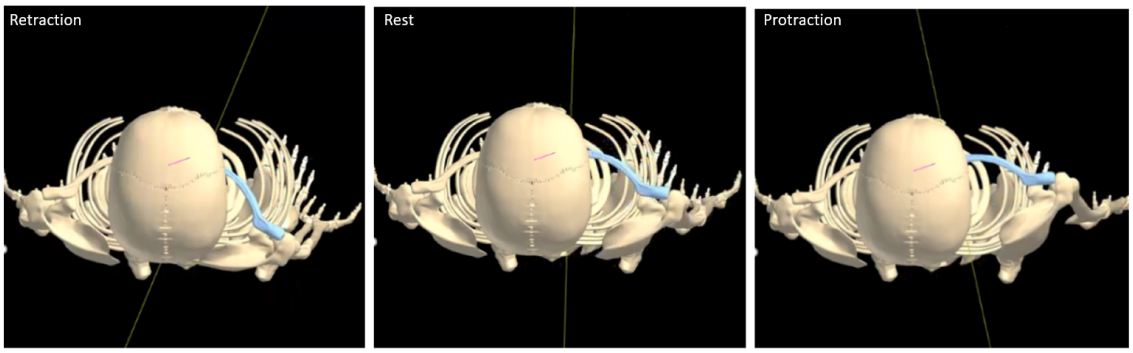

Figure 3.5.7: SC retraction/protraction example

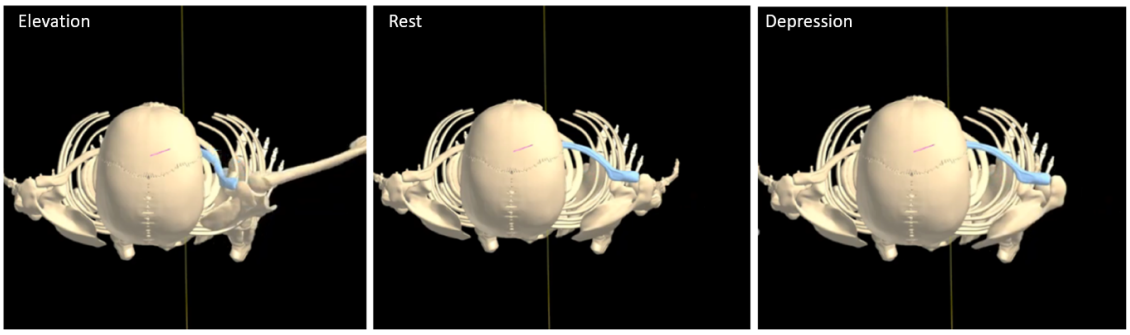

Figure 3.5.8: SC elevation/depression example

3.6 Shoulder Torque

The torque resulting from the mass of the arm is a combination of the gravitational torque and the torque of inertia as seen in Equation 3.6.1.

$$Tm = Tg - Ti \tag{3.6.1}$$

The arm dynamics were estimated by considering the parameters of the upper-arm, fore-arm, and hand, including their mass and respective centre of mass (COM) distances. Data from literature was used to calculate their inertial parameters [45], shown in Table 3.6.1. The arm has a total mass of 3.6Kg and has a centre of mass 294mm from the centre of the GH joint.

Table 3.6.1: Body segment inertia parameters for a 73kg male subject [45]. COM measuring from GH joint centre

Body Segment	**Body Mass (%)**	**Mass (kg)**	**COM (mm)**
Upper-arm	2.71	1.9783	162.6
Forearm	1.62	1.1826	401.7
Hand	0.61	0.4453	618.7
Total	4.9	3.6	294

The gravitational torque was estimated while the arm is at full 90° abduction, where the torque will be the greatest. The gravitational force and maximum gravitational torque are seen in Equations 3.6.2 and 3.6.3 respectively.

$$Fg = G * Marm = 9.81 * 4.1 = 35.36N \tag{3.6.2}$$

$$Tg = Fg * Rcom * sin(\theta) = 35.36 * 0.2938 * 1 = 10.37Nm \tag{3.6.3}$$

The maximum gravitational torque was found to be 10.37Nm at $\theta = 90°$. The minimum torque is 0Nm while the arm is at rest ($\theta = 0°$). Torque decreases with angle from the 90° abduction axis along the coronal plane.

The equations for inertia and Inertial torque are seen in Equations 3.6.4 and 3.6.5 respectively.

$$I = Marm * Rcom^2 \tag{3.6.4}$$

$$Ti = I * \alpha \tag{3.6.5}$$

Due to the low angular acceleration of the shoulder necessary during rehabilitation, the system is assumed to be quasi-static. Inertial torque is assumed to be 0Nm under these conditions. The maximum torque of the shoulder will therefore be equal to the acting gravitational torque.

For rehabilitation purposes, the torque of the shoulder during ADLs may define the necessary functional torque. Murray and Johnson [42] studied the torque required to complete basic ADLs, the results are tabulated in Table 3.6.2. The maximum required torque is 14.3Nm for flexion, which is above the gravitational torque due to external forces and the addition of inertial torque. However, the maximum abduction torque is 4.2Nm to complete basic ADLs, which is significantly lower than the maximum gravitational torque. A low abduction ROM is required to complete these ADLs, so the torque to overcome the forces of gravity are less significant than the maximum. Details on the ADL maximum ROMs are seen in Section 3.5, Table 3.5.2.

Table 3.6.2: Summary of the shoulder torque required for ADLs [42]

Force/moment	**Max (N m)**	**SD (Nm)**
Mx (N m) flexion	14.3	1.4
My (N m) abduction	4.2	1.8
Mz (N m) internal rotation	3.9	0.6

3.7 Shoulder Kinematics

Krishnan et al. [46] cites common challenges in the analysis of shoulder movement and kinematics such as;

- Complexity: The shoulder complexes movement is the result of several muscles and skeletal structures that interact to produce an output that cannot always be explained by a systematic model of rotations and translations.
- Over-constrained system: Although the individual shoulder bones can change orientation, their motion is often coupled and constrained.
- Movement variability: Upper-limb movements are discrete (a singular movement) involving a series of overlapping joint rotations [47]. Therefore it is challenging to monitor, analyse, and compare inter-subject and intra-subject kinematic data.

The functional shoulder motion may consist of simultaneous rotations and translations in one apparently simple movement. The kinematic model of the shoulder considers the skeletal structure and linkages as well as other muscular constraints. The skeletal structure of the shoulder complex encompasses the neck (from the sagittal plane intersection) to the upper arm. The shoulder complex consists of four bones: the clavicle, scapula, humerus, and thorax, as shown in Figure 3.7.1. The dynamic nature of the clavicle and scapula, and the large ROM of the humeral head facilitated by the girdle, allows for a wide range of combined motion.

The shoulder complex can generally be considered as a kinematic chain consisting of rigid links connected by joints, allowing the relative movement of neighboring links [48]. Kinematic chains can be classed as open-loop or closed-loop. In an open-loop chain, there is only one path along the chain where each link connects to the singular end of the next link, with the movement defined at each joint between links. In a closed-loop chain, each link connects to one or more links, with the chain consisting of multiple loops. The shoulder complex is a musculoskeletal system. Bones, muscles, ligaments, and nerves have an active effect on constraint and movement introducing a large amount of unknown complexity into the system. The shoulder complex itself is a closed-loop system considering these constraints. The scapula,

clavicle, and humerus make up a closed-loop kinematic chain of bones which defines the shoulder girdle, this connects the upper arm to the torso. However, the summation of the shoulders generalised movements can be considered an open-loop chain, where small discrete muscular connections are omitted from the model.

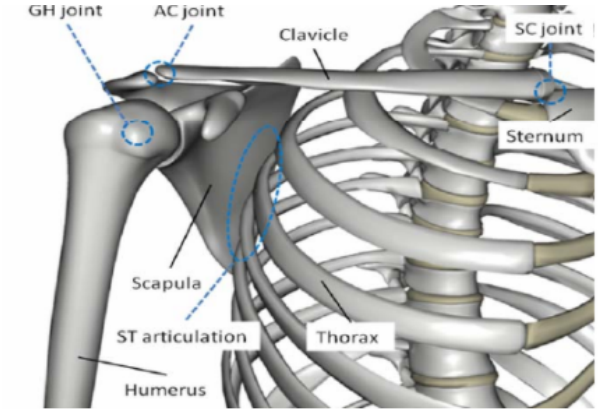

Figure 3.7.1: Anatomical structure of the human shoulder complex [48]

The contact points of the bones are defined as joints in the shoulder system. There are three synovial joints in the shoulder, these are joints where smooth bone movements between the adjacent bones occur. "The contact point between the sternum and the proximal end of the clavicle forms the SC joint. The distal end of the clavicle connects with the acromion process of the scapula, forming the AC joint. Furthermore, the humeral head articulates with the glenoid cavity of the scapula, forming the GH joint, which allows the humeral head to rotate in the glenoid fossa of the scapula. Additionally, the concave anterior surface of the scapula slides over the convex surface of the thoracic cavity by sandwiching a group of soft tissues, forming the ST joint" [48]. The bones of the shoulder complex are constrained and coupled at their joints which creates a combined assimilation of joints and links for each movement. This closed-loop coupled movement of the shoulder joints and bones is known as shoulder rhythm.

Lenarcic and Umek [49] modells the shoulder as an inner and outer joints. The inner joints represents the movement of the shoulder girdle, where the SC and AC joints were modelled as a universal joint, which are represented by two rotations. The inner joints represents The GH joint, and can be approximated by three rotations

constituting a spherical joint, with the axes centre being the centre of the humeral head. This kinematic shoulder model is included in a 6-DOF upper-limb model, shown in Figure 3.7.2.

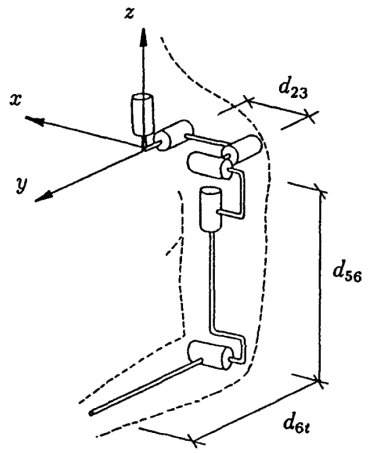

Figure 3.7.2: 6-DOF rotational kinematic model of the upper-limb [49]

Yang et al. [50] [51] models the upper limb as 9-DOFs. The shoulder is modelled with five DOFs, including 3 revolute and two translational joints (Figure 3.7.3). This model considers the GH joint as three revolute joints, having their axes intersecting at one common point. In addition, the effect of the scapula-thoracic translational motion is accounted for by two prismatic joints in the shoulder complex.

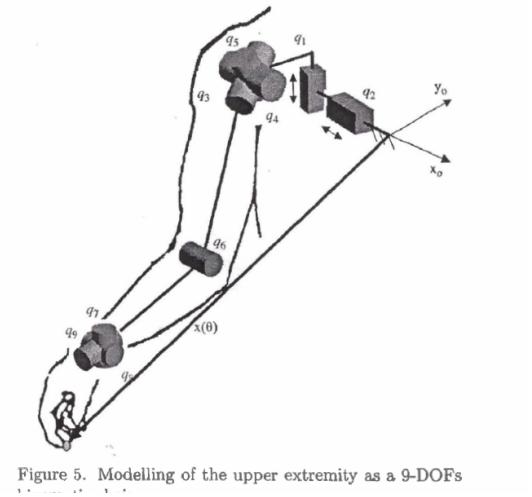

Figure 3.7.3: 9-DOF rotational and prismatic upper-limb kinematic model [51]

Li et al. [52] models the shoulder system with 6-DOFs, with three revolute joints and 3 prismatic joints (Figure 3.7.4). The GH joint is modelled as three revolute joints with intersecting axes, the movement of the clavicle and shoulder girdle translation is modelled by three prismatic DOFs.

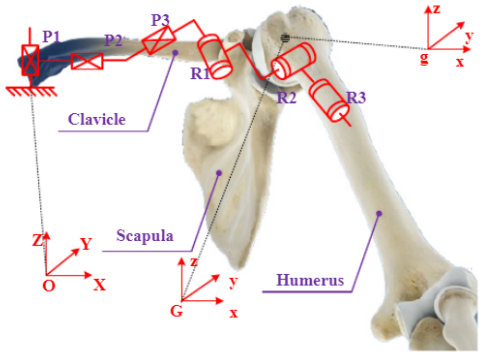

Figure 3.7.4: 6-DOF kinematic model of the shoulder [52]

The shoulder has also been modelled as a 7-DOF system with six revolute and one prismatic DOF [53], and a 9-DOF system that separates the shoulder complex into three segments (each with 3-DOF), considering the clavicle, scapula, and humerus as rigid links between them [54]. These models use an increased number of DOFs to precisely model the shoulders kinematics. For the application of an exoskeleton, whose kinematic model is based on the approximated general movements of the shoulder, this level of complexity is not required.

3.8 Electromyography

EMG is the detection of electrical signals generated by neurologically energised skeletal muscle cells during contractions. The signal output describes muscle activity and can be used for motion recognition and rehabilitation [55]. While some EMG devices use invasive electrodes, surface EMG electrodes can be placed on the skin above the muscle and provide a non-invasive, quantified, estimate of the muscle's actuation. Synergies can be quantified or observed in the energy patterns from the EMG signal [56].

EMG can be utilized as a trigger for the electrical stimulation and actuation via EMG biofeedback. For rehabilitation tasks, EMG can be used to monitor voluntary contractions and produce a quantifiable signal for control purposes. This is an effective method for patients who can activate selective muscles but lack the muscle strength to achieve the motion (paresis).

3.9 Review of Electromyography Techniques and Application

EMG is commonly used on many muscle groups. This review focuses on EMG applied to a complete set of shoulder muscles to determine recruitment patterns and activation levels during movement. Many studies were considered for this review, the selected studies were chosen due to their selection of muscle sets, signal filtering techniques, and detailed data.

Alizadehkhaiyat et al. [57], aimed to produce a complete data-set of shoulder musculature activation patterns for internal/external shoulder rotation. Thirty healthy subjects were included in this study, where EMG was used to measure the muscle activation energy of a defined set of 16 muscles during shoulder exercises. A similar method was used by the same authors (S Rajaratnam), investigating the characteristics and patterns of muscular activity during shoulder activity using EMG [58]. This encompassed a wider range of shoulder movements with muscle activity recorded for shoulder flexion, extension, abduction, and elevation for a set of 14 muscles from 20 healthy subjects. Wattanaprakornkul et al. [59] used EMG to investigate muscle activity amplitude for varying weight and muscle recruitment patterns during

flexion. EMG was recorded in 15 healthy subjects from a set of 12 shoulder muscles, with flexion performed standing in the sagittal plane at 0%, 20%, and 60% of subjects maximum load.

3.9.1 Electrode Placement and Muscle Set

Alizadehkhaiyat et al. used disposable Ag/AgCl bipolar surface electrodes to obtain EMG data from muscles accessible from the surface of the body. Standard electrodes with a 10mm conducting area were used, with an inter-electrode distance of 20mm to increase accuracy in small sub-regions of muscles. The anterior, middle and posterior deltoid (AD, MD, PD, respectively), upper, middle and lower trapezius (UT, MT, LT, respectively), upper and lower latissimus dorsi (ULD, LLD, respectively), upper and lower pectoralis major (UPM, LPM, respectively), serratus anterior (SA), and teres major (TM) were all measured using surface electrodes. Invasive bipolar hooked fine-wire electrodes were used to gather EMG readings from deep tissue muscles that aren't accessible from the surface of the body. The supraspinatus (SSP), infraspinatus (ISP), subscapularis (SUBS), and rhomboid major (RHOM) were all measured using these electrodes. Figure 3.9.1 shows the relative locations and placements of surface and fine-wire EMG electrodes.

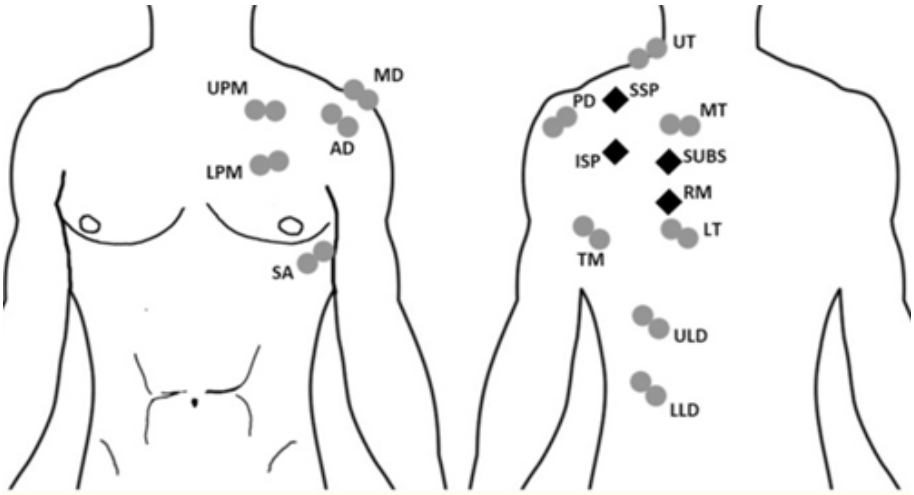

Figure 3.9.1: Placement of surface and intrusive EMG electrodes on the subject [57], Grey circles represent surface electrodes, and black diamonds fine wire electrodes.

A similar process was used in their following study [58] where two bipolar, disposable, self-adhesive pre-gelled Ag/AgCl dual surface electrodes were used to record the activity. The surface electrodes were used to record the EMG from the AD, MD, PD, UT, MT, LT, SA, TM, LD, and PM muscles. The electrodes had a 10mm conducting area to reduce the effect of cross-talk. These were placed parallel to the muscle fibres with an abrasive paste applied before electrode placement. Bipolar disposable hook wire electrodes were inserted aseptically for the intra-muscular recording of the SSP, ISP, SUBS, and RM. Wattanaprakornkul et al. also used two surface electrodes to record the EMG from the AD, MD, PD, UT, and PM muscles. The electrodes had a 10mm conducting area and 20mm inter-electrode distance. These were placed perpendicular to the muscle fibres with alcohol and abrasive gel applied to reduce the impedance of the skin. Indwelling electrodes were inserted into the SSP, ISP, SUBS, SA, LD, LT, and the middle trapezius (MT) to measure EMG. Standard practice is to place electrodes parallel to the muscle fibres, perpendicular placement is used to minimalise effects of FES on the EMG signal if being used simultaneously.

3.9.2 Signal Processing

EMG is a differential signal amplified with an instrumentation amplifier. Alizadehkhaiyat et al. and S Rajaratnam deferentially amplified their signal (Common mode rejection ratio (CMRR)>100db and a gain of 500db), sampled at 3000Hz and band-passed filtered (10-500Hz and 10-1500Hz for surface and fine-wire electrodes respectively). Introduced electrocardiogram (ECG) noise was removed using real-time signal processing. The raw EMG data was captured in a 100ms root mean squared (RMS) window to smooth the output data, with the teletremy unit applying an adaptive cancellation algorithm to remove ECG contamination[57] [58]. Wattanaprakornkul et al. alternatively 10Hz high passed, rectified, and 3Hz low pass filtered EMG data. [59]

3.9.3 Signal Normalisation

Alizadehkhaiyat et al. normalised data against a “maximum EMG” value to scale the data into quantifiable and directly comparable metrics [57]. Where the maximum

EMG was derived during a standardised measurement of rotational force (using a myometer). This was taken with the subject seated, shoulder and forearm in the neutral position, the elbow at 90° flexion. Similarly, S Rajaratnam also normalised data to the mean amplitude of the MD during shoulder flexion [58]. Wattanaprakornkul et al. post processed and normalised EMG data, using the maximum recorded voluntary contraction (MVC) which is the maximum RMS value from a data set, used to normalise subsequent data. Prior testing was done on subjects, where subjects would be asked to complete shoulder flexion at varying loads (with the shoulder in neutral position and forearm in mid-rotation), with the maximum load the subject could lift being the MVC. The baseline was also recorded for each muscle group and subtracted from subsequent data sets.

3.9.4 Signal Amplitude

S Rajaratnams [58] study shows the trends of muscle activation amplitude for shoulder flexion. Figure 3.9.3 shows the results of the study normalised to the mean amplitude of the MD during shoulder flexion. The MD, PD, UT, MT, and PM mean activation energies are shown for each movement, the remainder of the measured muscles are not shown as they don't show significant change between movements. There is a systematic increase of muscle activation energy from flexion, elevation, abduction to extension in all muscles except the PM, with the PD showing a significant increase of energy between extension and the other movements. PM generally has a low EMG signal with minimal change between values, except for an increase during flexion. The MD, PD, and MT all have similar trends also, though to note, the UT has a smaller response to abduction than the rest of the muscles.

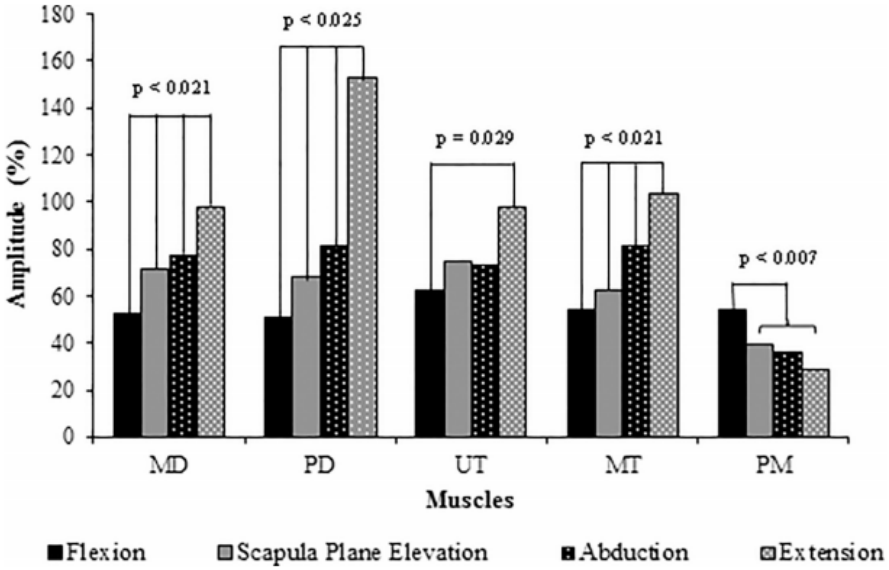

Figure 3.9.2: Mean signal amplidude during shoulder movements [58]

Wattanaprakornkul et al. compares a similar set of data with variable load for each muscle set. The normalised EMG amplitude of the muscle set during flexion for 0%, 20%, and 60% of the maximum load are shown in Figure 3.9.3. All muscles included in the study showed a systematic increase in activation energy with applied load. The AD, ISP, UT, LT, and SA showed high activation for all loads. The SA had the highest EMG for all loads, while LD showed very low activation energy for all applied loads. The PD showed significantly lower readings than the other portions of the deltoid, all of which have similar traits. The UT and LT recorded similar values with a linear increase of activity with load, the MD was significantly lower than these.

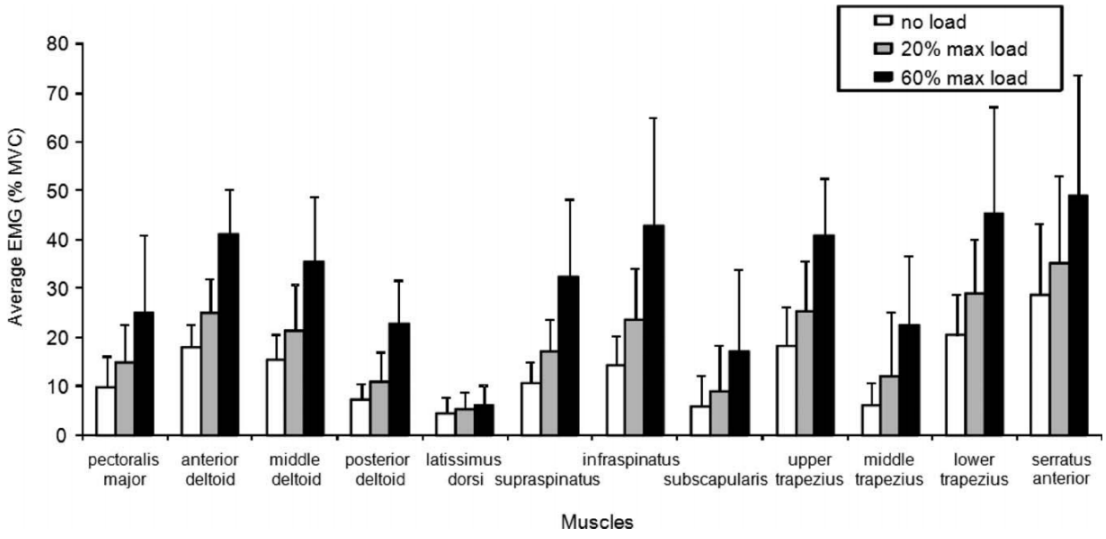

Figure 3.9.3: Mean signal amplitude during shoulder flexion at varying loads [59]

3.9.5 Recruitment Patterns

The patterns of voluntary muscle contractions and their successive activation are defined by recruitment patterns. The study by Wattanaprakornkul et al. showed an increase of the maximum EMG signal recorded, with load. The author states "The results indicate that the shoulder muscle recruitment pattern to produce flexion is established at low load levels and does not vary as load increases". Meaning that the muscle activity patterns remain the same regardless of the additional loads applied. Alizadehkhaiyat et al. notes that using an increased load should not alter the muscle recruitment patterns, which confirms this. Activation energy recorded before the start time indicated that the muscle has activated before physical movement is observed [59]. This phenomenon can be seen especially in the SSP, UT, SA, and LT. Other research also notes this, with delays of 20-25ms in upper-limb muscles recorded [60].

3.10 Electromyography Muscle Set

All three studies used a combination of surface electrodes and invasive hook wire electrodes to measure EMG muscle activation. Table 3.10.1 compares the muscle groups measured in each study, with the green shaded rows representing muscles tested with surface electrodes, yellow representing muscles tested with invasive electrodes, and red representing muscles not included in the testing set.

Table 3.10.1: Comparison of tested muscle sets in EMG studies

Muscles Measured	Alizadehkhaiyat et al. [57]	S Rajaratnam [58]	Wattanaprakornkul et al. [59]
AD: Anterior Deltoid			
MD: Middle Deltoid			
PD: Posterior Deltoid			
UT: Upper Trapezius			
MT: Middle Trapezius			
LT: Lower Trapezius			
SA: Serratus Anterior			
TM: Teres Major			
ULD: Upper Latissimus Doris			
LLD: Lower Latissimus Doris			
UPM: Upper Pectoralis Major			
LPM: Lower Pectoralis Major			
SSP: Supraspinatus			
ISP: Infraspinatus			
SUBS: Subscapularis			
RHOM: Rhomboid Major			

Two of the selected studies [57] [58] used similar signal processing techniques, both differentially amplifying the signal with a common mode rejection ratio (CMRR) >100dB; input impedance >100Mohm; gain 500dB. The signals were digitized at a sampling rate of 3000Hz and band-pass filtered at 10-500Hz. A 100 RMS window was used to smooth the resulting signal. Wattanaprakornkul et al. high pass filtered the EMG signal (10 Hz, 8th order Butterworth), rectified it, and then low pass filtered the output (3 Hz, 8th order Butterworth). This method does not offer any clear benefits and removes a significant portion of the relevant frequency spectrum.

The EMG hardware selected for the exoskeleton must include some form of anti-aliasing in the hardware, the remaining signal filtering will be done in the software for flexibility. Similar signal filtering to that in literature will be implemented. Further software-based signal filtering will be required to smooth the EMG signal and convert it into a control input, a RMS window of 100ms will be applied to achieve this. From the results of this review, the AD, MD, PD, UT, MT, LT, SA,

TM, ULD, LLD, UPM and LPM muscles will be measured during shoulder flexion/extension, adduction/abduction and internal/external rotation, with the data being normalised over time to analyse the muscle activation patterns. The amplitude data will not be normalised to an MVC as done in the reviewed studies, as the preservation of raw data is a priority. The results of this study are used to incorporate EMG based input control into the exoskeletons system.

3.11 Exoskeleton Classification

Exoskeletons are wearable devices that directly interact with the human body to exert force and motion onto the wearer. These can be made of rigid elements, such as plastics, metals, and elastic elements (rubber, nylon, wires etc). Stroke rehabilitation robotics and exoskeletons have many benefits over traditional methods and other technology such as cost, environment, and endurance. The cost of therapy can be reduced through cheaper equipment and less reliance on medical staff, portable devices enable rehabilitation to be achieved at home environments, and the duration of rehabilitation can be increased with fatigue management and increased participant interaction. This ever-growing field has a range of approaches in terms of actuation, sensing, control systems, and target objectives. Rehabilitative robotics can contain passive and active elements to achieve some form of actuation or restoring force. Although it is possible to define an exoskeleton as passive/active, often a combination of passive and active components are used to achieve maximum functionality.

3.11.1 Passive

A passive system does not require the input of electrical power to provide actuation, energy from human movement is stored and released by mechanical elements such as springs, elastic elements, and dampers [61].

In systems that interact with the human body, passive elements can be used to ensure the safety and comfort of the patient. Unrestrained movement or excessive forces in an unnatural direction may take the patients limb out of its naturally achievable ROM, which can cause strains or tears in muscle tissue, and in extreme cases may cause serious dislocations or injury. Passive mechanical stops are regularly used in exoskeleton systems to restrain the possible ROM of each link, these stops may be adjustable to allow larger or smaller achievable ROMs on a user-to-user basis. Adjustable length links are also commonly used to ensure the motion of the exoskeleton aligns with the patient's natural motion and joint intersections. Passive actuation elements are often used to provide a restoring or resistive force, and used in combination with active elements to achieve bi-directional motion.

3.11.2 Active

An active exoskeleton features one or more powered actuation elements that actively applies a force to the human body to excite movement [46]. Actuators such as DC motors, pneumatic inflatables (which include pistons and inflatable "muscles"), and linear drives (which are commonly pneumatic or hydraulic based coupled with DC motors) are common for active exoskeletons. The application and control of the force applied by the exoskeleton is very important in biomechanical systems.

Rigid link exoskeletons often use DC motors directly paired to the active joints to provide movement and power transmission. These exoskeletons are effective but are often very large and heavy, with the lack of compliance in rigid elements being a safety concern if not properly managed.

Soft-bodied exoskeletons are becoming increasingly popular, with pneumatic actuators and Bowden cables used to transfer force to the user. The use of Bowden cable power transmission allows the motors to be placed distally from the actuated joint, providing more opportunities to negate the need for rigid links and to distribute weight and unwanted torque forces away from the joint.

3.12 Additive Manufacturing

The material and manufacturing method of the exoskeleton are dependant on each other. Different manufacturing techniques have limitations in available materials, the complexity of the build, and lead time. When choosing the material for the exoskeleton, build variables to consider are strength, weight, rigidity, and accessibility [62].

Additive manufacturing is the process of "adding" successive layers of material to build physical components/structures, such as 3D printing. 3D printing enables rapid prototyping and mass customisation at a low cost for a variety of materials. However, 3D printing is less common in manufacturing due to its slow build rates, size limitations, poor mechanical properties, and anisotropic characteristics. The most common materials used for printing are plastic or polylactic acid (PLA), acrylonitrile butadiene styrene (ABS), and polycarbonate (PC) plastics. 3D printing introduces its own challenges, with anisotropic characteristics in prints being one of the most important. This anisotropy means that an object has different physical properties(such as strength, flexibility) along different axes, potentially producing variations between prints. To ensure that the maximum tensile strength is achieved, the orientation of prints must be considered. Cantrell et al. [63] tested the characteristics of 3D printed PC printed in different orientations to determine how prevalent anisotropy is. An array of raster angles (+45/-45, +30/-60, +15/-75, 0/90) were tested, where the raster angle refers to the angle between the nozzle and x-axis during printing. It was found that in PC (and in general 3D printed parts) anisotropy is present. It is recommended that parts are inspected (and even weighed) after printing to detect any potential defects or imperfections in the surface. A raster angle of +45/-45° gave the highest material properties with a shear modulus of 670MPa, yield strength of 22.8MPa, and ultimate strength of 36.9MPa as summarised in Table 3.12.1. Tanikella et al. [64] tested the tensile strength of commercial 3D printed polymer filaments, where PC had a maximum tensile strength of 49.08 MPa and a maximum load of 2041.64N which is significantly higher than any other filament.

Table 3.12.1: Material properties of 3D printed parts at +45/-45° raster angle [63]

Material	Poisson's Ratio	Young's Modulus (MPa)	Yield Strength (MPa)	Ultimate Strength (MPa)	Breaking Strength (MPa)
PC	0.39 +- 0.03	1890 +- 60	39.7 +- 0.9	56.6 +- 0.5	54.0 +- 0.7
ABS	0.36 +- 0.03	1960 +- 60	30.3 +- 0.6	32.8 +- 0.6	29.6 +- 0.5

3.13 Review of Exoskeleton/Robotic Devices

Many exoskeletons have been built and tested. This review mainly focuses on upper limb/shoulder active exoskeletons for post-stroke rehabilitation.

3.13.1 Soft Exosuit for Upper-Limb Assistance

Cappello et al. [65] [66] [67] suggests that rigid body exoskeletons have many limitations in terms of force, kinematics and materials. Human biomechanics can be used to provide support for exerted loads. Bones and tendons on the human body can be used in a way to constrain the system and enable normal functional movement, where mechanical "soft actuation" is applied by air, tendons, elastic elements etc.

Cappello et al. proposes a 1-DOF soft, compliant cable-driven elbow exoskeleton (Figure 3.13.1). Bowden cables are used to transfer force from a series elastic element (SEA) on the user's back to the elbow joint, SEAs are used to achieve a greater level of system compliance and easier bi-directional movement (as motor actuation is not rigid). SEAs in series with the Bowden cable transmission provides better ergonomics as they place motors in a location where their weight is carried by the trunk of the user, and it negates any rigid interaction. It is noted that Bowden cables introduce factors such as friction and backlash into the system. Friction is generated when the bending angle of the cable transmission changes with the relative position of the actuation/joints. This friction depends on the cable's length/curvature and reduces control performance unless it is properly compensated [68]. Backlash is caused by slack in the cable transmission system, a feeder system is used on the device which compensates for slack in the system.

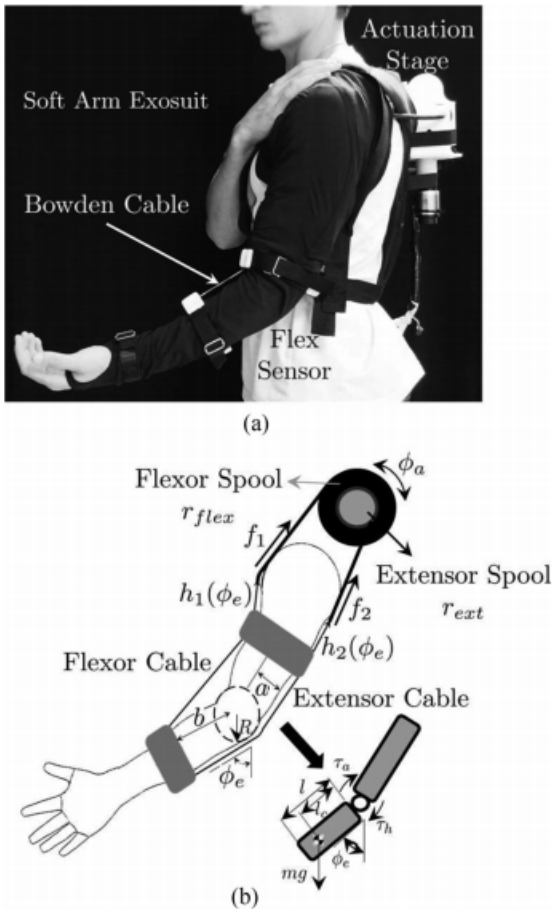

Figure 3.13.1: Soft cable driven exoskeleton [65]

The build of the exoskeleton consists of a soft frame devoted to holding the actuator. When the actuator is active the torque bi-product is transferred to the frame by compliant elements. This frame is held by a brace used to distribute the load onto the user's shoulder. As this is a soft-exoskeleton load distribution is considered in the build and fabric of it. Durable, form-fitting and stretchy elastane/polyamide is used to fit the form of the user, where nylon webbing is used in parts to handle loads and support tension by redirecting the external forces onto load-bearing bone structures. Velcro and buckles are used to increase friction between the exoskeleton and the user to prevent slippage.

EMG activity experiments were conducted, with the RMS of the EMG signal used to estimate effort, intention, and trigger assistance. Basic flex sensor models were used

to detect intention. To get the speed characteristics of the arm, the bending angle of the elbow was smoothed using a Butterworth filter and differentiated to provide acceleration. Load cells in the Bowden cables were used to estimate the assistive torque of the device. This project was developed into a pneumatic exoskeleton which is outlined in Section 3.13.2.

3.13.2 Soft Wearable Robot for the Shoulder

The active system designed by O'Neill et al. [69] is a soft wearable robot to assist in the movement of the shoulder for those who suffer neuromuscular conditions which stops them from completing ADLs. The actuation of this design features two pneumatic actuators that act to support the upper-arm during abduction and horizontal flexion/extension movements of the shoulder. Pneumatic actuators produce force based on the air pressure input and cross-sectional area. As noted in the paper, the total absolute pressure that can be handled from the actuator is 200kPa. This was restricted to this pressure as many of the smaller scale compressors have a limit of 200kPa, meaning to increase the pressure would require larger compressors, so a trade-off between power and size is required. To abduct the arm the moment value referenced was 15-20Nm to overcome the arm and a 1kg load weight [45].

A neoprene vest is worn by the user which has the robotic components attached. A flexible plastic plate is placed below the underarm and is used to support the robot body and horizontal actuators. The abduction actuator (ABA) is secured to the upper arm by a wide adjustable velcro strap. The chambers of the ABA pneumatic actuator is split into 5 inflatable chambers, this was done to ensure that the material doesn't wrinkle during use, which results in a reduction of the ABA stiffness and compromises its support integrity. The exoskeleton model is shown in Figure 3.13.2

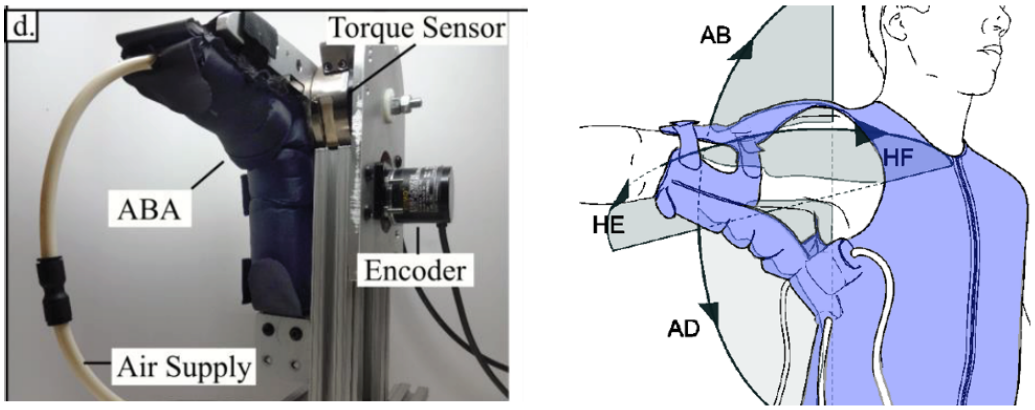

Figure 3.13.2: Soft phonemic actuated exoskeleton [69]

Soft actuators are more compliant to the human body kinematics compared to rigid links as they do not constrain movement in any way. There is a much lower risk of harm to the user and the control system is more simple as fewer components are required [69]. However, due to the simplicity of actuation, soft pneumatic bodies cannot achieve a higher number of DOF as easily as rigid links. Pneumatic actuators tend to act in a non-linear fashion, making accurate control and monitoring difficult. EMG is used to read muscle activity and control the system with four differential surface electrodes. The EMG signals were rectified and filtered with a 4th order 10Hz Butterworth low pass filter. The soft robotic shoulder support technology is available for licensing.

3.13.3 Design of a Passive upper-limb Exoskeleton for Macaque Monkeys

The design proposed by Lu et al. [70] is a 6-DOF upper-limb passive exoskeleton, which includes 4-DOF to model the shoulder complex. The model has been designed as a passive system for kinematic motion sensing for neural research and animal training. The macaque monkey is constrained to the chair by its neck and torso, and the exoskeleton is attached to the right arm. The exoskeleton is externally supported so minimal weight is experienced by the limb. A 3D system is used to present targets to the monkey and the upper-limb voluntary motor movements are tracked while the neural signal is recorded and synchronised with the motor movement data. As can be seen in Figure 3.13.3, shoulder complex joints 1-3 have

rotational axes which intersect at a common point, where joint 4 has a rotation axis along the arm. The exoskeleton is attached to the upper-limb via two 3D printed cuffs with attached elastic braces. A curved rail around the cuffs a timing belt with a pulley and sliding roller to record the motion of the limb to the host computer for synchronisation. Although this prototype is intended to record the motion movements only, the internal timing belt/cuff system could potentially be utilized to also exert external/internal rotational movement onto the upper-limb if actuators were implemented.

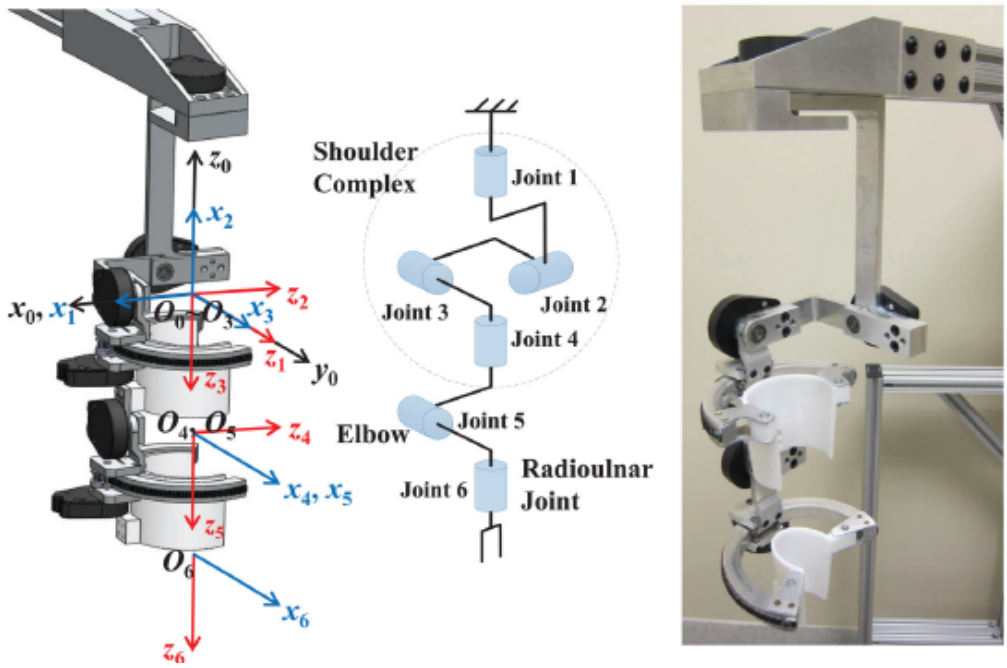

Figure 3.13.3: Left - complex model with joint, middle - simplified joint model, right - as-built exoskeleton model [70]

This design presents an interesting model of the shoulder joint, which allows for a large ROM while not over constraining the upper extremity's movements.

3.13.4 CLEVERarm

CLEVERarm, designed by Soltani-Zarrin et al. [71] [72], is an 8-DOF active exoskeleton that includes 6 active joints and 2 passive joints. The exoskeleton models the motions of the elbow, wrist, GH joint, and shoulder girdle. Five of the active joints are used to model the shoulder complex which facilitates 2D motion of the GH joint along the frontal plane of the body. The remaining active joint models the elbow, and the two passive degrees model the wrist. Three circular revolute joints are used to model the GH joint. An interesting feature to note from this configuration is that the end effector link is angled at 35° to align the exoskeletons direction of movement with the natural angle of the arm. Figure 3.13.4 shows a series of 3D models of the design.

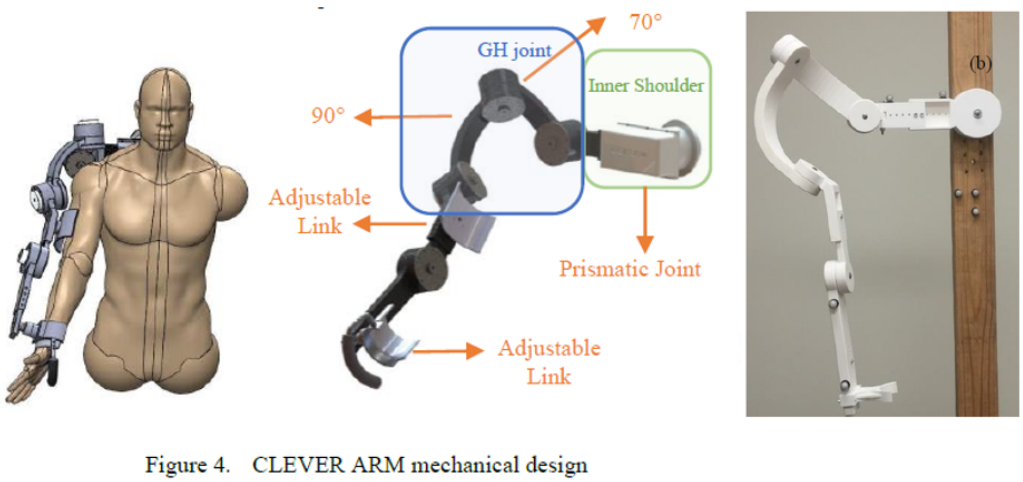

Figure 4. CLEVER ARM mechanical design

Figure 3.13.4: Left - 3D exoskeleton and human attachment model, middle - simple design diagram, right - printed and mounted simple passive frame [72]

The revolute joints are actuated by brushless DC motors, with attached gearboxes, while the linear joint is driven by a direct-drive linear actuator. Each individual joint has an encoder to provide motion feedback. The joints have the following characteristics;

- The back rotary joint uses a Maxon EC-90 motor with a 20:160 gearbox to provide 53.3Nm of torque.

- The connected linear joint uses a Tecnotion UM06 linear actuator to provide 58Nm of torque.
- All three joints in the GH spherical system use a Maxon EC-60 motor with a 17:100 gearbox to provide 31.09Nm of torque.

Further distal DOFs do not need to be considered for this study, though the weight of the exoskeleton body at the extremities will generate a large force on the system. Each joint must generate enough torque to overcome the weight of successive links. The exoskeleton was constructed with a combination of materials such as steel alloy, aluminum, and carbon fibre reinforced alloy. Excluding the motors and support base, the mass of the exoskeleton body is approximately 3.9kg. The entire exoskeleton can be seen in Figure 3.13.5.

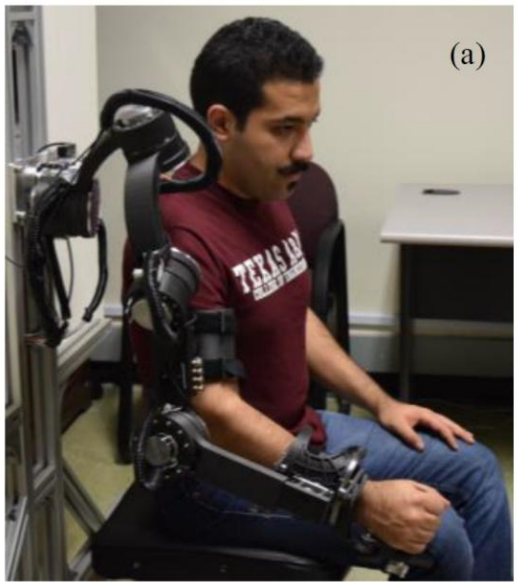

Figure 3.13.5: Motorised CLEVERarm functioning on human subject [72]

Virtual reality environments are used alongside the robotic exoskeleton as a control mechanism to assist with motion tracking and therapy. The control program simulates regular ADL movements encouraging consistent muscle motions.

3.13.5 Upper-Limb Powered Exoskeleton Design

The design by Perry et al. [73] is an active assist-as-need rigid body exoskeleton with externally mounted actuators, utilizing surface EMG (sEMG) to elicit movement from the motorized body. 7-DOFs are modelled with each DOF implemented with a revolute joint. Figure 3.13.6 shows the system.

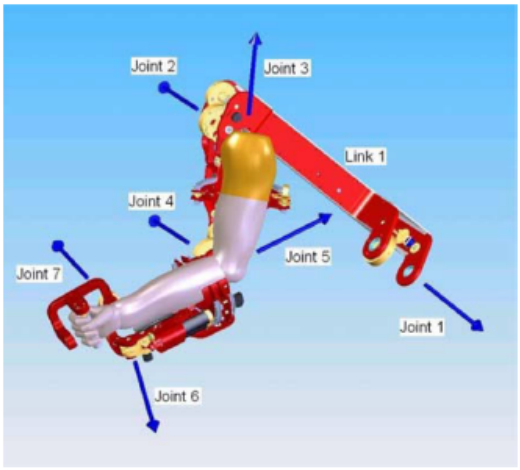

Figure 3.13.6: 7-DOF upper-limb powered exoskeleton [73]

For the actuation of the joints, brushed DC motors were used. The shoulder and elbow joints used a low weight 6.2Nm motor while the wrist used a 1Nm motor. Gear ratios are used to increase the torque capacity of the active joints, exerting 9Nm onto the shoulder. The larger motors were mounted on an external stationary base to reduce the weight exerted on the patient's arm, while the lighter, lower torque motors were mounted directly on the exoskeleton. Cable drive systems were used as they can transmit force remotely easily and safely. This exoskeleton has excellent safety measures in place to protect the user. Physical stoppers are placed at joints to ensure that accidental over-extension of a joint does not occur. In addition to these, three different emergencies stop switches are implemented to shut off motor functions and power entirely.

3.13.6 HARMONY

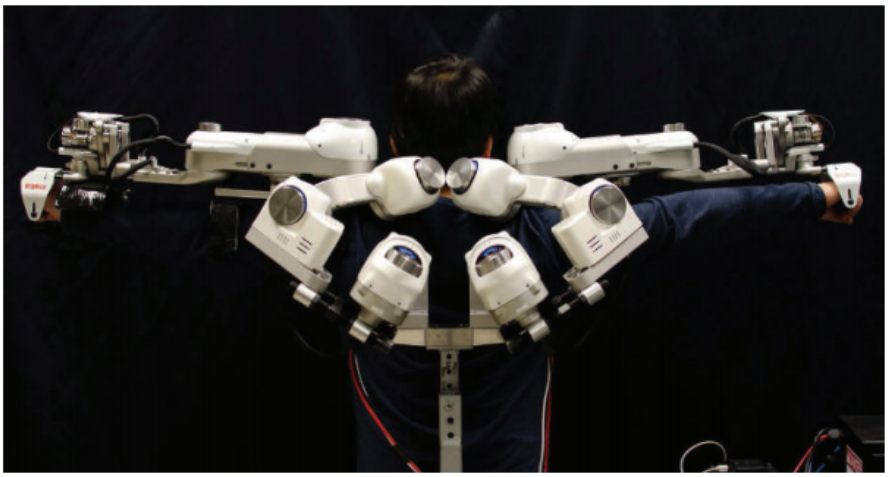

(c)

Figure 3.13.7: HARMONY robotic exoskeleton

HARMONY (Figure 3.13.7), designed by Kim and Deshpande [74] is a fourteen DOF upper-limb rehabilitation robot. There are 5-DOFs for each shoulder complex: three revolute DOFs at the GH joint, and two for translation, each DOF consists of a DC motor with an SEA. The GH joint is approximated as a ball-and-socket joint, realised by three revolute joints with intersecting axes. For the GH joint translation, a shoulder girdle mechanism was developed, which consists of one rotary joint and a "parallelogram", which is a multi-link structure that has one actuated DOF. Using the parallelogram structure, circular motions could be shifted in any direction. This parallelogram kinematic design is unique to the HARMONY exoskeleton. Three adjustable parameters (Figure 3.13.8) are used to align the exoskeleton's GH intercept with the subjects, compensating for any variability in user and ensuring proper spherical motion around the joint.

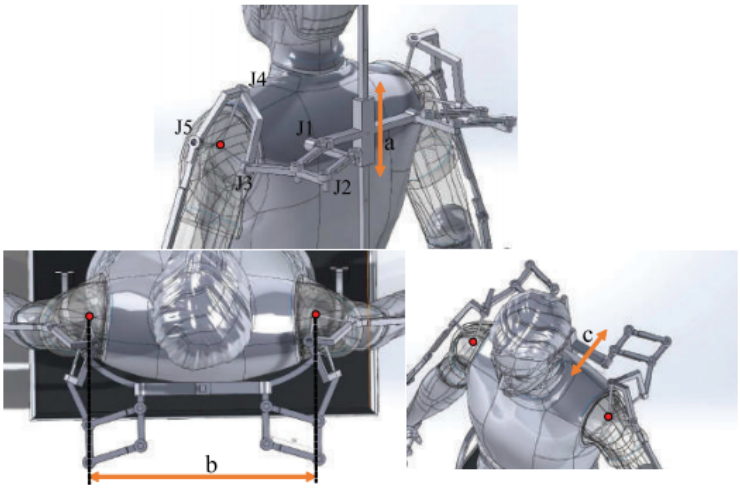

Figure 3.13.8: Kinematic design of HARMONY exoskeleton featuring labelled adjustable parameters. [74]

HARMONY is actuated at each joint by flat profile, high torque, brushless DC motors. It can provide 34.4Nm of torque at the shoulder, 13Nm at the elbow, and 1.25Nm at the wrist. Four multi-axis force/torque sensors at the interaction ports are fitted to measure the output force. The weight of the exoskeleton body is 31.2kg, a chest harness is required to attach the exoskeleton to the frame, this acts to take the load off the user.

A 3D motion work area analysis was completed to verify the achievable ROM by tracking the centre of rotation (COR) of the GH joint and at the centre of the wrist. The ROM of the exoskeleton was derived from this analysis. The achieved adduction/abduction range is 60° to 118°, extension/flexion range is 45° to 160° , and internal/external rotation range is -80° to 79°.

Passive hard stops are used at every joint to limit motion, and emergency stops for the operator and user are also accessible on the exoskeleton. Safety ROM limits are also incorporated at a software level. Additional software safety precautions are limited joint speed, limited torque/force and self-collision recognition. The Operating system is a Linux based computer communicating with the motor drivers via EtherCAT for real-time control.

3.13.7 Parallel Actuated Exoskeleton

The design by Hsieh et al. [75] is a 6-DOF parallel actuated exoskeleton with two actuated and four passive DOFs allowing assisted flexion/extension and adduction/abduction movement of the shoulder. Figure 3.13.8a shows the exoskeleton design. This exoskeleton uses passive DOFs in a spherical interlinking structure to allow movement and transfer force, which is an interesting feature. Actuation is provided independently by two linear SEAs. The "five revolute" and "four revolute" spherical mechanisms, and a gravity-balancing mechanism, are used minimize the load on the motors and increase the device compactness.

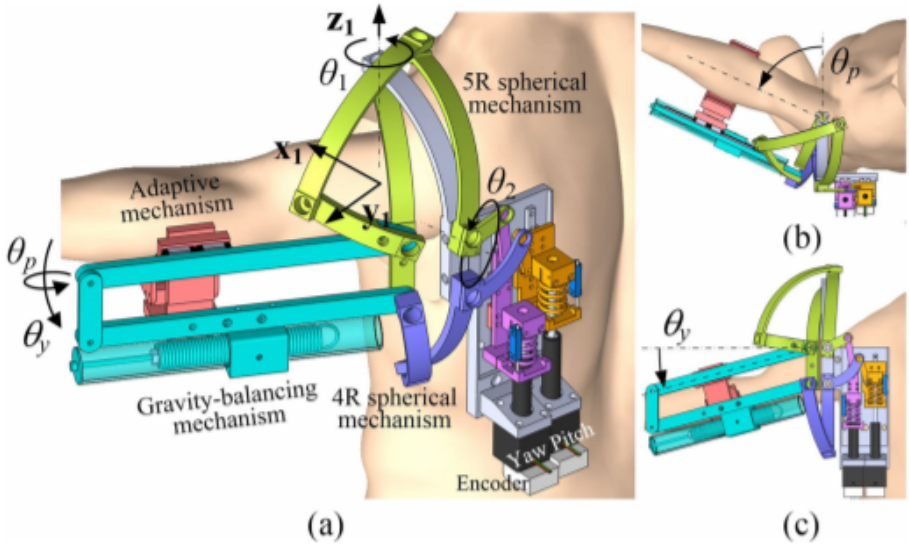

Figure 3.13.9: Model of the 6-DOF parallel exoskeleton. a) diagram of mechanisms, b) movement of the exoskeleton along the transverse plane (pitch), c) movement of the exoskeleton in the coronal plane (yaw) [75]

The linear stepper motor (with encoder) is connected in series to a 33N/mm spring, whose end is connected to a free moving sliding crank unit. A potentiometer is used to quantify the deformation of the spring and derive the spring force. This force is used as an estimate of interaction forces, allowing force/impedance control to be realised. The SEA motors were attached to the ground on an external frame to reduce any inertial interference introduced into the system, because of this larger motors could be used to provide a higher range of torque.

With reference to the angle notations in Figure 3.13.8, the achieved ROM along the transverse plane was -20° to 75°, with an applied torque and torque of 44Nm. The achieved ROM along the coronal plane was -40° to 70°, with an applied torque of 24Nm. The annotations of pitch/yaw do not directly correlate to shoulder movement of adduction/abduction and flexion/extension, but it can be inferred that the yaw motion is the largest contributing factor to these exercises.

3.13.8 ARMin III

ARMin III, designed by Nef et al. [76] [77], is a 4-DOF upper-limb rehabilitation robot. The shoulder complex is modelled by three actuated joints, with one other actuated joint for the elbow. All joints are actuated by DC motor drives, these are labelled as M1-M4 in Figure 3.13.10. Drives M1 and M2 are driven by a DC motor directly coupled with a 100:1 harmonic drive gearbox. Drive M3 is a DC motor directly coupled with the 1:30 harmonic drive gearbox, whose output is coupled to a curved slider by a 1:14.5 belt drive. All DC motors have encoders, with additional wire potentiometers fitted which are used as a redundant measurement to reduce position errors. The system runs on a Matlab/Simulink XPC target computer with a loop time of 1ms. The author states that higher torque values were chosen in order to reduce/overcome forces introduced by the human subject such as spasms and high resistance, as these are hard to model due to their volatile behavior. For this exoskeleton, the achieved transverse rotation range is 47° to 135° and has a torque of 33.28 Nm. The coronal rotation range is 46° -140° and has a torque of 37.76 Nm. The internal/external rotation range is is -91° -92° and has a torque of 38.5 Nm. The device is 18.755kg (excluding controller, hardware, and frame).

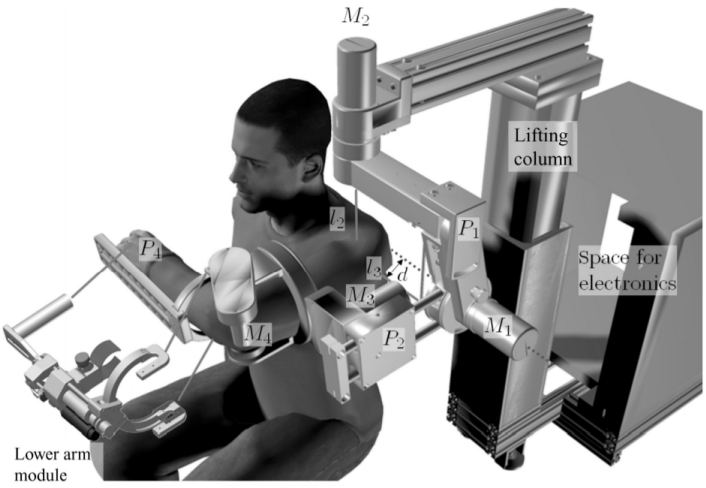

Figure 3.13.10: Model of ARMinIII exoskeleton

Safety has been extensively covered by a combination of passive, active, and software-based countermeasures. The digital potentiometers are used as a redundant positioning measurement to detect any errors in the encoders. Passive safety features include mechanical ROM limits, bio-compatible cuffs, smoothed edges etc. The real-time controller has a 100Hz activity watch-dog timer, current/speed monitoring, and collision detection are also enabled. The safety circuit isolates the motor drives from power if any safety issues are flagged. The motor drives are back drive-able so in the case of an accident or power outage they can be moved manually. Motor drive M1 also has passive weight compensation to ensure that it does not collapse in the case of a power outage too. The most extreme safety measure in place a dead man's switch, held by the operator, which isolates power if released.

At the time of writing, Five ARMin III devices were undergoing clinical evaluation in hospitals in Switzerland and in the US. The ARMin is in its 5th iteration of development. However, research based documents for further models have not been released in detail.

3.14 Further Discussion of Literature

3.14.1 Actuation

The most common types of electrical actuation on reviewed devices are DC motors. DC motors are used usually for their accessibility, high constant torque, ease of control, and compact size. However, to provide enough torque at the right speed, DC motors have to be geared down and this causes them to have a high mechanical impedance. This impedance causes issues in human-mechanical systems as they cannot be back driven, and offer little compliance. Additionally, their weight is often a contributing factor to unwanted forces introduced in systems.

Of the active exoskeletons reviewed, six of the seven exoskeletons utilised some form of electrical actuation. Of these six exoskeletons, five used DC motors for active revolute DOFs [65] [72] [73] [74] [76] and two used linear DC motors for active translational DOFs [72] [75]. The issue with motors is the more torque you need, the larger/heavier the motor. This is a significant issue for robots that place the motors at the joints of the links, as the weight of the system increases, affecting the size and portability of the system as well as the load felt by the user.

From the reviewed exoskeletons, the issue of the actuator's significant weight force acting on the user has two solutions.

- Motors are placed distally from the actuation point at a location where the load can be distributed onto the user without discomfort, such as the user's back.
- Motors are placed at the joints and the robot is placed on an external frame, often requiring the user to be seated for trials.

Perry et al. states "as each motor carries the weight and inertia of the more distally placed motors, the importance of high power-to-weight ratio increases from shoulder to wrist" [73].

For distally placed actuators, cable transmission is used to transfer the torque from the motor onto the target joint [65] [73]. Cable drive systems have been used to reduce the inertia of exoskeletons and to increase compliance. However, there are

losses in the power transmission and Bowden cables introduce factors such as friction and backlash into the system [65]. In cable transmission, and even more localized drive systems (such as ARMin III), a "gear ratio" is used to increase the torque of the system by having the actuated joint on a larger diameter spool than the actuator spool.

Of the two "soft" exoskeletons reviewed, O'Neill et al. [69] used pneumatic actuation to enable shoulder adduction/abduction. An advantage of pneumatic actuation is the safety and compliance of the actuator. Its low weight on the user, fast response, and high applied force are also benefits. However, although the wearable device is low weight, the infrastructure to produce pressure is not. Pneumatic actuators are not a common feature in rehabilitation robotics, because it is not widely supported and easily implemented. Complex, custom made, units, often need to be made for this form of actuation, though many standard commercial units are available [78]. The need for air supply and its non-linear control nature are drawbacks as it relies on external special connections and is difficult to accurately control.

Other actuation methods include FES and springs. FES is the applied electrical stimulation to the body's muscles to stimulate contractions and incite motion. Castro et al. [79] used curved scissor links interconnected by revolute joints and compression/extension spring actuation. Springs are also used in exoskeletons to give a measure of force interaction[75] .

3.14.2 Torque, ROM and DOFs

The DOFs, torques, ROMs, and weights of the reviewed rehabilitation robots are tabulated in Table 3.14.1. The majority of exoskeletons included in the review use the standard movements of flexion/extension, adduction/abduction and internal/external movements as a DOF metrics. Some devices [75][76], used pitch and yaw, or movement in the coronal and transverse planes as metrics for defining their ROM. Although the standard movements occur in these planes, it is difficult to directly compare these results. Hsieh et al. state that therapeutic exercises mostly require the yaw motion (flexion/extension and abduction/adduction) [75], where these motions will likely be a combination of pitch and yaw.

The applied torque varies in the reviewed exoskeletons, with DC motors applying torque to the shoulder at 9Nm [73] to 44Nm [75]. HARMONY provides 34.4 Nm of torque at the shoulder. CLEVERArms motors can provide a maximum of 31.9Nm. The parallel actuated exoskeleton [75] can output 24Nm in the coronal plane and 44Nm in the traverse. High torque values are required for these exoskeletons due to their large weight/size, as a significant amount of torque is required to actuate its end effector, these weigh up to 18.8kg per side of actuation. The soft pneumatic exoskeleton design[69] cities that 15-20Nm is required to overcome the weight of the arm (with a 1kg weight in hand).

Table 3.14.1: Characteristics of reviewed robotic devices. *excluding controller, frame, and additional hardware

Exoskeleton	**DOFs**		**Maximum Torque (Nm)**	**ROM(°)**			**Weight (kg)**
	Active	**Passive**		**F**	**E**	**AB/AD**	
Soft Pneumatic Exoskeleton [69]	2	0	15-20	48	26	59	0.48
CLEVERARM [71]	5	0	31.9	-	-	-	3.9*
Upper-Limb Powered Exoskeleton [73]	7	0	9	180		180	-
HARMONY [74]	7	0	34.4	160	45	58	31.2
Parallel Actuated Exoskeleton [75]	2	4	24-44	-	-	110	4
ARMin III [76]	3	0	38.5	-	-	94	6.5*

The exoskeletons which incorporated DC motor actuation typically modelled the shoulder complex as 2-5 DOFs, with most of the models using direct motor actuation for each DOF. Hsieh et al. incorporated passive DOFs into the driving mechanisms, using passive DOFs in a spherical interlinking structure to allow movement and transfer force [75].

3.14.3 Feedback and Control

Feedback for control is essential in any rehabilitation or biomedical device. In most of the exoskeletons reviewed, the main feedback measurement for control was joint angle. For devices that have a direct motor drive, encoders can be used to measure this. ARMin III uses optical incremental encodes, and CLEVERarm uses both incremental and absolute encoders at each joint to ensure reliability. The soft elbow-actuator design [69] uses a resistive flex sensor to measure the bending angle of the elbow joint at an accuracy of +-1°.

Applied force is an important sensory type of feedback for control, CLEVERarm

and HARMONY both use the same approach by incorporating force/torque sensors at the physical interaction points between the exoskeleton and the human subject. These sensors provide 6-axis force and 4-axis torque measurements. Other force-sensing methods involve using a spring/potentiometer system in the parallel exoskeleton, where a potentiometer is used to measure the deformation of a spring with a known spring constant [75]. This system provides an estimate of the interaction forces which are then used in a force/impedance-based controller. Hsieh et al. [75] also suggests using SEAs, to obtain accurate force and impedance control at the exoskeleton-limb interface. Other devices reviewed used the motor current draw as an indicator of output torque, and in systems that incorporated Bowden transmission, load cells in parallel with the power transmission gave an accurate force indicator [65].

From the devices reviewed, a common controller type was an impedance controller, which effectively controls force/torque based on motion feedback. PID control was also used in selected devices. PID is a common control strategy, which uses gains and sensory error to achieve a desired output, such as position or speed. These controllers are easily implemented, but difficult to incorporate multiple sensors for assist-as-need control. For the soft cable-driven exoskeleton [65], an admittance controller is used, which aims to compensate for gravity/frictional force and to achieve a desired trajectory and speed. This can adjust its level of assistance based on the voluntary force of the subject, measured by load cells attached to the Bowden power transmission as previously described.

EMG measurements, for selected muscle activation energies, are used in exoskeletons as a trigger or as a sensory control input [65][69]. This can be used to implement real-time assist-as-need type control, where the provided motor output (whether it's speed, position, or force-controlled) is proportionally adjusted based on the EMG signal input. A benefit of this is that it is applicable for patients with varying degrees of mobility, and is likely to increase patient engagement in therapy due to its interactive nature.

3.14.4 Portability

Of all of the active exoskeletons reviewed, only the design by Cappello et al. could be considered portable [65]. Portability suggests that the device can be transferred from one place to another with relative ease. Often when describing portability, characteristics that are considered usually relate to, low weight (Its ability to be easily lifted by the subject), compact size, and a lack of reliance on external inputs/power. For a rehabilitation device, true portability has many benefits as it reduces the requirement to go to the hospital for therapy, which could be done in a comfortable environment (e.g. home) at any time. Being able to complete portions of rehabilitation at home will likely help improve recovery due to its accessibility (especially important for ADLs) and reduce the likelihood of developing compensatory injuries. From the review of robotic exoskeletons, the portability of the devices are usually hindered by one or more of the following categories;

Weight and Size: All of the devices reviewed, excluding the soft exoskeletons, were too heavy and large to be considered portable. The size of the motors, components, and the weight of the materials used, contribute to the overall weight of the system. Having the devices rely on fixed frames for support also adds to the weight and size issues. These devices all required connection to a PC or other type of user interface (UI), all of which is permanent/semi-permanent. Often these restrictions require the patient to sit down, restricting the rehabilitation exercises that can be completed.

Power and Specialised Connections: Most of the reviewed devices required a physical connection to an external power supply or to a PC for control and data gathering (such as an EtherCAT connection for HARMONY). Most of the reviewed devices do not cite the power requirements, but a connection to a large power source or mains power is assumed for the frame-supported devices. Additional specialised connections include an air supply. The soft pneumatic exoskeleton requires a constant supply of compressed air, which requires extra components to operate outside of a hospital setting.

Propriety Software: Devices such as HARMONY and ARMin III require software on the connected hardware which is not open source. Often this will be a custom build of Linux, 3D motion capture software, or MATHlab. Some of these issues could be resolved by buying licenses for each exoskeleton developed for the relevant software. There is also a significant learning curve for the user to learn how to navigate complex new programs if the device is intended to be user-controlled. Using a microcontroller (MCU) or similar device eliminates the reliance on physical external control or paid specialist software.

Supervision Requirements: The larger specialised exoskeletons, such as ARMin III, require a supervisor/therapist operating the machine at all times, which limits the use of the machines to a hospital environment.

Of the reviewed devices, many are not appropriate for outpatient use due to their reliance on the aspects described. However, with developments in Bluetooth/wireless communication, battery's, software, and continuously minimizing components, more upper-limb exoskeletons will have the ability to be portable.

3.14.5 Compliance/Comfort

Compliance in biomedical and applied exoskeletons is essential to allow voluntary free movement and to not over constrain the system. Compliance is generally referred to as a device's ability to allow a degree of free movement in the system so that when actuation/force is applied the user does not feel discomfort due to rigid actuation systems or structural components.

Soft actuators [65][69] are innately more compliant to the human body kinematics compared to rigid actuation as they do not constrain movement. Often form-fitting fabrics and additional load-bearing strategies are used to safely distribute any loads [65]. Cable drive systems are also used to place motors distally from the actuated joint where its load/torque can be more comfortably distributed (such as on the back of a user). This also helps reduce the size and weight of exoskeletons at their extremes, improving comfort and compliance if implemented well. SEAs are also used to introduce an elastic compliant element into the drive system of exoskeletons,

allowing for a degree of human motion due to natural deformation. SEAs are also used to estimate the torque applied to the system for control and safety measures [74], [65].

Compliance contributes to the comfort of the user by allowing voluntary movement. However, comfort differs from compliance as it is based on how external forces interact with the user and makes them feel. Often the weight and size of the exoskeleton are minimised in order to improve comfort, the dispersion of excess actuation torque, mounting the exoskeleton to an external frame, and compliant exoskeleton-body attachments (cuffs) are also used to increase comfort for the user. Adjustable parameters are also featured on most of the exoskeletons reviewed to align the exoskeletons to the skeletal frame of the user. Specifically, when the GH joint is modelled as a 3-DOF spherical joint, the exoskeleton is usually adjusted to align its movement intercept with the centre of the GH joint. The misalignment of this can cause discomfort and injury by actuating a joint in an unnatural movement pattern. The shoulder complex can be kinematically modelled a number of ways as seen in Section 3.7. The kinematic representation of shoulder movement may not necessarily mimic exact human motion, misalignment in the exoskeleton is allowable provided it does not exert any unwanted forces onto the user.

3.14.6 Safety

All of the devices reviewed had considered safety and implemented countermeasures. Passive physical stops to limit the ROM, and software-enabled stops to limit the joint angles, were used extensively in the exoskeletons. HARMONY and ARMin III are two good examples of exceptional safety practices. HARMONY uses passive hard stops, emergency stops, software ROM limits, limited joint speed, limited torque/force, and self-collision recognition. As described previously ARMin III is exceptional to the point of extreme with their safety measures, the most unique of which are back drivable motors, weight compensating drives, and a dead-man switch for the operator.

3.15 Design Requirements

The exoskeleton proposed will consider the kinematic models of the shoulder investigated in Section 3.7 and their relative movement patterns. This kinematic model will look to simplify the shoulder complex while not restricting/constraining movement in any way. Kinematic analysis and modelling will be completed to verify a non-constrained ROM and link relations. The exoskeleton will allow for a ROM based on research findings in Section 3.5, which considers the skeletal ROM, muscular constraints, and ADLs used in common rehabilitation practice. As this is for ADL based rehabilitation, only active motion ROM characteristics will be considered. The minimum achievable ROMs are defined as such; the achievable ROM should be 154° in flexion, 74° in extension, 163° in abduction, 47.5° in internal rotation and 86.5° in external rotation. All of this range will be achievable by the exoskeleton. However, the entire range does not need to be achieved by actuated movement alone, users may actively move the exoskeleton to achieve larger ROMs past the actuated limits. The majority of shoulder models investigated failed to define if adduction from the arms resting position is possible, or defined it as 0°. The shoulder can move with adduction for a small angle from rest, this movement is usually accompanied by shoulder elevation. A specified adduction ROM is not essential for the exoskeleton, but is worth considering.

The developed exoskeleton should be able to operate without any of the aforementioned connections, software, or supervision reliance's defined in Section 3.14.4. In addition to these portability requirements, the exoskeleton should be light-weight, as to not be reliant on any permanent structures and to be easily supported by the subject. Therefore, the exoskeleton's entire weight must not exceed 5000g. The size of the exoskeleton should be small enough that it may attach to the user without any external connections to the ground, fit into conventional transport and be able to fit through a standard home doorway (1980 x 860mm). an upper limit of $0.5m^3$ is therefore defined as the maximum workspace volume of the exoskeleton.

Compliance, comfort, and safety are grouped in the same family as they often are interlinked. The exoskeleton must include adjustable parameters to allow for changes in orientation and user size. Depending on the defined kinematic model this will be used to align the exoskeleton DOFs to the relevant joint intercepts. As previ-

ously noted, the misalignment of exoskeleton joint axes with human joint axes is a common issue with exoskeletons. Tthe developed design should ensure the axis of rotation aligns with the natural rotation of the user, or ensure that any misalignment in the exoskeleton does not exert any unwanted forces onto the user. Safety features must be incorporated at a passive and software level. To build further on this the joint angles of the exoskeleton must use some form of sensor to determine its current position and velocity to provide feedback for software safety features.

When choosing the material for the exoskeleton, build variables to consider are strength, weight, rigidity, and accessibility [62]. The exoskeleton must be high strength and low weight, it must withstand the weight of the arm and any distal forces acting on it during shoulder movement. The material needs to be rigid enough to not cause excessive displacement of the exoskeleton joints when a load is applied. However, in some components, an amount of mechanical bending is desired to introduce an element of compliance into the system. This bending shall not be irregular, with the resulting displacement not causing unregulated changes in the natural motion of the exoskeleton. This flex should also be temporary, leaving no lasting deformation or damage to the exoskeleton.

Sensor units on the devices will be used to determine the ROM and velocity of the exoskeleton. The device will have two main functionalities; basic speed/position-controlled movement, and assist-as-need control to improve subject effort/participation. The former will use simple controllers, such as PID to measure the output of the actuator and exoskeleton, input will be adjusted based on this error. The latter will use EMG based actuation, this will use EMG to read the muscle activity and estimate the intended force based on the amplitude. Application methods and the testing set defined in Section 3.9 will be used to develop and implement this model.

Movement of the arm can be provided through either passive or active actuation, systems reviewed featured actuators such as springs, Bowden cables, DC motors, pistons etc. Considering the portability requirements of the system, the exoskeleton will be lightweight and therefore not require excessive force to move its own mass. As defined in Section 3.6, the maximum torque required to overcome the force of gravity on the actuated arm is 10.37Nm. However, literature showed that a maximum of 14.3Nm and 4.2Nm are required to complete basic ADLs. The torque specifications will be segmented into three brackets; Torques of 4.2Nm to 10.37Nm

will define the lower specified torque bracket, 10.37Nm to 14.3Nm define the middle bracket, and 14.2Nm and above define the upper bracket of acceptable torques. The chosen actuator shall be able to achieve these torques and transfer this to any actuated joints.

4 Mechanical/Kinematic Design

The design of the BITERS exoskeleton was intended to achieve all of the requirements defined in Section 3.15. The use of kinematic modeling, computer-aided design (CAD), simulation/analysis and investigation into material strengths and applied forces were required. The passive exoskeleton frame was designed first, which was based on human kinematic representations, and considered the future application of actuation. In addition to, and to reiterate some of the defined requirements, the passive mechanical model of the exoskeleton was designed to have the following general attributes:

- Able to achieve the desired ROM for all defined shoulder movements.
- Able to support by the subject's shoulders without constraining movement or causing fatigue.
- No transfer of unwanted force, generated by the subjects arm mass or distal forces, onto the user
- To interact with the patient only at the defined points, movement of the exoskeleton outside of these locations shall not intersect with the patient at any time.
- Abide by portability requirements defined in the requirements; including being small and lightweight (less than 5000g).
- Incorporate elements of compliance to avoid a fully rigid/constrained system.
- Feature adjustable parameters in links for user-exoskeleton alignment.

The active exoskeleton is based on the passive system, with added electrical/sensory components which enable actuation. The exoskeleton used DC motors and PI/P control to actuate the rotational DOFs by a bidirectional Bowden cable system. The active model was designed with the following objectives:

- Provide sufficient force to actuate the arm (4.2Nm to 10.37Nm).
- Reduce power/force losses between the actuator and actuation point.
- To not apply force to the user through misaligned intentional actuation force or unintentional actuation torque effects.
- Consider additional portability requirements, including power consumption and reliance on specialised software/connections.

The exoskeleton's mechanical design/build adopted an iterative development structure to attain optimal performance, this is formalised in Figure 4.0.1. This Section details the processes in the development of the BITERS exoskeleton.

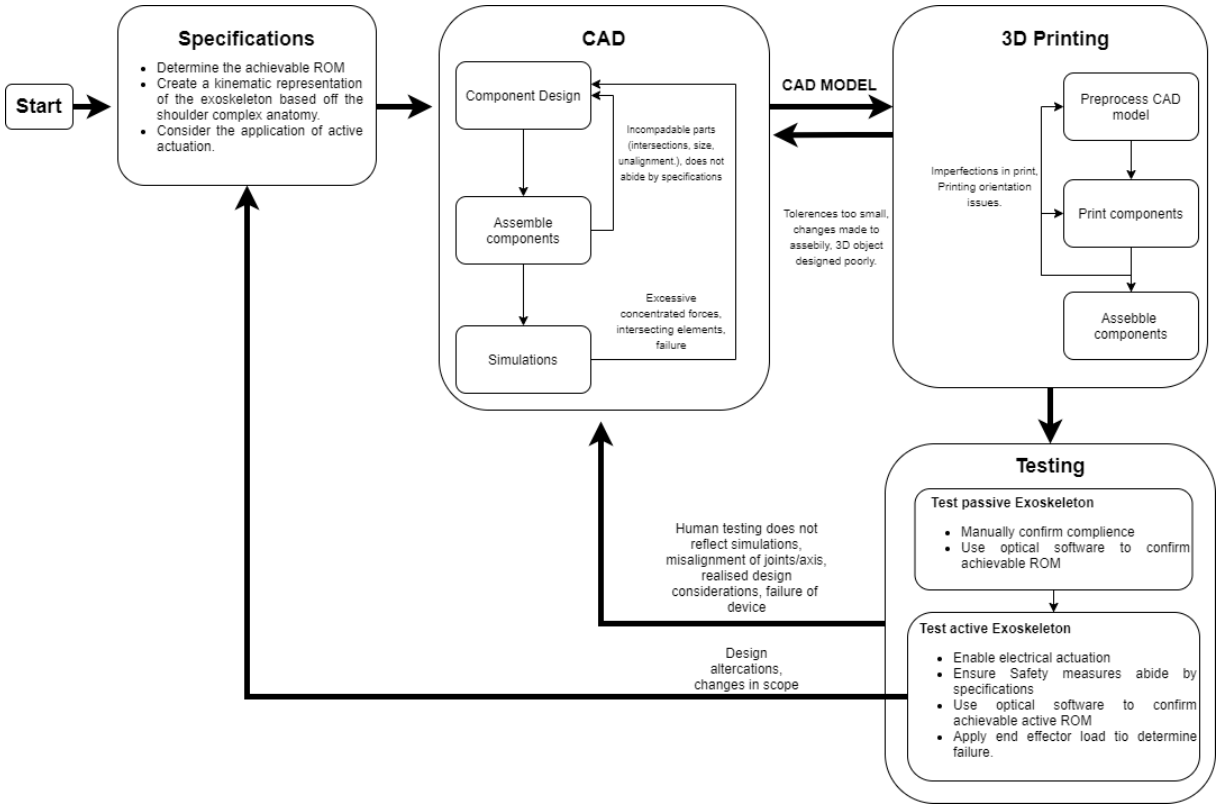

Figure 4.0.1: Iterative Development Management Structure

4.1 Design Overview

CAD software (SOLIDWORKS, 2018, Dassault Systems) was used to model the shoulder exoskeleton in an iterative approach, determining the parameter values for the links and mechanisms that result in a large ROM and adequate similarity to the human form. Links and joints were designed to fit around the human shoulder at all points in its ROM, which was the main design consideration for all components of the exoskeleton. Figure 4.1.1 and Figure 4.1.2 show the exoskeleton on an anatomical model in abduction and flexion respectively to demonstrate the linkage interactions in reference to the human body.

The kinematic model of the exoskeleton has been modelled as a 5-DOF open-loop chain, encompassing the centre of the torso out to the upper arm (Humerus), as further defined in Section 4.2. The sternoclavicular elevation/depression is modelled by a revolute DOF (joint 1) connected to the centre of the torso, this allows relative up/downwards movement of the GH joint from a distal rotational point. The acromioclavicular sliding movement is modelled by a prismatic DOF (joint 2). The GH joint allows the rotation of the humeral head and is approximated by three rotational joints (joints 3-5) which form a spherical assembly whose axes intercept with the centre of the humeral head. Joints 1 and 4 are both passive rotational DOFs. These joints use self-aligning bearings in series between links to allow free movement and support the bending moment. Joint 4 is the second joint in the GH assembly and allows movement of the other GH DOFs (within its limited range) and natural internal/external rotation. Joint 2 is realised by a linear sliding bearing with a 150mm range in series with a 40mm compression spring (6N/mm) to provide a restorative force. Joints 3 and 5 allow the actuated movements of abduction/adduction and flexion/extension, respectively. These joints have a similar bearing arrangement, with the bearings either side of the non-actuated linkage to limit unwanted bending motion in the joints. Bowden cables are used to transfer force from DC electric motors to the two active DOFs to allow a full range of actuated movement.

All load-bearing links were 3D printed with 50% infill PC (Polycarbonate) Blend. PC was chosen due to its high tensile strength, low weight, accessibility and its material elastic properties. These properties introduce an element of compliance into

the system. These links were manufactured with a 10mm thickness to ensure structural integrity and appropriate rigidity, while still allowing for a small amount of compliance. PLA was used for non-load bearing fixtures and was printed in the same manner. Consideration was given to the reinforcement of other components, with all rotational Bowden wheels and safety stops being reinforced with aluminium bolts. 12mm Acrylic Perspex was laser cut for the exoskeletons backplate, which was mounted on aluminium rods to increase the rigidity of the backplate and reduce limiting human interaction. Padded yoke straps with three self-tightening clips fit the exoskeleton to the users back. All parts were assembled in a CAD assembly for further optimisation. This ensured correct geometry within the system and was used for further simulation and modelling. Part mates were used to define the interactions of faces and parts to accurately imitate the physical barriers and attachments the exoskeleton will have.

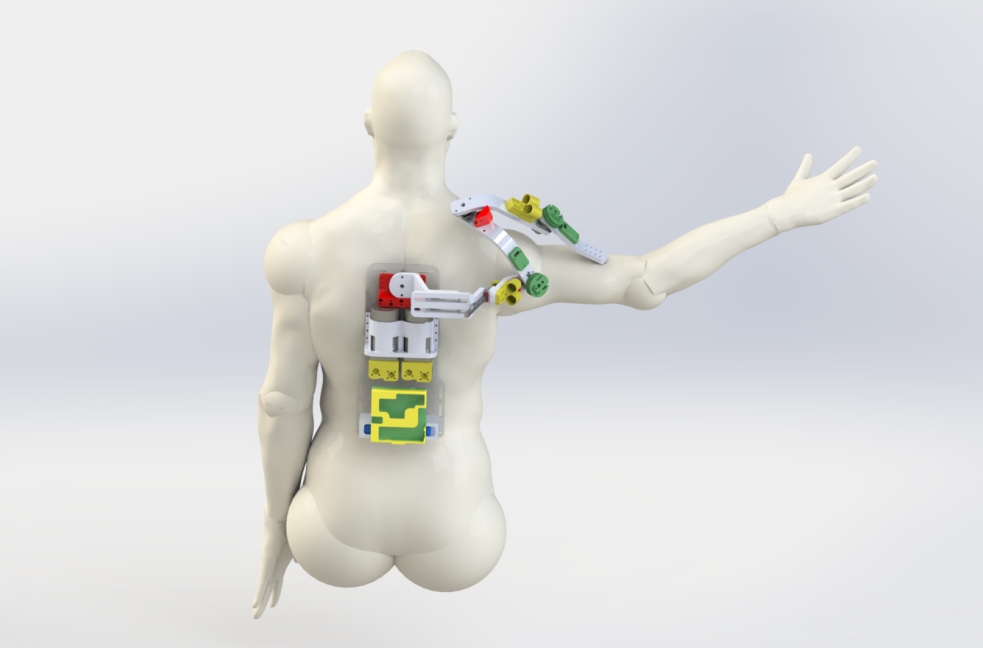

Figure 4.1.1: Anatomical model in abduction demonstrating exoskeleton interactions

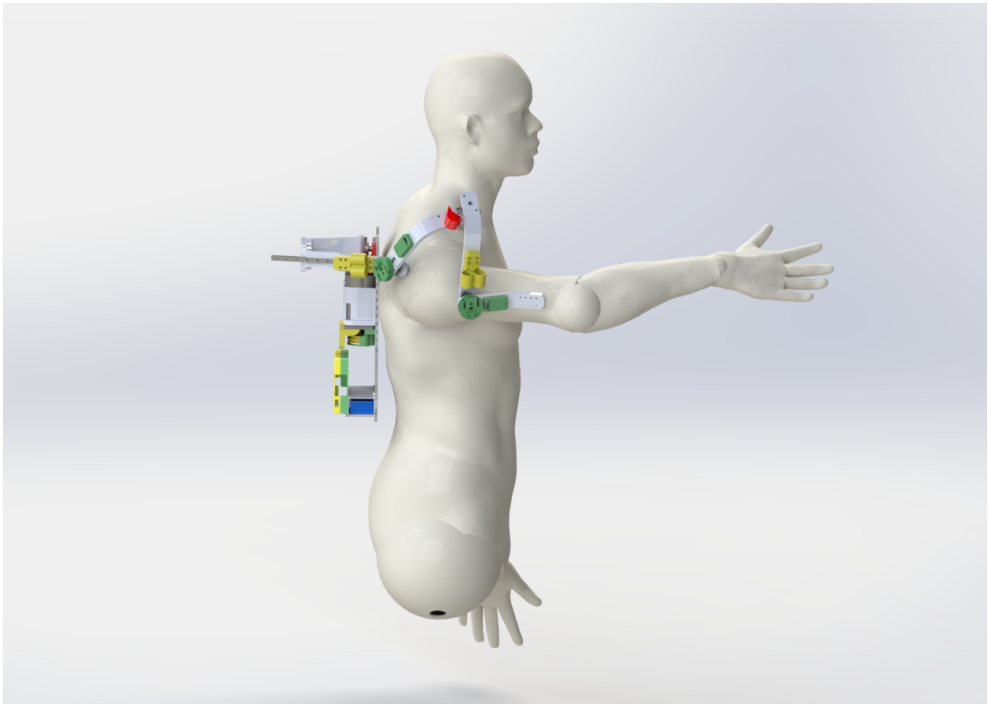

Figure 4.1.2: Anatomical model in flexion to demonstrating exoskeleton interactions

The model's static loading characteristics were validated by a finite element analysis (FEA) static simulation, to indicate stress points and quantify deformation. The kinematic analysis was performed using DH parameter modelling, and motion tracking workspace analysis, to determine the achievable ROM of the exoskeleton model.

4.2 Kinematic Design

It is important to differentiate between the kinematic model of the shoulder and the exoskeleton. The former acts to precisely model the skeletal/muscular elements (links, muscles, joints, discrete movements etc) of the body in terms of translations and rotations. The latter aims to simplify the shoulder's elements and discrete movements into key translations and rotations, whose links and DOFs will approximate the normal movement of the human subject with a full ROM. The kinematic compatibility between these two models is essential to the intricate motions of the shoulder complex and ensuring that normal motion is not restricted. Sufficient DOF must be given to the exoskeleton to allow the alignment of critical joints and motions, so functionality mimics that of the shoulder while not over-complicating the system.

The exoskeleton has been modelled kinematically as a series of links and joints encompassing the torso out to the upper arm (humerus), with movement defined at the joints between links. Findings in Section 3.5.1 and literature in Section 3.7 formed the basis of the kinematic model. The GH joint facilitates the rotation of the humeral head in the shoulder girdle, allowing a large upper-arm ROM. It is approximated by three rotational joints which form a spherical assembly where the points of intersection of the 3 axes of rotation is at the centre of the humerus head. For the inner DOFs, the acromioclavicular sliding movement is modelled by a prismatic DOF, while sternoclavicular elevation/depression is modelled by a rotational DOF connected to the centre of the torso, which allows relative up/downwards movement from a distal rotational point. A combination of these two DOFs should accommodate for any discrete shoulder complex movement outside of the defined scope in Section 3.5.1. Figure 4.2.1 shows the general proposed kinematic design of the exoskeleton (without consideration for actual link position).

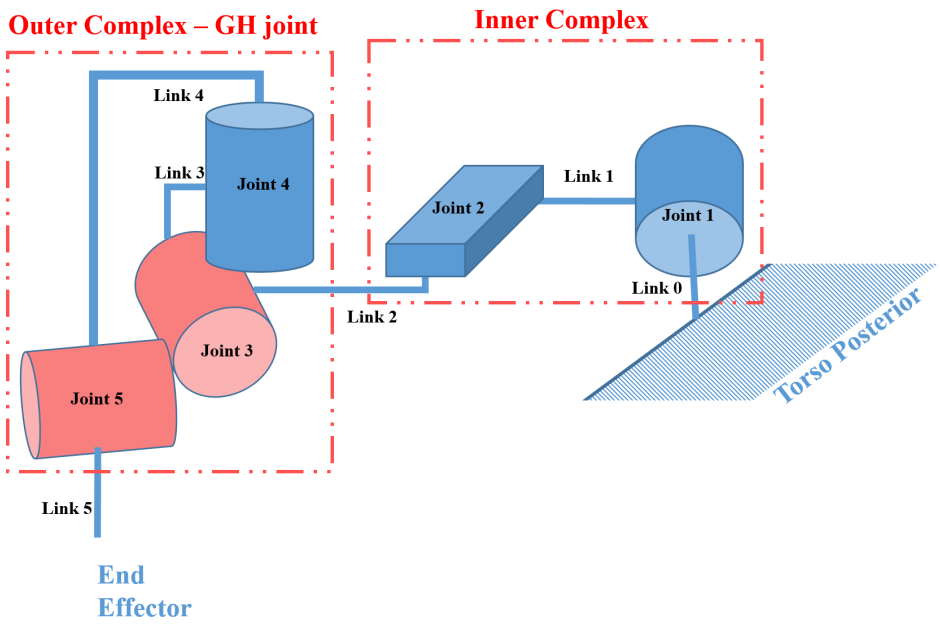

Figure 4.2.1: Generalised kinematic representation of the exoskeleton. Actuated joints are red, passive joints are blue.

The exoskeleton is separated into two sub-areas: the inner and outer complex. The inner complex consists of the rotational and prismatic joints 1-2. The rotational joint will be orientated on the centre of the back of the torso, rotating about an axis perpendicular to the coronal plane to allow further abduction movement beyond the achievable ROM of just the GH joint. Link 1, connecting joint 1 to the prismatic joint, will need to extend out the coronal plane to ensure there is no collision with the human body during scapula sliding movements. As specified in Section 3.5.1 the prismatic joint will angle inwards at 75° to approximate the posterior/anterior movement of the scapula sliding and translation of the GH joint.

The outer complex consists of the three rotational DOFs, with perpendicular intersecting joint axes to model the spherical GH joint. These joints shall all be connected in series from the prismatic joint. The human shoulder does not form a straight line from the centre of the torso outwards, therefore sufficient space is given to allow scapular movements in the posterior direction. The angle of the outer shoulder complex (scapula, AC, GH) must also be accommodated for, this is rounded around the shoulder girdle/GH joint.

The first rotational DOF in the GH model, joint 3, accommodates active shoulder adduction/abduction and angles inwards at a 35° from the horizontal. This angle not only accommodates the shape of the shoulder, but subsequent links in the serial chain will travel around this axis, angling them anteriorly away from the neck/head of the user. The second rotational DOF in the GH, joint 4, is passive and has a large ROM. By aligning this joint with the GH joint intercept and with the exoskeleton accommodating normal motion, this will automatically allow for free-moving internal/external rotation and facilitate the combined motion of the other DOFs. Link 3 needs to be long enough that it extends over the shoulder complex and provides sufficient space for shoulder elevation and other discrete muscle movements. To keep the workspace of the exoskeletons links away from the user, this may also be angled towards the GH joint from further back to allow for a shorter forward facing extension. Similarly, the fourth joint must be aligned with the GH joint centre, with the link between the fourth and fifth joint (link 4) extending enough to avoid collision with the outer of the shoulder/upper arm and angled to reduce the exoskeleton's outer workspace. Finally, the link from joint 5 to the end effector (contact point with the body) will be angled at 35° to decreases the space between the upper arm and the exoskeleton, while aligning with the angle of the human arm.

4.2.1 Applied kinematic Design

Modelling the relationships between the elements of the body, exoskeleton links, actuation loads and other forces and parameters is complex. Misalignment of the joints between the exoskeleton and wearer can cause discomfort or injury onto the user due to unwanted forces. It must be ensured that the kinematic model is functionally capable of enabling human motion. Therefore, it is important to further develop the concept so it accurately portrays the exoskeleton's true form so that it can then be modelled and simulated. The requirements of the DOFs and connecting links orientation/angle of trajectory defined in the Section 4.2 were applied to the model. The resulting modified kinematic model is shown in Figure 4.2.2, which includes the requirements of the developed exoskeleton links and joints to build on the generalised shoulder complex model.

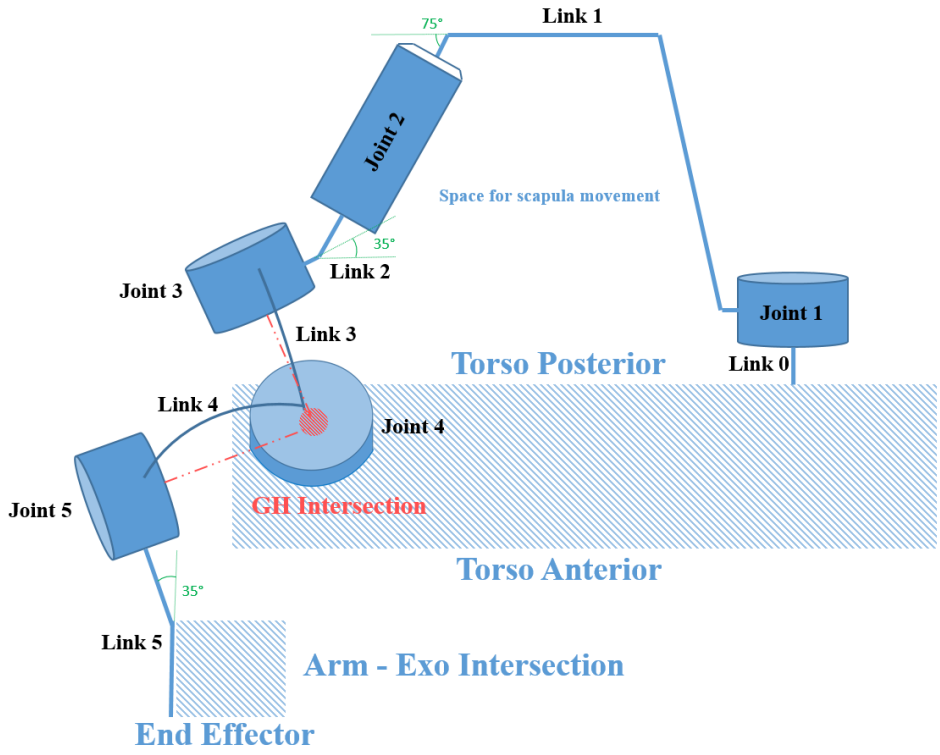

Figure 4.2.2: Accurate kinematic representation of the exoskeleton - top view

The axes of the rotational joints which make up the spherical model of the GH joint do not need to completely align with the GH intercept. A degree of tolerance is allowable due to the compliance in the structure. Similarly, for the prismatic joint, the approximate angle and direction of the scapula sliding movement is acceptable as the lack of a physical connection between the body-linear joint and compliance in the system will ensure safe directional movement (even if misaligned).

The length and angles of the curved links and the angles of joint axis were designed and tested in the physical design refinement phase. This phase aimed to reduce the size of the exoskeleton, and increasing the exoskeletons workspace while avoiding unintended physical contact between the links and the user. Features such as link thickness, width, angle, curvature and structure load-bearing properties were considered in this phase. Circular and curved structures were used due to their geometric rotational abilities, and to avoid self-collision during movement. The prismatic joint is a linear slider bearing set at 75° to the horizontal with a 40mm compression spring at the frontal end of link 2 to provide a restoring force. The rotational joints are

realised by pairs of self-aligning bearings. Similar to Soltani-Zarrin et al. CLEVER-arm exoskeleton, the end effector link is angled at 35° to align the exoskeleton motion with the users natural movement, reducing the area between the exoskeleton and the user at the end effector. Figure 4.2.3 shows the links and joints of the final design.

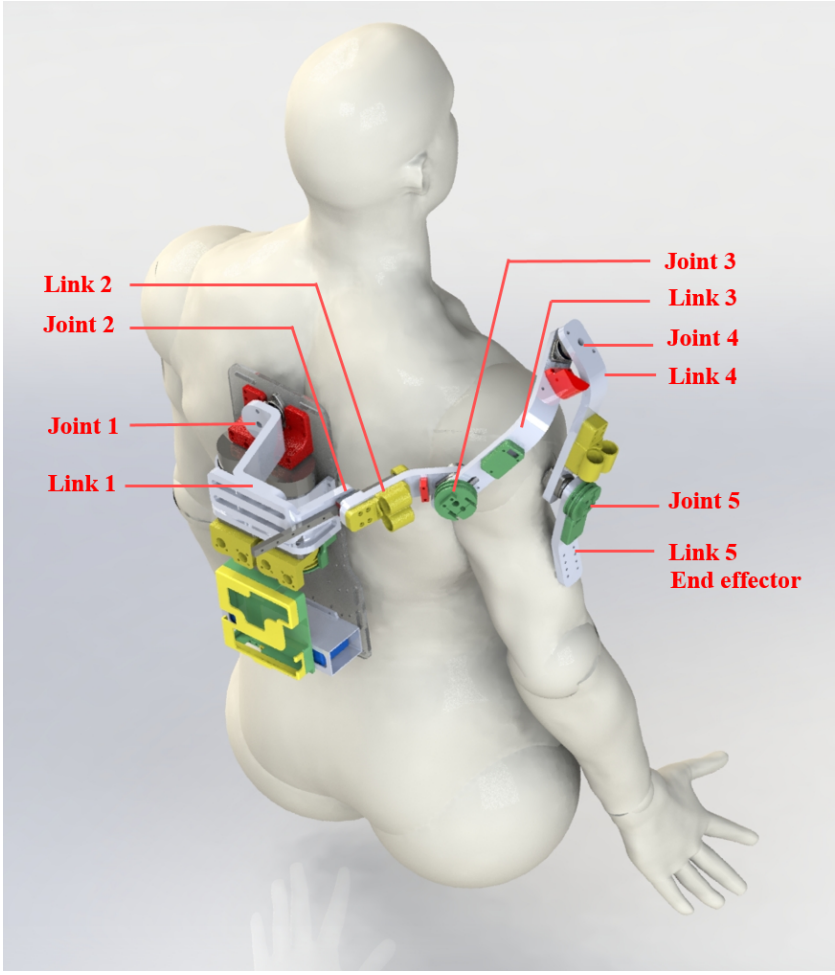

Figure 4.2.3: Annotated joints and links of the exoskeleton

4.2.2 DH Kinematic Parameters

The Denavit-Hartenberg (DH) convention is used to model the kinematic of the exoskeleton. The homogeneous transform of the link coordinate axes are represented by a set of four parameters. These parameters for the *ith* link are the link length (ai), the link twist (αi), the link offset (di) and the joint angle (θi). These parameters define the geometry of link i with respect to the previous link (link $i-1$) [46]. The kinematic model of the exoskeleton (Figure 4.2.2) is analysed to define the frame coordinate systems, the DH variables are defined through measurements on a CAD model. The purpose of deriving this system of transforms to conventionally derive the forward kinematics which can be used to determine a workable ROM of the exoskeletons end effector. This can then be compared to the real ROM achievable using visual tracking equipment. Ideally, these should be "identical", however discrepancies may occur due to un-modelled factors. These could include the discrete movements of the user's shoulder complex, compliance in the exoskeleton, mechanically constrained movement of the exoskeleton and anatomically constrained movement of the user.

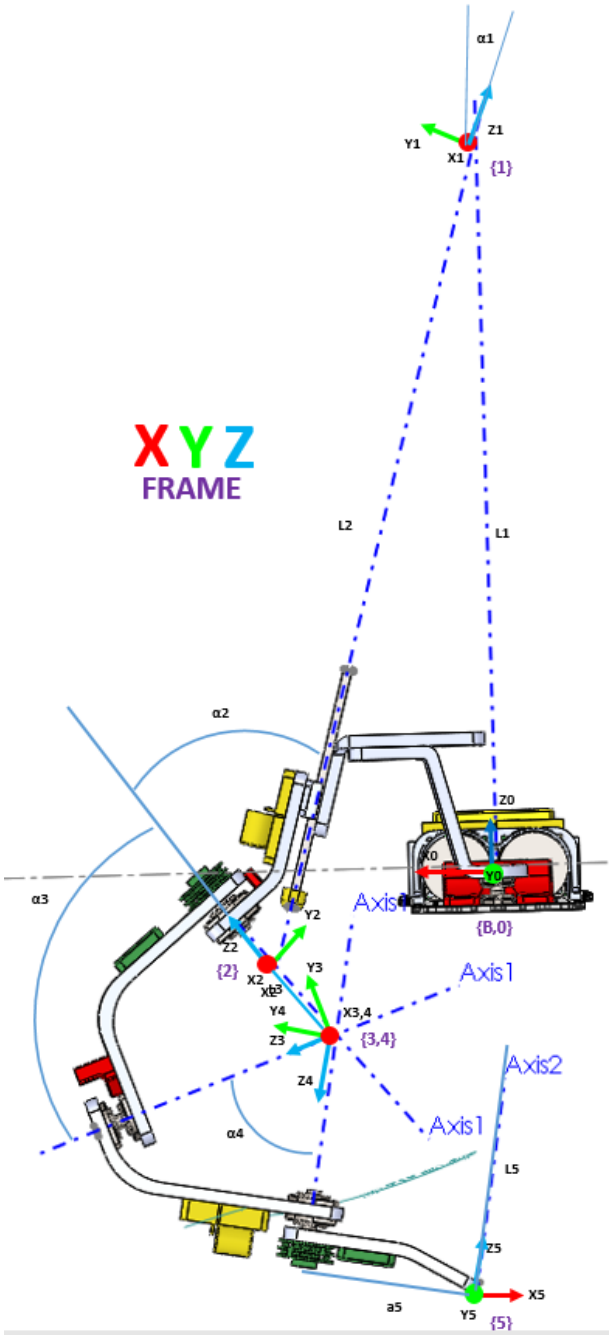

Figure 4.2.4: DH coordinate axes shown on exoskeleton model

Figure 4.2.4 shows the assignment of the frames of each link, following the DH convention for the exoskeleton. The model is positioned in the fully extended configuration. A base frame is at a fixed Y-axis displacement from frame {0} as that is where optical tracking markers were placed, as further discussed in Section 4.4.4. Other figures generated to represent the DH coordinate systems are shown in Appendix B.

The corresponding DH parameters for the proposed exoskeleton design are shown in Table 4.2.1. These parameters are defined as such; $\theta 1$ has a range of -40° to 0° and is the rotation at the first DOF. D2 has a range of 665mm to 765mm and is the displacement of the linear DOF (DOF 2) from the projected {2} frame. $\theta 3$ has a range of -90° to 0° and is the rotation of the third rotational DOF. $\theta 4$ has a range of 0°to 120° and is the free-moving DOF in the GH spherical joint (DOF 4). $\theta 5$ has a range of -65° to 154° and is the rotation at the final rotational joint (DOF 5).

Table 4.2.1: DH parameters

Link	$\theta(^\circ)$	d(mm)	a(mm)	$\alpha(^\circ)$
Base	0	85	0	0
1	$\theta 1 - 90$	$L1 = -577$	0	$\alpha 1 = 15$
2	180	$(L2 = 665)$-d2	0	$\alpha 2 = 55$
3	$\theta 3$	$L3 = 73$	0	$\alpha 3 = -70$
4	$\theta 4$	0	0	$\alpha 4 = -60$
5	$\theta 5 - 90$	$L5 = 195$	$a5 = 137$	180

4.3 Design Details

The realised form of the exoskeleton includes five joints (four rotational and one prismatic) and five connecting links. The joints facilitate movement in the axis of their respective DOFs. The links are the physical connection between each joint in sequence and define the absolute joint orientation/angle. Mechanical components to house the electrical components and Bowden transmission system are required to facilitate the active actuation of the exoskeleton. The positioning of the exoskeleton mechanical components are shown in Figure 4.3.1.

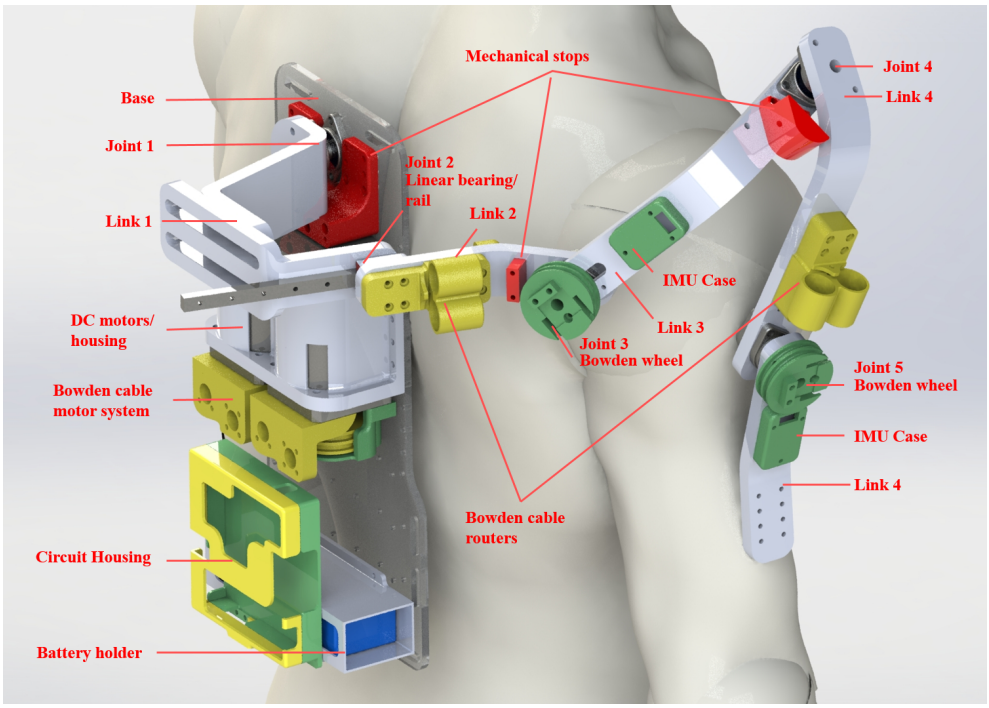

Figure 4.3.1: Exoskeleton components

4.3.1 Joints

Joints impose five constraints on a body moving in free-space. Leaving the realised joint with a single DOF. This DOF may be rotational (revolute joint) or translational (prismatic joint). Joints are the physical embodiment of the DOF's described in Section 4.2, facilitating rotational and linear movement. The joints may be passive to allow free movement, or active, using actuation to cause movement. Joints are found

between typically two links. Passive stops limit the achievable ROM of each joint.

Revolute Joints. The revolute joints use pairs of self-aligning bearings in one of two formations to connect the surrounding links and provide smooth, secured, rotation. KFL08 8mm shaft diameter flange bearings are used, constructed of Chrome Steel and Zinc Alloy. The components in the joint are held together by an 8mm aluminium bolt through the centre of the joint axis acting as a shaft, with a grub screw in the side of each bearing coupling it to the shaft. Active joints are comprised of a bearing either side of the non-actuated link of the joint (Figure 4.3.2). This reduces the possible angular displacement of the shaft by increasing the distance between the grub screws. The actuated linkage has unrestrained motion and moves with the inner cylinder of the bearings.

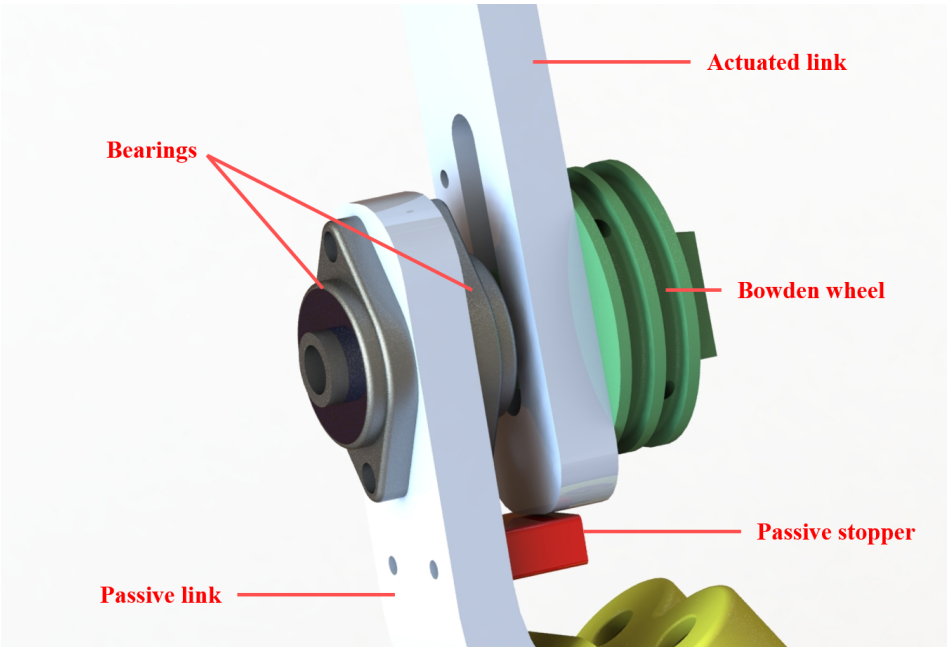

Figure 4.3.2: Rotational bearing configuration for actuated joints

The bearings are used in series between the links for passive rotational joints (Figure 4.3.3). This allows a small amount of angular displacement of the bolt as the grub screws are close together. The increased distance between links allows a small bending moment under load. This is done to increase compliance in the system by allowing discrete movements in joints/links which do not require exact alignment.

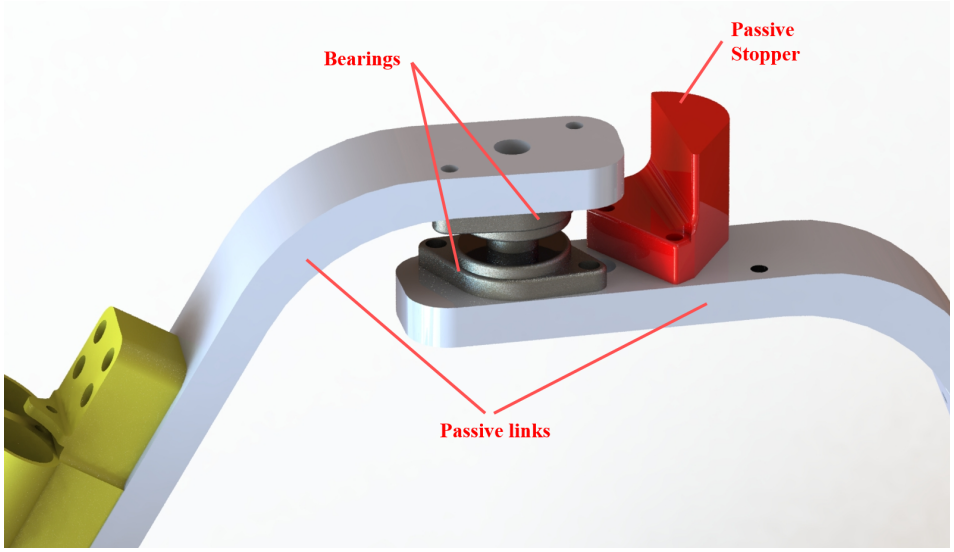

Figure 4.3.3: Rotational bearing configuration for passive joints

The bolt through the centre of each joint axis reinforces the component against torsional force applied by the bi-directional Bowden cables. A bolt displaced to the side of the joint centre locks movement along the adjustable axis of the actuated link. Circular washers were printed in PLA and fitted under the bearing housings to restrict movement in select joints.

Prismatic Joints. A compression spring is used in series with a linear slider to model the AC scapular sliding movement and SC retraction/protraction. A 150mm MGN15 steel alloy linear rail guide with a linear bearing is used for the prismatic joint. This also encourages correct shoulder positioning (an issue for subjects with shoulder subluxation) as it provides a restorative force directed towards the users posterior if the shoulder is slumped forward. The linear slider has movement limited to 100mm forward with a compressing 40mm spring at the base and 50mm backwards. The movement of the linear bearing can be constrained to avoid putting the shoulder out of the bodies achievable ROM, which may result in injury. The spring must provide enough restorative force to support the shoulder joint, therefore a spring with 6N/mm was selected, which equates to 240N over the length of the spring. Providing 240Nm of force, the spring can actuate approximately 24.5Kg of shoulder mass, which is sufficient. Figure 4.3.4 shows the spring position on the

linear rail, a rectangular PLA connector is used to distribute the linear roller bearings force evenly over the spring.

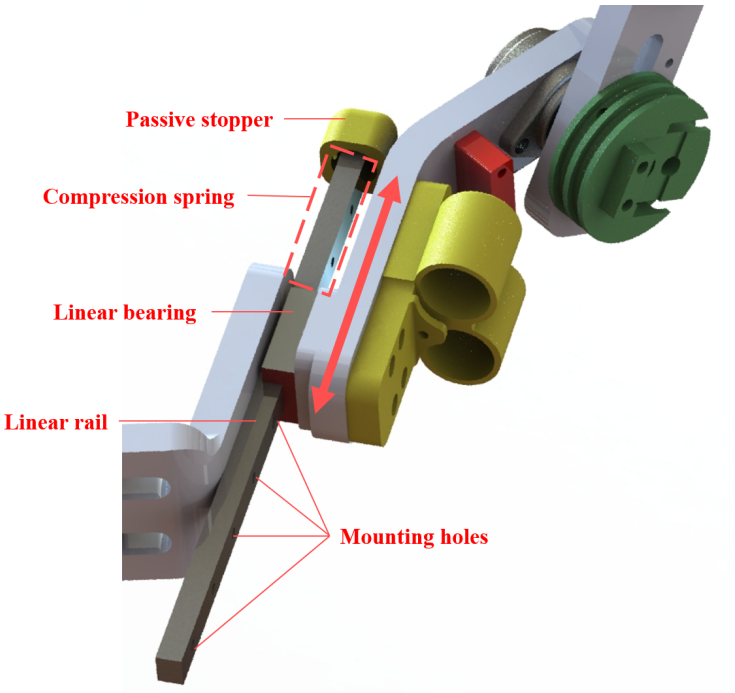

Figure 4.3.4: Prismatic joint design

4.3.2 Links

The links in the system connect each joint to facilitate the coordinated movement of the whole system. These are shaped to fit around the form of the upper limb without colliding with the patient's body at any undefined points in its reachable workspace. The joint angles and spacial tolerances defined in Section 4.2 are achieved through the varied modelled connecting links.

Material Properties. 3D printing was used to print exoskeleton links in PC because of its strength, low cost, accessibility, weight and manufacturing turn-around time. Links were printed with a Prusa MK3 3D printer. Prusament PC Blend was used for all load-bearing elements of the exoskeleton. PCs are a group of thermoplastic polymer materials, which are one of the strongest printable filaments. PC blend is a combination of PC, which, by itself, is not recommended for 3D printing as it has a

high thermal expansion and a tendency to crack and deform, and additives, which reduce cracking and distortion while still achieving the high strength characteristics of PC when printed. Section 3.12 details the material properties of PC and additive manufacturing techniques. PC blend has a Tensile Yield Strength of 58 MPa and a Tensile Modulus of 1.6-1.9 MPa dependant on orientation [80]. Even with additives, PC was difficult to print and produced defects such as deformation, heat warping and cracking. Various iterations of printing were required, with each print inspected for sub-optimal layers to ensure that no weaknesses or stress concentrations were developed. The bed heat (110°C) and nozzle heat (275°C) were important to define and keep constant to reduce the likelihood of imperfections in the print.

Printing orientation can have a large impact on a part's strength. Elements must be designed and printed with consideration of the direction and magnitude of forces which will be applied to them. Figure 4.3.5 shows forces applied normal and parallel to the layers, the overall strength of the part is much higher when the load is applied normal to the printing direction rather than parallel. The force is spread across the length of the piece. When applied to the parallel, the lack of continuous material paths and the stress concentration created by each layer joint, contribute to its weakness.

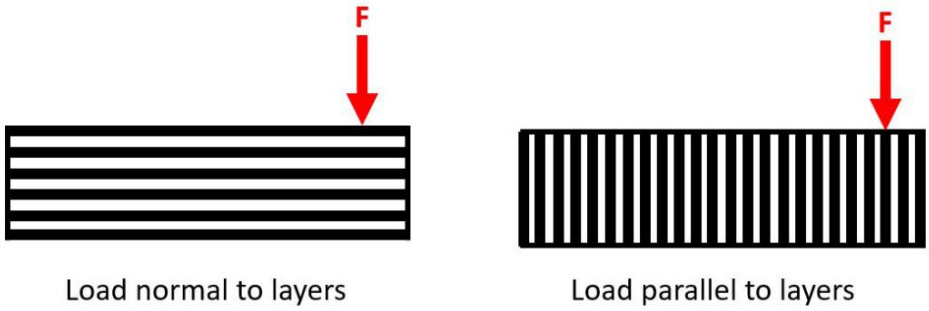

Figure 4.3.5: Example of load being applied normal and parallel to layers

The force applied normal to the print direction "principle" is applied to every link of the exoskeleton. When printed this way, PC has a degree of flexibility, creating a compliant system. Figure 4.3.6 shows the direction of printing for link 3, where the load acts normal to the layers as described above.

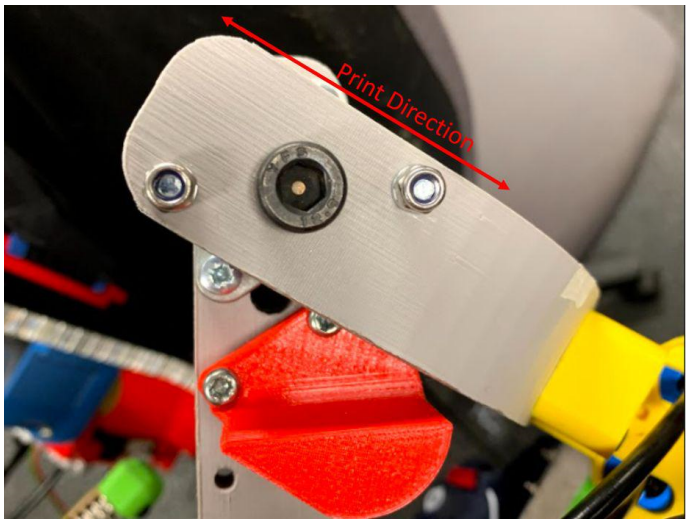

Figure 4.3.6: Direction of printing for exoskeleton link

To approximate the deflection of the links, the links are modelled as cantilever beams from the point of bending (from the vertical) to the joint where the force is applied. This can be calculated using Equation 4.3.1, which models the deflection of a cantilever beam with a load, P, acting on the end. This was derived by integrating the second-order differential equation of the bending moment equation [81]. The parameters for the equation are visualised in Figure 4.3.7.

$$\delta = PL^3/3EI \tag{4.3.1}$$

Where P is the magnitude of the force, L is the distance between the base and acting force, I is the second moment of inertia, and E is the Young's modulus of the beam. Link 3 has the largest distance between the vertical axis of a link and the load-bearing joint, giving an L of 90mm. The moment of area is derived from the length of the link and a cross-sectional width of 10mm. The Young's modulus for 3D printed PC is defined in Section 3.12 as 1890MPa. However, a reduced PC infill is used for the links (50%) so the Young's modulus is scaled to 950MPa as a conservative assumption. In the 3D printed links, the outer shell will resist the majority of the force, with the infill density having little effect. The applied force, P, was 30-60N to model reasonable maximum applied forces to the exoskeleton (as detailed and defined in Section 4.4.3). The resulting deflection was found to be 0.97mm to 1.94mm

at the end of the linkage for 30N-60N respectively. This deflection is acceptable as it abides by the requirements outlined in Section 3.15.

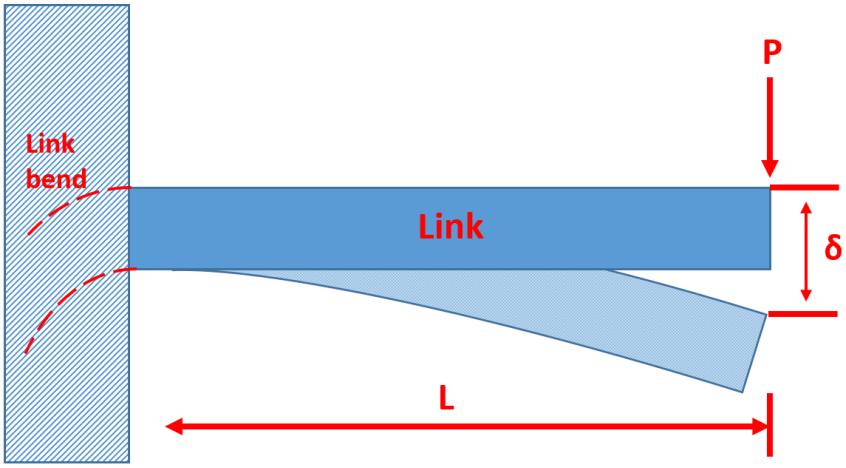

Figure 4.3.7: Exoskeleton link modelled as a cantilever beam

The bending property of the printed links is shown in Figure 4.3.8, where a force is applied normal to the joint. This compliance was anticipated, given the material properties of PC. This exceeds the calculated displacement. However, further static simulations showed similar displacement characteristics, as discussed in Section 4.4.3.

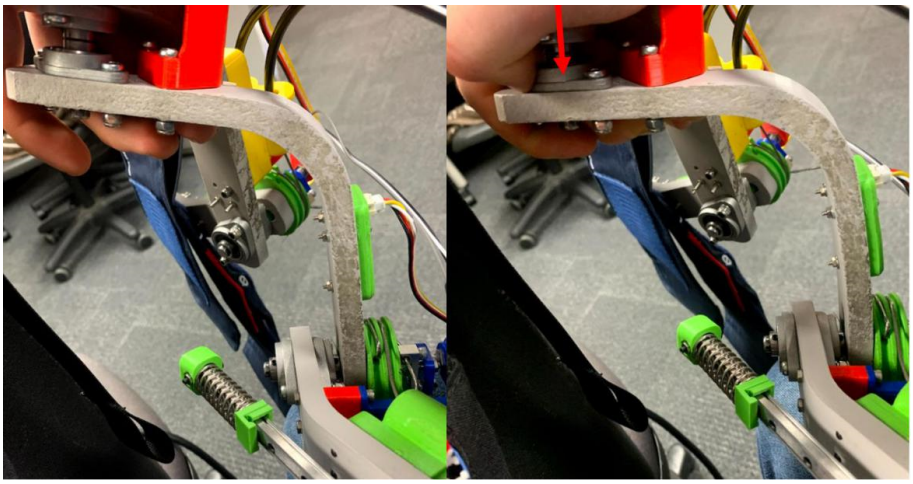

Figure 4.3.8: Complience in exoskeleton link resulting from applied force

Adaptability. The exoskeleton has been modelled to accommodate varied shoulder widths of users. Adjustable prismatic links have been included in the design to allow customisation of the exoskeletons physical dimensions to an individual user. The main adjustable parameter is the backslider (Figure 4.3.9), which consists of two links bolted together by 4 bolts, allowing for 100mm of adjustability laterally. Joint 1 can also rotate 180 to rest on the opposing side of the body for actuation of the other shoulder (with adjustments to the cable drive system).

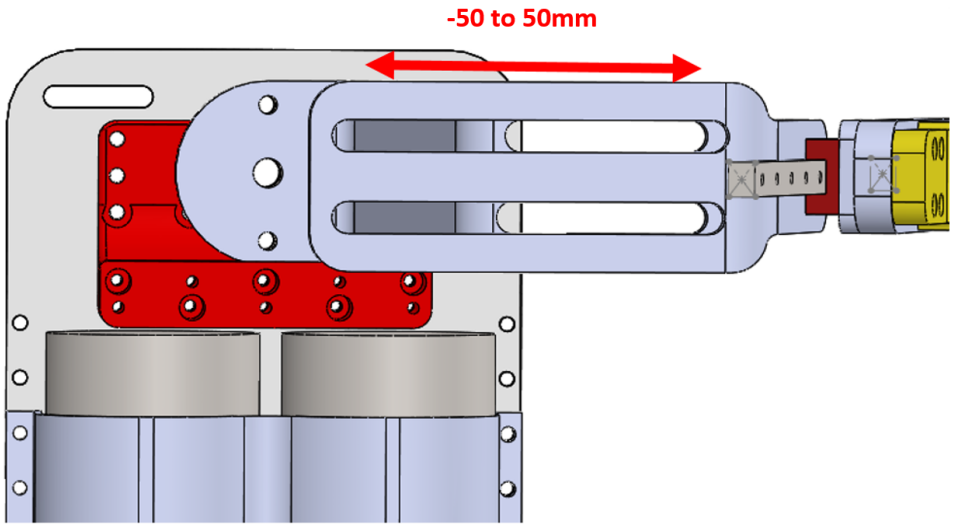

Figure 4.3.9: Adjustable horizontal exoskeleton links

Links connected to actuated joints are also adjustable, with a maximum continuous linear bearing movement of 150mm possible. This can be limited by a removable bolt at +- 15mm increments. In addition, the linear rail can be coupled further forward/backwards along the link it is attached to, providing an additional 100mm of adaptability. All rotational joints fit into a slot in their respective links, this allows for 30mm of adjustment for each DOF. Passive mechanical stops on the system also have multiple configurations which work to restrict or increase the ROM of each link. These mechanical stops have two/three different orientations, and various designs of stoppers have been developed with shapes to restrict movement outside of the links direct overlapping area.

4.3.3 Actuation

The desired applied torque, weight, size and control of the exoskeletons active system was considered when selecting actuation methods and components.Electric motors connected in series with Bowden cable transmission were chosen due to their high achievable torque, size and minimal backlash. Bowden cable systems decrease the inertia of the device, and allow soft actuation from distally positioned motors. A compression spring is used to provide restorative passive actuation of the shoulder.

DC Motors. The Rhino RMCS-2201 (Rhino Motion Control Solutions) integrates a high-torque DC 18000RPM base motor with a reduction gearbox (1000:1) for 10RPM output. It includes a 0.2° resolution quadrature optical encoder on its output shaft enabling position and speed control. The motor has a maximum holding torque of 11.77Nm [82], this is within the required torque range of 4.2Nm to 14.3Nm as specified in Section 3.15, with a tolerance given for power losses in the Bowden drive system. The Rhino motor is connected to the UART port of the embedded controller for UART control, the motor is powered from a 14.8V battery source.

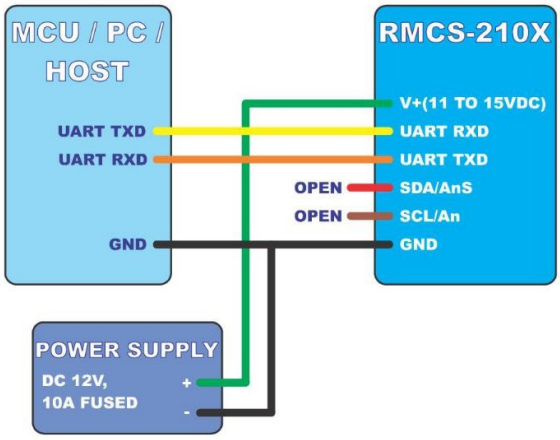

Figure 4.3.10: Rhino motor system control [82]

The Rhino motor has built-in user-adjustable PI control, based on the feedback from the optical encoder. The control allows smooth speed ramp up and down (using a damping variable), and reduces backlash and irregular movements.

Bowden Power Transfer. Bowden cables are used to transfer force from motors on the users back to the two actuated DOFs. The Bowden cable system is comprised of a single Bowden cable per actuated joint, the cable is fed through the Bowden wheel and wound in opposing directions. The cables are tracked around the circumference of the wheel, with surrounding ridges keeping it on track (and to avoid tangles) which keeps it out of the path of the other windings and locks the cable in a "U" shape. Using a single cable for each DOF reduces any slack (and therefore backlash) as it is a self-tightening system, allowing for smooth bi-directional movement. The Bowden wheel is mounted onto the shaft using a 5mm grub screw mounting hub, a cylindrical slot in the centre of the wheel allows the shaft to sit inside, providing reinforcement against tension force from the Bowden cables around the wheel edges (Figure 4.3.11). A 3D printed mount is made to house similar 5mm clamping hubs to fix the Bowden cable outers in place at the heights of their corresponding rails. An opposing mounted cable restrictor fits around the wheel (with a circular extrusion around the inner circumference of the components) restricting Bowden cables to their rails in the case of unwinding/looseness. The orientation of these components can be seen in Figure 4.3.12.

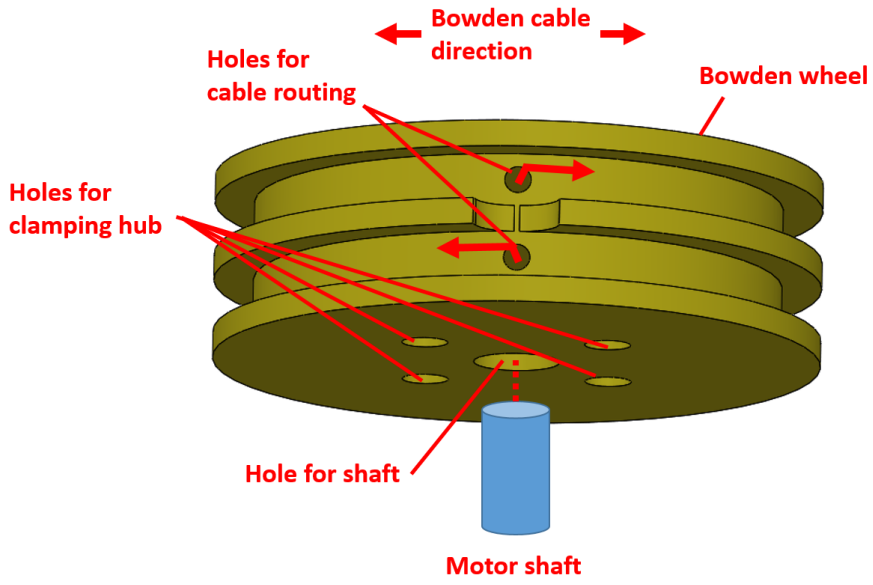

Figure 4.3.11: Bowden cable direction of movement on motor wheel

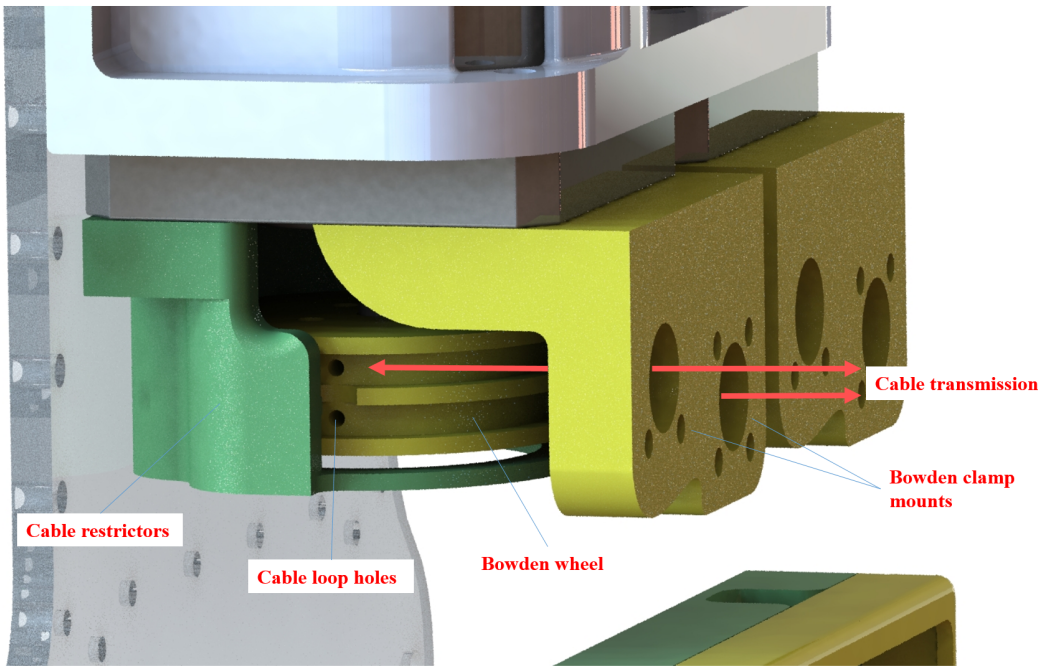

Figure 4.3.12: Bowden cable system 3D printed wheels/components

Friction between the cable and cable outer is generated when the bending angle of the cable transmission changes with the relative position of the actuation/joints. This bending depends on the length and curvature of the cable. Long cables were used so the cables could be routed to avoid angular bends and pulling tension, and therefore reducing friction. Adequate length was also allocated to accommodate the translation and rotation of the actuated joints in space.

Termination of the Bowden cable is essential to provide continuous tension in the system and avoiding slip. A Bowden reel was 3D printed in PLA to terminate the Bowden wire at each of the two activate joints (Figure 4.3.13). The Bowden cable is wound twice around the wheel (to allow significantly more ROM than required) and then fed through a cylindrical hole through the wheel. Slots on the other side of the hole allow the cable to be wrapped around the plastic body, then screw terminated by an aluminium element. The clamping force provided by the screw and the holding force of the wires restrained form, terminates the wire successfully while also enabling it to be tensioned, adjusted and replaced if need be.

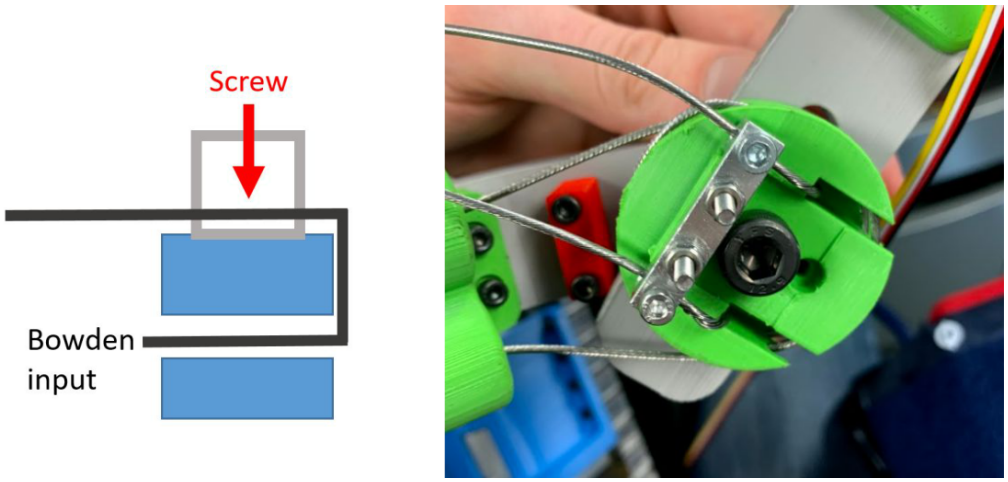

Figure 4.3.13: Bowden cable termination design

4.3.4 User Interface

12mm Acrylic Perspex was laser cut for the exoskeletons back/mounting plate, this thickness was determined by iterative testing. Perspex plates of lesser thicknesses resulted in bending from the overall weight of exoskeleton and actuator torque. Perpendicular force on the bolts which mount the joint 1 stopper, caused cracking across the bolt holes. Because of this, fewer holes were cut and the bolts were embedded internally in the stopper to lessen the moment of the force, holes through the entire structure alternated with the embedded bolts were included to reinforce the PLA structure. The large thickness of the mounting plate adds significant weight to the overall exoskeleton. However, the plate acts as a fixed rigid body on the back, protecting the user from applied loads. Two aluminium square rods were fixed either side of the backplate to prevent bolt heads causing pain to the user and to lessen the interference area between the exoskeleton and patient (as this will restrict motion). Padded Yoke straps were fixed either side with PLA printed contacts as seen in Figure 4.3.14. PLA filament was used to print the non-load-bearing parts, this is more rigid and brittle than PC, but is less expensive, faster and easier to print. These are fitted with padded shoulder protection, adjustable straps and front and side adjustable clips.

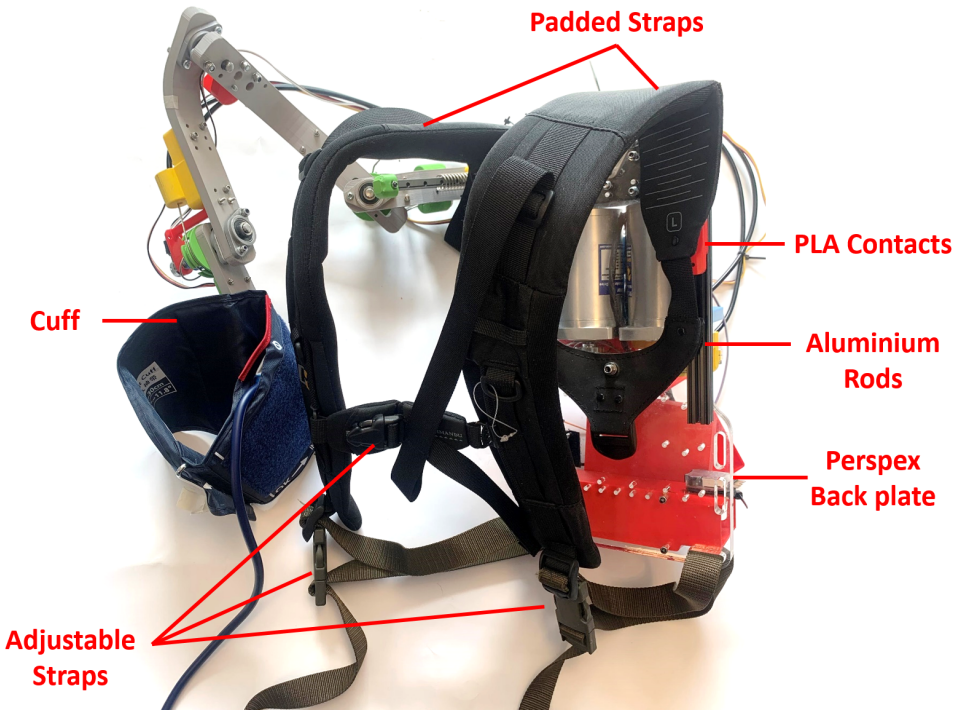

Figure 4.3.14: Exoskeleton mounting equipment

A pneumatic cuff attaches the end effector to the user's arm. Plain velcro was used for earlier prototypes but did not provide an adequate balance of compliance and stiffness required. The cuff is designed to be easily fitted by the user. Also, its large contact and longitudinal stiffness reduces slip of the end effector.

Figure 4.3.15: Pneumatic cuff

4.4 Validation

4.4.1 DOF verification

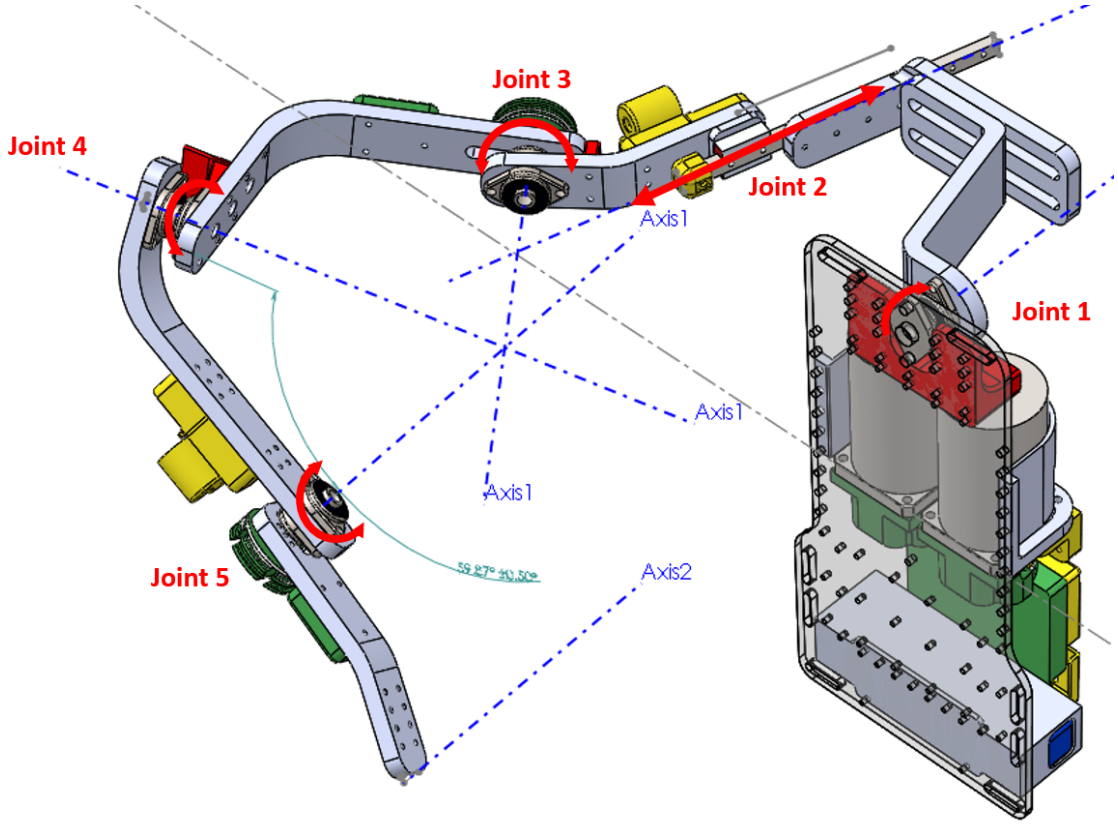

Figure 4.4.1: CAD model of exoskeleton with all joints and axes illustrated

To verify that the assembled CAD model of the exoskeleton contains the required DOFs that reflect the kinematic requirements, a SOLIDWORKS motion study was completed. SOLIDWORKS motion studies are graphical simulations of motion for parts and assembly models, which can simulate the effects of gravitational and other forces to determine the resulting motion of the model. The quantity of restrained and unrestrained DOFs can be determined through this process. [83]

An unconstrained part in space has three axes (X,Y,Z) with one translational and one rotational DOF per axis, for a total of 6-DOF. Within the motion studies tool, the number of DOFs can be determined by comparing the total DOFs in the system and

removing the unrestrained or redundant DOFs. A motion study was completed on the CAD model of the exoskeleton, results of this study are shown in Table 4.4.1. As expected, five unrestrained DOFs were present in the model, which reflects the expected number of linear/rotational DOFs in the kinematic model. Thus, the CAD model has 5-DOF, as specified by the design requirements. However, a workspace analysis is necessary to ensure that these DOFs allow the required ROM.

Table 4.4.1: Simulated DOFS: Gruebler Count

Gruebler Count (approximate DOF)	DOF
41 moving parts	246
61 cylindrical joint(s)	-244
51 planar joint(s)	-153
4 parallel primitive(s)	-8
9 generalized constraint(s)	-9
Total number of redundant constraints	173
Total (actual) DOF	5

4.4.2 Exoskeleton Workspace

The Matlab Robotics Toolbox (Peter Corke, version 10.4) was used to define the translations/rotations to the end effector using the DH parameters from Section 4.2.2. A total of 60000 random configurations from within the possible variable parameters were generated to give the XYZ coordinates of the end effector position in reference to the rigid body base. The convex hull of the workspace is obtained from these configurations. This hull indicates the maximum theoretical unrestrained ROM of the exoskeleton. The modelled exoskeleton workspace hull has been imposed on an anatomical model for reference, as can be seen in Figure 4.4.2. Axes have been left on the workspace so they may be directly comparable to further imagery.

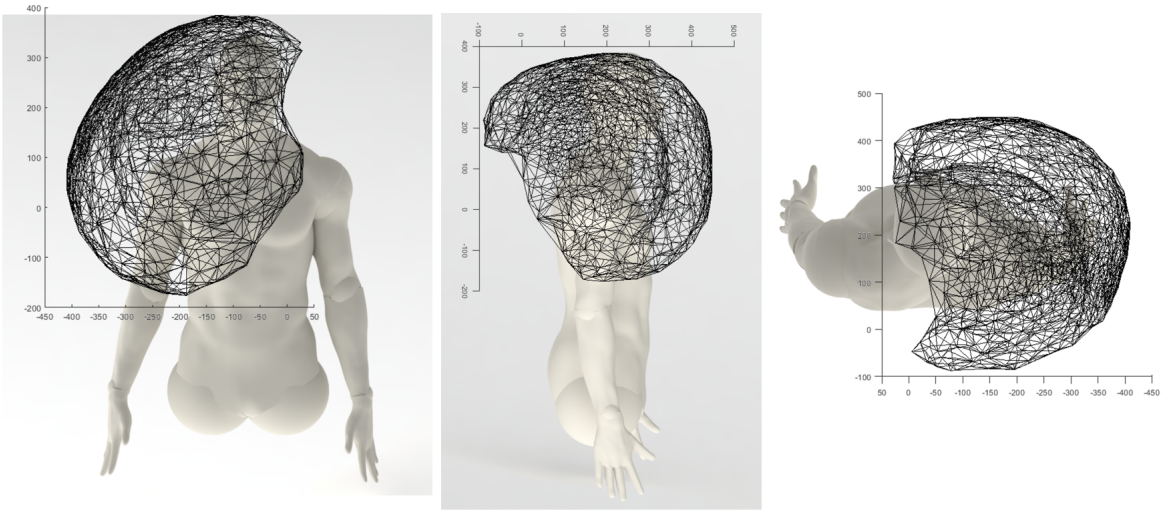

Figure 4.4.2: Measured exoskeleton workspace imposed on anatomical model. Left-front view, middle-side view, right-top view

Figure 4.4.3 and Figure 4.4.4 show the front and side view of the exoskeleton workspace respectively. The workspace shows a cavity around the shoulders joint, and a clear spherical workspace which indicates that it was a large, natural ROM. This is further analysed and compared to the actual ROM achieved by the exoskeleton using optical tracking hardware.

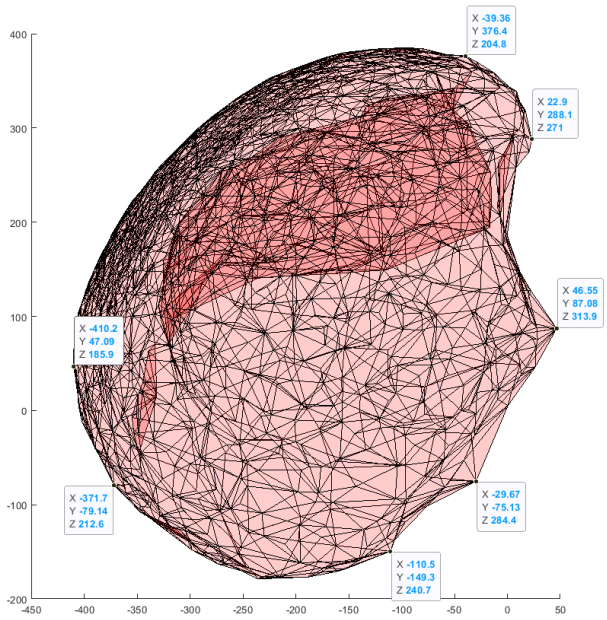

Figure 4.4.3: Modelled exoskeleton workspace - frontal view

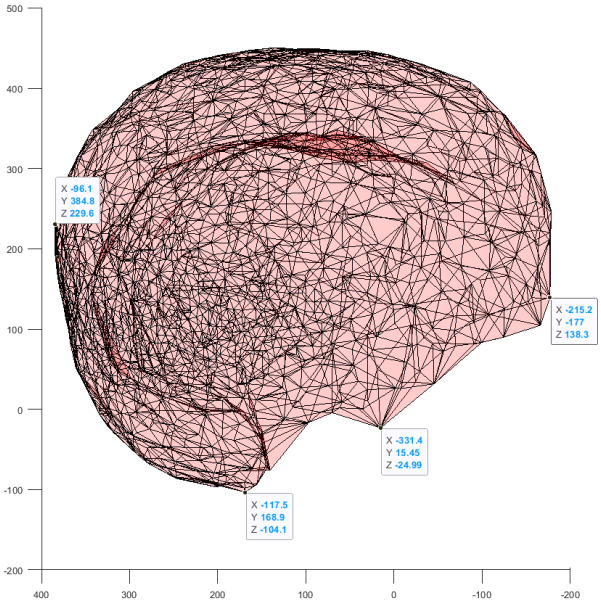

Figure 4.4.4: Modelled exoskeleton workspace workspace top view

Analysis of the workspace shows that it measures 448mm in the x-axis, 577mm in the y-axis and 541mm in the Z direction. The volume of the exoskeleton workspace is $0.0358m^3$, with an approximate absolute-cubed outer volume of $0.14m^3$. This satisfies the maximum workspace requirement of $0.5m^3$, as outlined in Section 3.15. Figures of the 3D workspace can be seen in Appendix C.

4.4.3 Deformation/Stress Analysis

A finite element analysis (FEA) static simulation (SOLIDWORKS Simulation, 2018) was done to indicate stress points and to quantify deformation of the exoskeleton model. A varied sized curvature-based mixed mesh was applied to the model, for parts with fine features/contours and a coarse mesh for larger links. The meshes characteristics are as follows; maximum element size of 33.46mm, minimum element size of 6.69mm, four Jacobin points defined and a total node count of 185989 nodes. The base-plate was fixed and made rigid to constrain movement in the simulation. Parts were modelled with correct material properties, with the auto-adjusting bearings modelled as rigid and the links as defined in Section 3.12. A force was applied to the end effector and opposing torques onto each Bowden wheel as seen in Figure 4.4.5 to get an understanding of the system's behaviour under load.

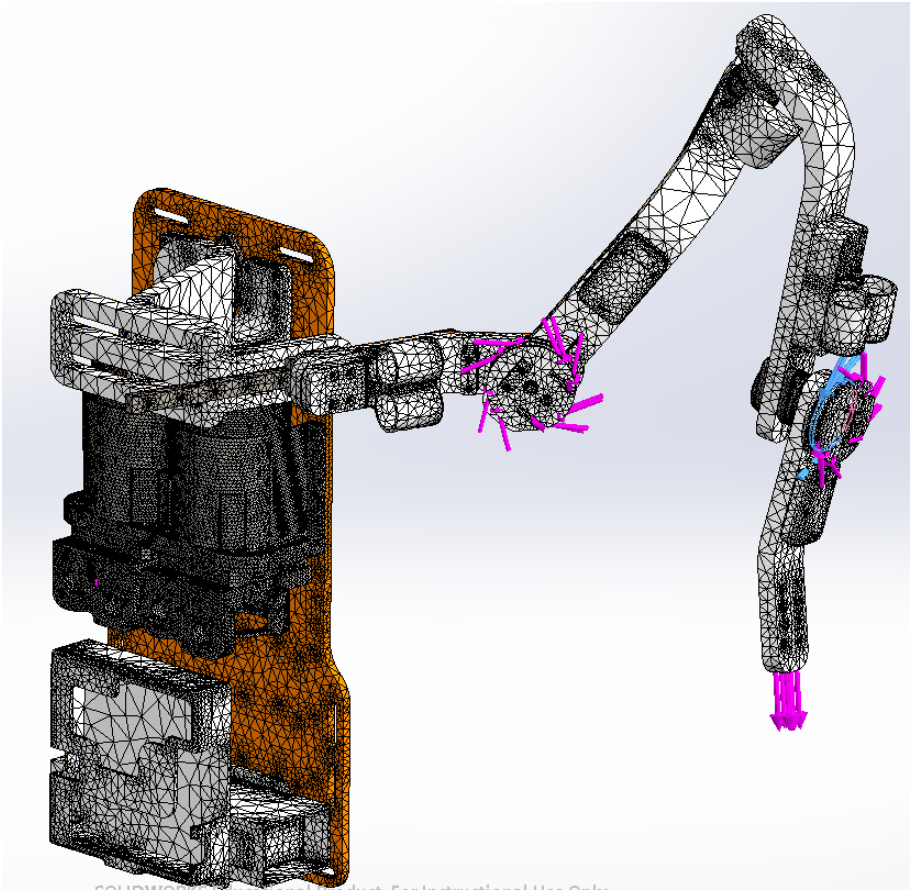

Figure 4.4.5: Applied mesh to CAD model of exoskeleton

The simulation showed clear deformation around the Bowden wheels, with concentrated force also acting in the link slots where the link and Bowden wheel connects. Figure 4.4.6 shows an indication of the resulting stress. Deformation in the links can also be seen. However, a certain degree of compliance is a required specification of the exoskeleton so this flex in the links could be used as a safety feature, this will be constrained but not eliminated by selecting materials which allow for these characteristics. The Bowden wheel will be reinforced with an 8mm bolt through to minimise deformation.

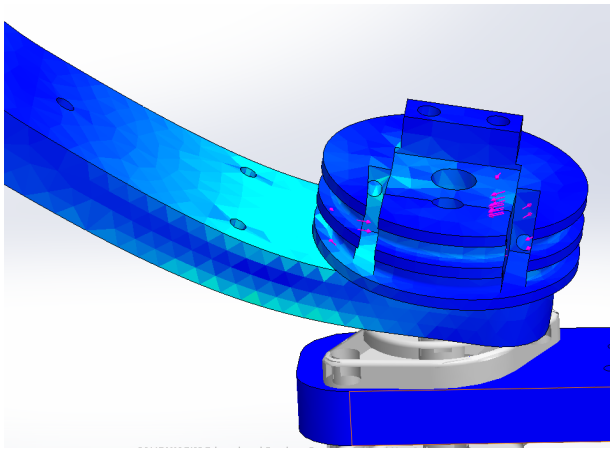

Figure 4.4.6: Stress at Bowden wheel from applied torque. Lighter hues represent higher amounts of stress.

Another key feature is the stress concentration on the linear bearing rail (Figure 4.4.7). As the exoskeleton modelled is a series chain, all forces distal from joint 2, due to weight of the exoskeleton and applied load, will be applied onto the linear bearing. A rigid high tensile strength material for the rail and a large surfaced bearing is essential to the structural integrity of the exoskeleton.

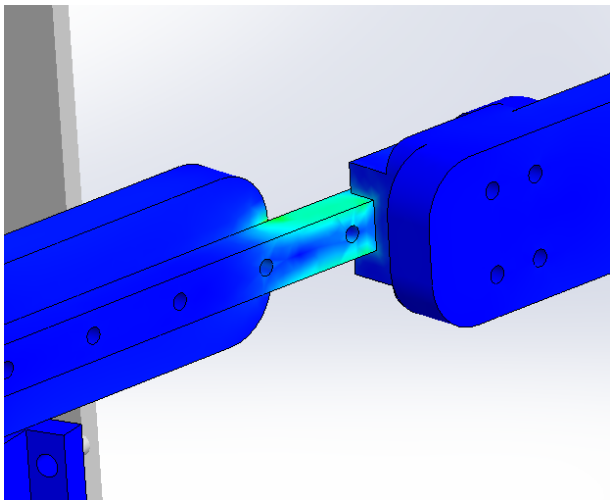

Figure 4.4.7: Stress at linear rail from the acting force. Lighter hues represent higher amounts of stress.

A model of the applied load forces was simulated for a static simulation displacement test. With the moment of the arm approximately 30mm from the revolute joint, and with a realistic torque of 9Nm-20Nm at the actuated joints. The applied force can be assumed to be 30N-60N, using the moment of force Equation 4.4.1. *Ures* is the magnitude of the resulting displacement vector as shown in Equation 4.4.2.

$$T = F * x \tag{4.4.1}$$

$$Ures = \sqrt{(Ux^2 + Uy^2 + Uz^2)} \tag{4.4.2}$$

A distal force of both 30N and 60N was applied to the end effector of the model in the direction of gravity, with displacement measured from the resting position as shown in Figure 4.4.8 and Figure 4.4.9 for applied forces of 30N and 60N respectively.

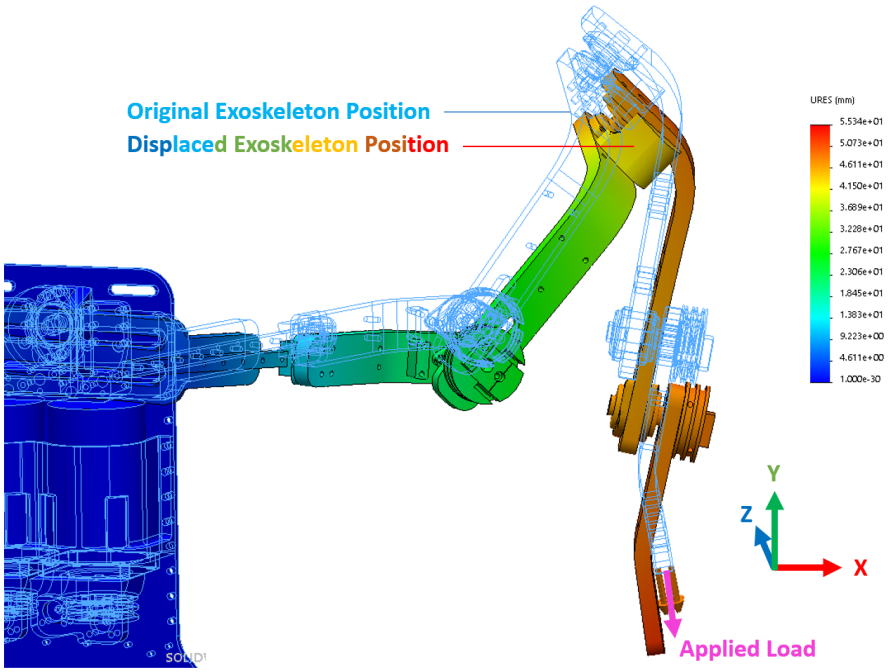

Figure 4.4.8: Displacement graphic for 30N applied load

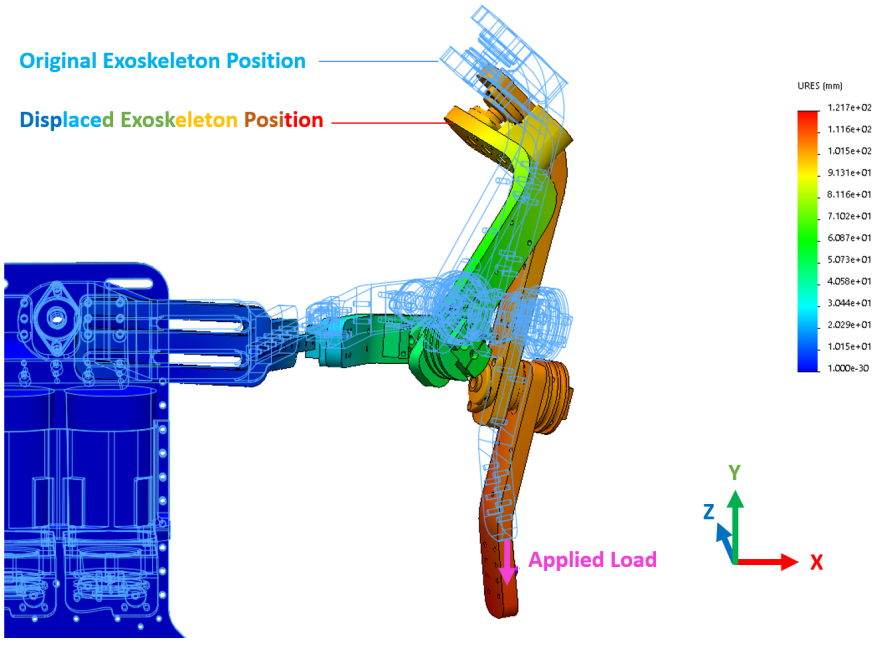

Figure 4.4.9: Displacement graphic for 60N applied load. The surface of the objects are displayed as a gradient of colours, with each hue representing a specific degree of deflection of *Ures*.

A higher load equates to a larger displacement, as expected. The end effector experiences the highest displacement of all links in the design, with 55.3mm of displacement for a 30N applied load and 121mm for a 60N applied load. These displacements were mostly experienced in the downwards y-axis. There is also a forward twisting torque which is significant in the distal rotational DOFs, reducing as the load moves towards the central point. Displacement is plotted for points at the end effector, all joint centre axes, and along the linear rail/inner shoulder complex for applied forces of 30N and 60N in Figure 4.4.10. The physical positioning of the nodes are provided in Appendices D.

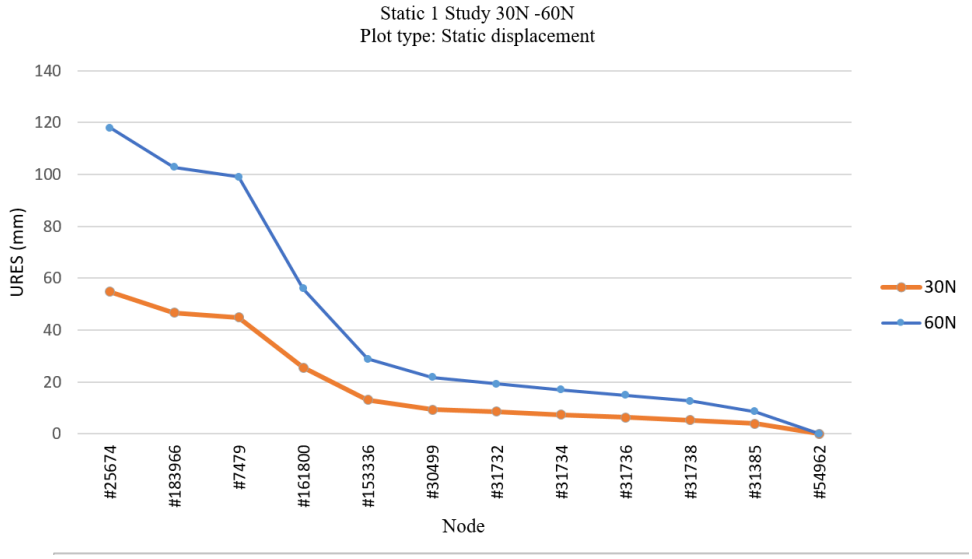

Figure 4.4.10: *Ures* Displacement for 30N and 60N applied load

The trend-lines of these show that the force to displacement at a singular point along the exoskeleton theoretically has a linear relationship. The trend-lines of the displacements are the same shape and the displacement for 30N force is approximately half that of 60N. Displacement decreased laterally from the actuated end effector to the centre rotational DOF. The assumption can then be made that any bending in the system accumulates. Changes in properties of the inner joints and links will therefore have a larger effect on the displacement of the end effector.

4.4.4 Range of Motion Analysis

The ROM of each joint was verified individually. However, it is important to ensure that all joints working together provide the necessary 3D ROM of a human arm. Further data on the achieved 3D workspace is necessary to determine the performance of the exoskeleton against the workspaces of the kinematic model. This was verified using a motion tracking system (OptiTrack).

Reflective 14mm spherical markers were used to track individual points on the exoskeleton, and 19mm diameter markers were used for the rigid body reference point. 12 cameras were used to give a wide coverage so the full motion of the exoskeleton was captured, the system was calibrated to 0.1mm accuracy. Considerations during testing included:

- Ensuring that the camera field of view overlaps for a large area (capture volume).
- Non-reflective tape was used to cover reflective materials/metals on the exoskeleton, to prevent/reduce unintentional spurious returns.
- Markers were placed to avoid overlap and occlusion by placing them apart and on varied levelled stands.

Three reflectors were placed on each segment of the exoskeleton for passive testing, and three reflectors were placed on the "base" of the device to define the exoskeletons coordinate system using a rigid body for reference. One reflective marker was placed on the axis of each joint, and three markers for the base. Figure 4.4.11 shows the position of the reflective markers for active exoskeleton testing, the base rigid body can be seen at the centre of the exoskeleton. A reflector was also placed on the end effector to define the achievable motion in its entire range.

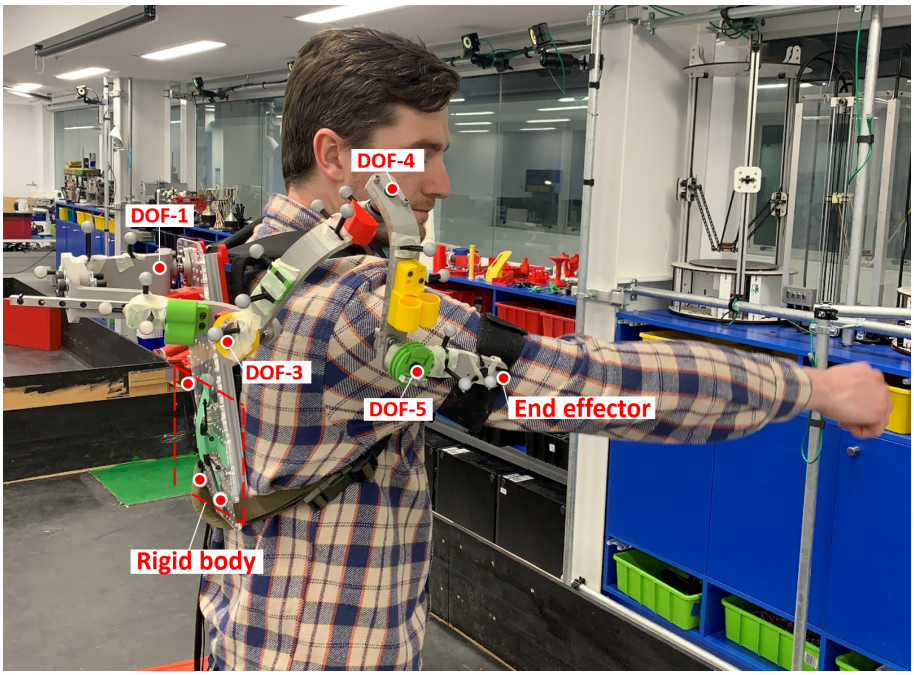

Figure 4.4.11: Marker system locations for motion tracking using OptiTrack

This study was approved by the Human Ethics Committee at the University of Canterbury (HEC 2020/75). This application covers the use of the passive exoskeleton, applied actuation and motion tracking of the upper-limb/shoulder complex.

Testing was completed sitting down with the markers as defined above, the position of the cameras can be seen to scale in Figure 4.4.12. ROM testing was conducted by recording datasets where the exoskeleton reached the full extent of its ROM during continuous exercises. Electrical actuation achieved its capable ROM, assisted by manual actuation (facilitated by the first rotational DOF in the kinematic chain) so the exoskeleton can reach above its actuated range.

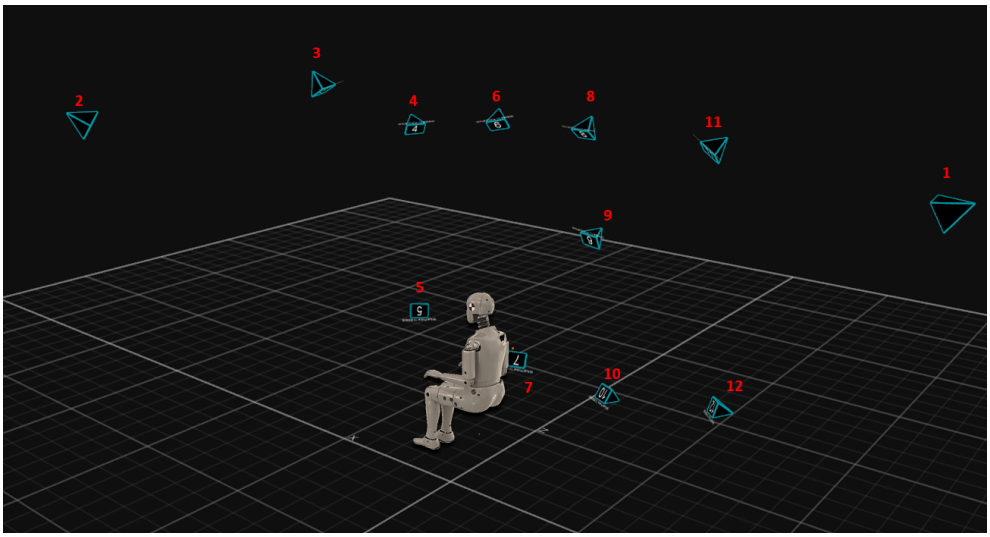

Figure 4.4.12: OptiTrack camera positioning

A cloud of 3D points is produced that represents the position of the reflective markers in 3D space. Captured at 250Hz, the label data is smoothed with a cutoff frequency of 6Hz and repaired with cubic interpolation. This process was implemented for all data in the dataset. By tracking the position of the end effector and the rigid bodies, the orientation of the end effector could be determined with respect to the body frame. Processing was performed with rigid bodies represented by quaternions to facilitate interpolation and filtering using spherical linear interpolation. The end effector position with reference to the rigid body is plotted and formed into a convex hull, the resulting outer curved hull can be seen in Figure 4.4.13. The hull is a map of the real achievable workspace of the exoskeletons end effector.

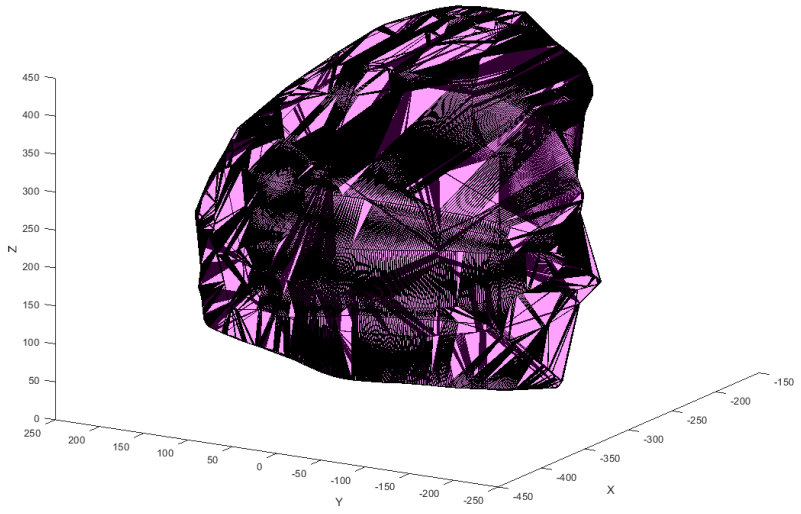

Figure 4.4.13: Tracked exoskeleton motion workspace convex hull

The measured exoskeleton workspace hull has been imposed on an anatomical model for reference, as can be seen in Figure 4.4.14. The axes have been left on the workspace for comparison to further imagery.

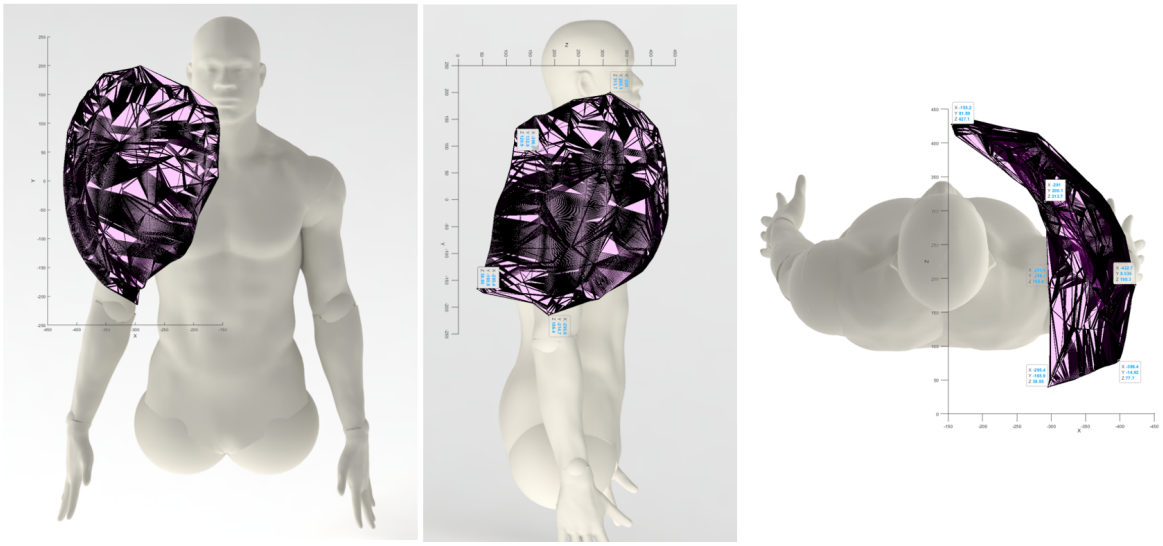

Figure 4.4.14: Measured exoskeleton workspace imposed on anatomical model. Left-front view, middle-side view, right-top view

Further analysis of the real workspace shows that it measures 280mm in the x-axis, 400mm in the y-axis and 400mm in the Z-axis. These axes reflect the exoskeleton axes defined in Section 3.5. Annotated figures to indicate the ROM of flexion/extension and abduction from the convex hull are shown in Figure 4.4.15 and 4.4.16respectively. The resting position of the end effector is (X=-296mm, Y=-215mm, Z=186mm). This aligns with the coronal plane of the wearer's body. Based on the curvature and the area of the plotted data points, a circular outline is fitted to the workable area. The circumference of this circle models the unrestrained arcing motion of the end effector in all directions. This circular movement can be assumed as the GH joint is modelled with a spherical joint. Flexion from the resting position to (X=291mm, Y=200mm, Z=314mm) is a relatively consistent arc, it peaks and then has an increased gradient until it intercepts with the coronal plane. This results in 157° of forward flexion. Extension from resting position to (X=-295mm, Y=-166mm, Z=39mm) has a rather linear relationship. However, a lack of data points in this area did not complete this relationship (also due to its smaller length of workplace, any arc will be harder to observe). This results in 30° of backwards extension. From the limit of extension, end effector continues behind the coronal plane, gradually converging towards the plane intersection.

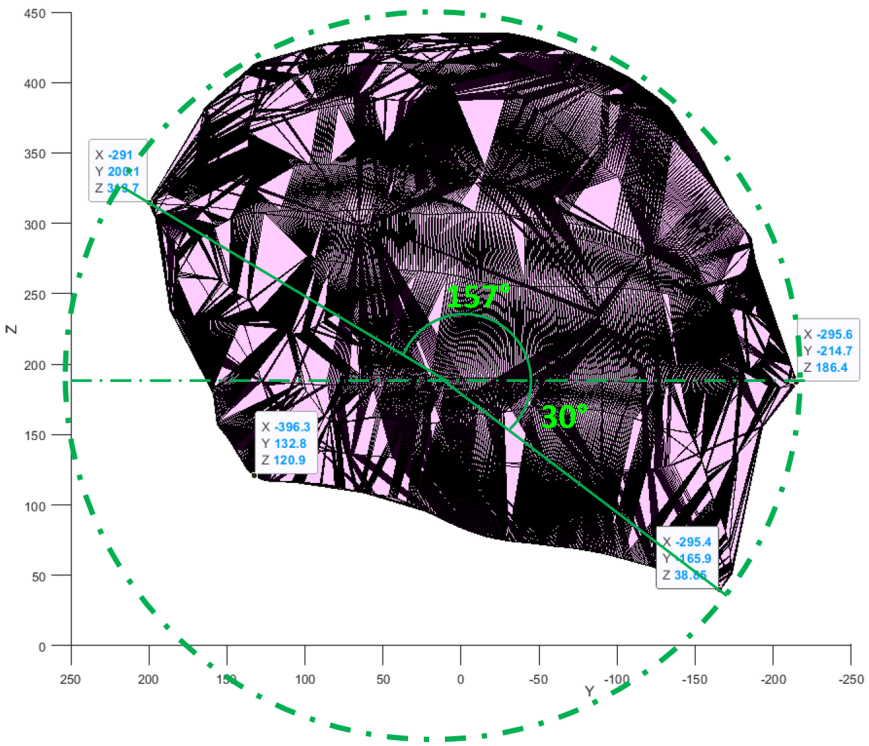

Figure 4.4.15: Motion tracked ROM convex hull (flexion) on sagittal plane

Abduction from the resting position to (X=-396mm, Y=133mm, Z=121mm) is a consistent arc parallel to the coronal plane, from this position abduction it begins to converge to the coronal plane. However, there is a constant abduction movement all the way to near the coronal intersection along the transverse plane (X=-304mm, Y=-199mm, Z=303mm). From this point, no more abduction is achieved and the end effector travels along the transverse plane until the arm begins adduction. This results in 153° of forward constant abduction parallel to the coronal plane, with a full range of 177° with the inclusion of mild translational movement. A limited amount of adduction from rest can be achieved but the direction of this motion was dominated by shoulder elevation. Shoulder internal/external rotation cannot be directly measured as it is a natural product of the other movements. However, to achieve an inwards curving arc (that is not just rotations of abduction and flexion) rotation of the arm had to occur. The resulting 3D optical tracking data shows curving arc and rotation, which was manually verified through testing. Further figures of the 3D workspace can be seen in Appendix E.

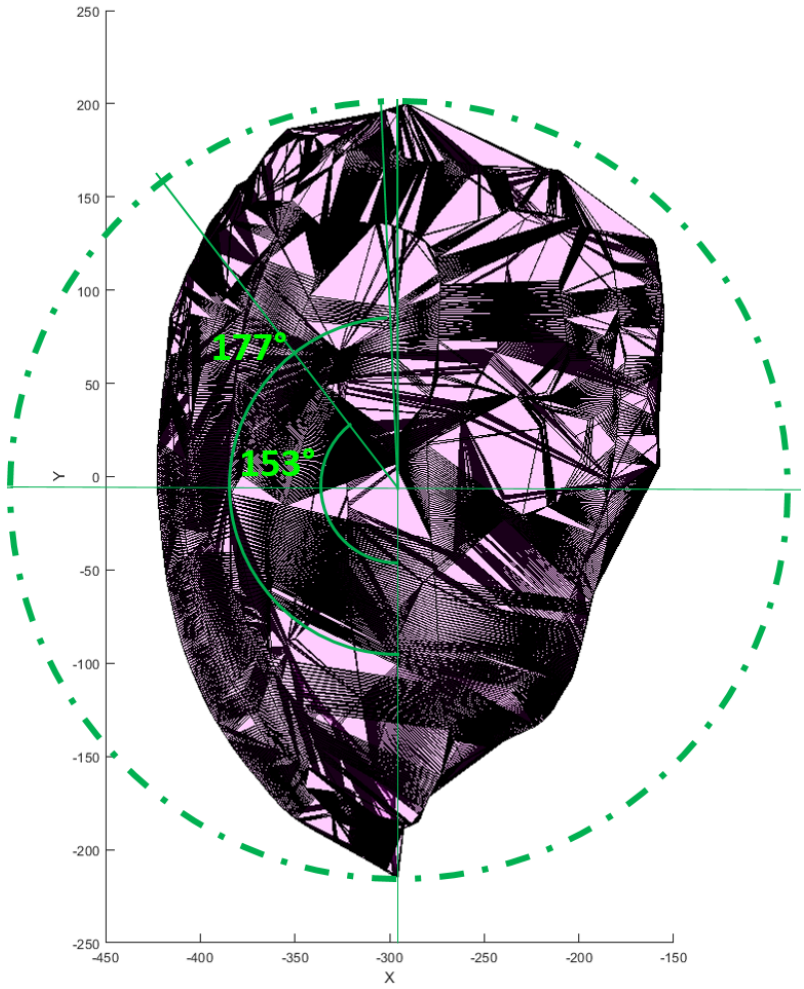

Figure 4.4.16: Motion tracked ROM convex hull (abduction) on coronal plane

Analysis of the workspace shows that it measures 265mm in the x-axis, 421mm in the y-axis and 395mm in the Z direction. The volume of the exoskeleton workspace is $0.00446m^3$, with an approximate absolute outer volume of $0.045m^3$. This satisfies the maximum workspace requirement of $0.5m^3$, as outlined in Section 3.15. The reachable workspace of the motion-tracked exoskeleton can be compared to the modelled workspace, where the modelled workspace consists of the maximal achievable simulated ROM for the exoskeleton. Figures 4.4.17 and 4.4.18 show the convex hulls of the DH parameters in red and motion data in purple plotted independently in 3D space. Where Figure 4.4.17 shows the frontal view of the exoskeletons ROM and Figure 4.4.18 the top translational. The measured data matches the modelled data,

with the alignment and similar curvature of the workspaces verifying that the DH coordinate frame systems and parameters were correctly modelled. Analysis of the two workspaces validates the design and confirms that it meets the requirements.

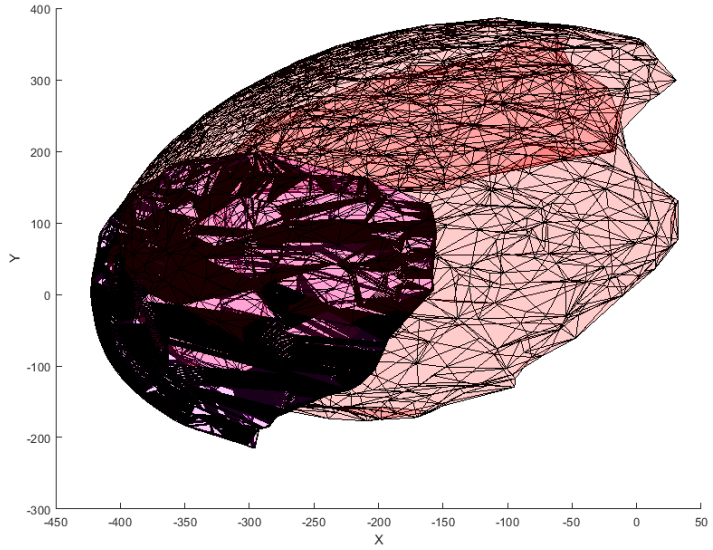

Figure 4.4.17: Measured and modelled workspace comparison coronal frontal view

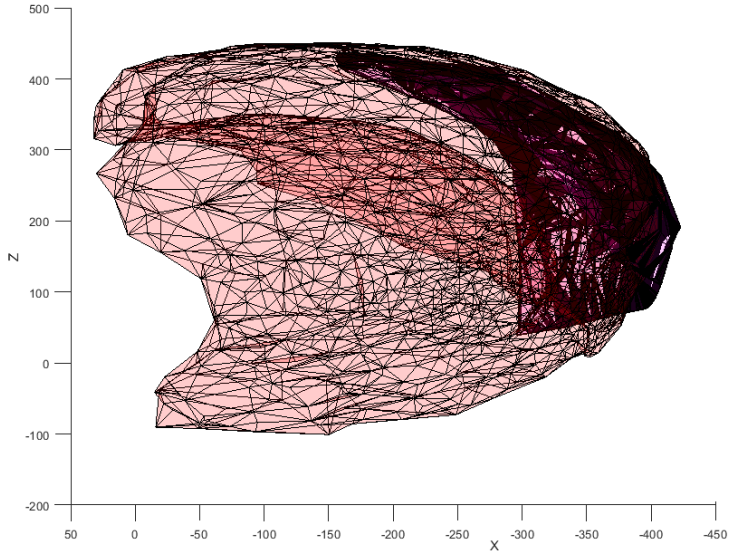

Figure 4.4.18: Measured and modelled workspace comparison transverse top view

The ROM measured from the motion tracking system is significantly lower of that of the kinematic model. The resulting volumes of the modelled and measured workspaces were $0.0358m^3$ and $0.00446m^3$ respectively. Which shows that the motion-tracked model achieved 12.46% of the modelled workable area. The leading cause for is un-modelled human/muscular constraints. Where the model can reach every available point in the range of each DOF, the likely achievable points are much less than this. For one, the muscles in the shoulder complex and the diameter of the arm restricts movement to a certain degree, where the exoskeleton can technically exceed this. The free-moving rotational DOF in the outer complex is only passively stopped in the backwards direction and allows for an almost complete rotation of free movement as to not constrict any patient movement. Theoretically, it can achieve this entire range and the model allows this, but when applied, the arm cannot physically rotate or move at the desired angles. Arm diameter and joint geometry restrict this motion. This leads to the model being able to achieve impossible configurations of the exoskeleton as shown in Figure 4.4.19 which increases its available workspace area.

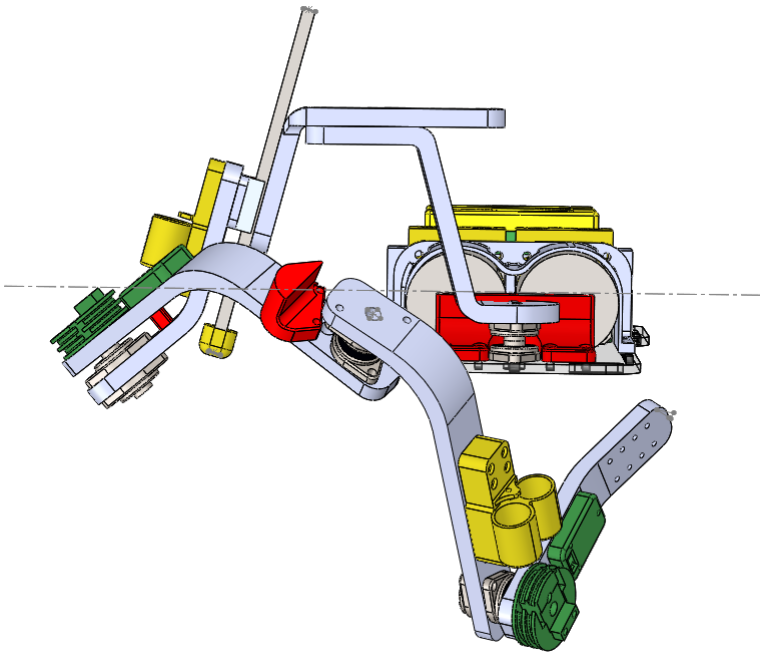

Figure 4.4.19: Configuration of the modelled exoskeleton that is kinematically valid, but unreachable by a human user

The measured workspace was based on a relatively small set of data, with the motion data having 16000 points and the modelled data having 60000 points. The modelled points are a random set, spaced uniformly across available joint ROMs. These points will reach unlikely configurations and achieve a large workspace when plotted as a convex hull. In comparison, the motion-tracked points are successive to each previous point and will only represent a small change in coordinates so the data covers a smaller area. Continuing from this, when recording motion data it is difficult to reach the full range of the device in every direction, omitting key data points which would increase its area.

The effects of mechanical compliance can be seen in Figure 4.4.18, where the workspace of the motion-tracked exoskeleton is displaced below the modelled workspace. Compliance in the links is likely responsible for disfigured aspects of the motion-tracked workspace, as this is an un-modelled variable (model assumes rigidity) which is relatively unknown as it is heavily dependant on the orientation and force applied to the exoskeleton. As outlined in Section 4.4.3 between 55mm to 121mm of displacement of the end effector could be expected with an applied load. The workspace is displaced downwards by 43mm which confirms the effects of compliance in the system.

4.5 Summary of Mechanical/Kinematic Design

The kinematic model of the exoskeleton has been modelled as a 5-DOF open-loop chain, encompassing the centre of the torso to the upper arm (Humerus). The kinematic design features 3 passive joints and 2 active joints.

CAD software was used to determine physical exoskeleton parameters that result in a large ROM and adequate compliance to the human body. Features considered in the design of the shoulder complex model were the axes of natural shoulder movement and shape of the human body. The shape, geometry and angles of the exoskeletons links and joints were determined from this model. Three revolute joints, constituting a spherical joint, are used to provide the three DOFs required for the motion of GH joint. These allow for active motion in the flexion/extension and adduction/abduction directions, while also passively allowing internal/external rotation. A prismatic linear slider accommodates for sternoclavicular forward/back motion and a central rotational joint to accommodate for autioclavicular elevation/depression motion. The inclusion of this linear slider with compression spring actuation, is a novel feature of the exoskeleton, simplifying the kinematic model while accommodating for a large range of discrete shoulder movements. In addition, this DOF works to translate the exoskeleton/users workspace anteriorly against a resistive force, and allow free movement posteriorly. DC motors (Rhino RMCS-220X) placed distally on the users back, with Bowden cable transmission, actuate the joints to provide up to 11.7Nm of torque.

All load-bearing links were 3D printed in PC. PC was chosen due to its high tensile strength, low weight, accessibility and its material elastic properties. Displacement simulations show that the end effector experiences the highest displacement of all links in the design, with 55.3mm of displacement for a 30N applied load and 121mm for a 60N applied load. The deflection of these links are constant, leaving no lasting deformation or damage to the exoskeleton. The links, mechanical stops, Bowden wheels and linear rail are all adjustable parameters. Adjustable prismatic links, rails, have been included in the design to allow customisation of the exoskeletons physical dimensions to an individual user.

DH parameters were used to define a kinematic modelled 3D workspace of the ex-

oskeleton. Motion tracking was used to determine the ROM characteristics of the exoskeleton. Flexion was measured to be 157°, extension 30° and abduction 177°. The resulting volume of the modelled and measured workspaces were $0.0359m^3$ and $0.00446m^3$ respectively. This satisfies the maximum workspace requirement of $0.5m^3$.

The exoskeleton was design, built and tested, and meets all of the mechanical design requirements specified in Section 3.15.

5 Electrical Design

The electrical and electronics implementation of the exoskeleton supports the actuation, sensing, and control of the system. The BITERS exoskeleton is powered by a 14.8V lithium polymer (LiPo) battery which provides power to the 12V XL4015 buck converter, MP1584 5V buck converter, and Rhino RMCS-2201 DC motors. The system is controlled by a Teensy 3.5 microcontroller (MCU). The 5V regulator supplies power to the Teensy and the I2C multiplexor, which multiplexes the inertial measurement units (IMUs). The Teensy's on-chip 3.3V regulator and digital pins supply power to the remainder of the sensors as reflected in Figure 5.0.1. The Teensy supports the software control architecture of the exoskeleton. This section encompasses component selection, power management, PCB manufacturing, and considerations when developing the electrical system for the exoskeleton.

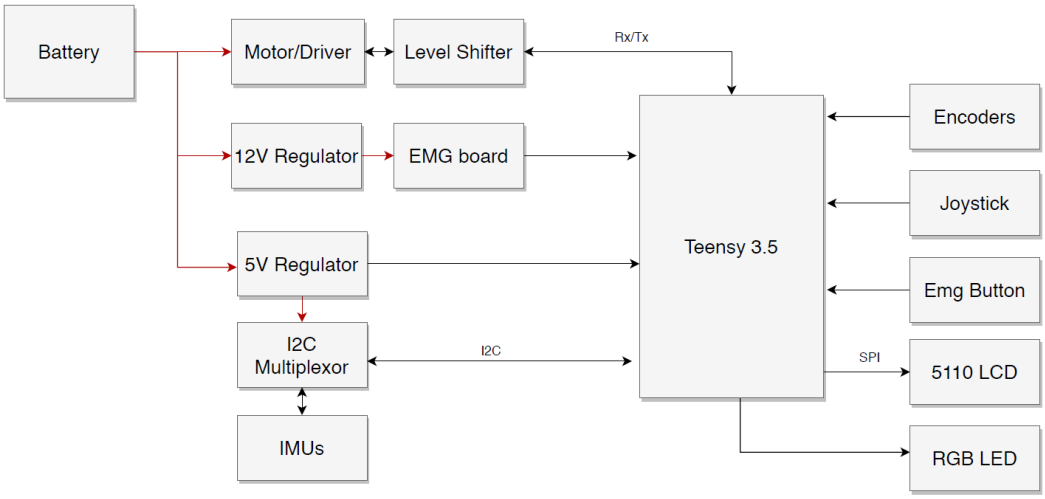

Figure 5.0.1: Electrical block diagram for exoskeleton system

5.1 Components

MCU. The Teensy 3.5 MCU supports the software control architecture of the exoskeleton. The MCU provides a USB link to power the board if no external power supply is present and enables data transmitted over the serial interface. The Teensy was chosen because of its multi-purpose pin functionality and number of programmable GPIO pins, supported by C++ programming.

Regulators. There are two specified voltage regulators on the main circuit board and one embedded in the Teensy 3.5. The 5V regulator is an MP1584 DC-DC buck converter that can tolerate a 6.2V-26V input voltage and can provide up to 3A at 5V with a loss of 8%. This regulator provides voltage to the Teensy voltage input port and the I2C multiplexor via decoupling capacitors. The 12V regulator is an XL4015 DC-DC variable buck converter which can provide an output of 8V-36V and up to 5A with a loss of 4% power. Providing voltage to the external EMG board via ceramic decoupling capacitors, and is detailed in subsequent sections.

Sensors. The input sensory system consists of potentiometer encoders on joints, joystick, emergency stop button, and IMUs. The potentiometers are 10K variable resisters with a rotation of 270° which fit onto a custom D-shaped attachment at the two actuated DOFs. Since these are just variable resistance pots the Teensy can read the connected ADC and derive the angle of the rotational joint. These encoders are used for speed/position inputs to the proportional assist-as-need control outlined in the subsequent sections. The potentiometers are also used to enable software stops, which support mechanical stops by force stopping the motors when they exceed the allowable ROM (before mechanical stops are engaged). A joystick is also a form of variable resister, as it is comprised of a push button and two spring-loaded 10K resisters. The joystick is used to manually control the direction of the motors/exoskeleton links when in manual control mode, and is also used to navigate the menu displayed on the Nokia 51140 screen.

An emergency stop button is essential for this system, it is connected to an interrupt-driven pin on the Teensy and toggles when pressed. It is standard practice to have emergency stop buttons connected in series with the positive power supply. How-

ever, as the button is located in the handheld unit the losses and noise introduced by bringing the 14.8V power supply to the circuit and back were too great.

The 9-axis Grove IMUs have 3-axis gyroscopes, 3-axis accelerometers, and 3-axis magnetometers. These IMUs communicate via I2C protocol and are connected to the I2C multiplexor on the main circuit. The intention of the IMUs is to provide a redundant measurement for the axis angle and speed. This ensures the safety of the user by detecting when the link is outside of the allowable workspace, or detecting discrepancies in the potentiometer data. A combination of the gyroscopic and accelerometer data can be fused to accurately gather this data, with the potential to provide an absolute position of the entire exoskeleton (including tilt, pitch, roll, height etc). There are three IMUs, one on each of the actuated links, and one positioned flat on the baseplate to provide a reference reading to triangulate position from.

User Interface. The output user interface system consists of the Nokia 54110 LCD screen and the RGB smart LED. The Nokia display runs on the Teensy 3.3V display and is back-illuminated via a 100 Ohm resistor. The display is used to provide user feedback by way of menu screens, data display, and directional indicators, and can be seen in Figure 5.1.1. The Nokia display is controlled by the joysticks position and switch states. The RGB LED is intended to be used in "exercise mode" (defined in Section 6), where the user controls the exoskeleton by EMG muscle intention, to complete an exercise. The LED will be red if the user is moving in the wrong direction, yellow if still completing the exercise (but completing the correct movements), and green when the exercise is complete and the user can return to rest. The LEDs are effectively "redundant" indicators to assist the LCD display. LED's have been used to simplify the user feedback experience by only offering one of 3 states at any given time. The simplicity of indication allows the user to focus on the current exercise. In addition, green and red LEDs are universal indicators of positive and negative feedback respectively. Therefore, the user will understand their meaning without excessive cognitive load.

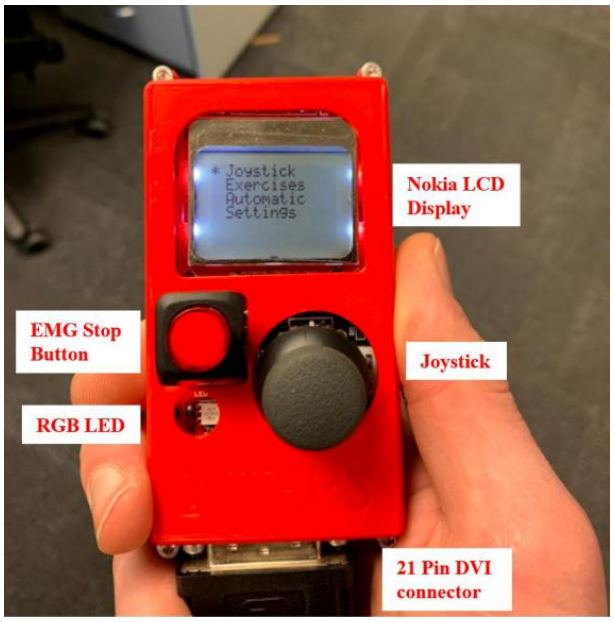

Figure 5.1.1: Hand held control unit

Motor/Actuators. The rhino RMCS-2201 motor specifications are defined in Section 4.3.3 and can draw a maximum of 7.5A at 12V-15V. These motors are connected directly to the power supply on the main board through a series of parallel decoupling capacitors, which are used to stabilise the voltage during high or pulsed current draw. The Teensy supplies the UART control signals to the motors through a communications level shifter, as the motors are 5V logic Rx/Tx and the Teensy is 3.3V logic. Although the Teensy pins are 5V tolerant, the level shifter was included as a protection measure in the error case where the motors pull the UART logic higher than the allowable range.

5.2 Schematics

The schematics for the main circuit and the hand unit are provided in Appendix F, extracts will be discussed briefly where necessary. Kicad 4.0.7 was used to design the schematics and footprints. The library was custom built, with the majority of the footprints/symbols designed specifically for this project (the exception being the Teensy 3.5). The schematic defines the interconnections of signals and power supplies alike and is a graphical representation of the electrical system, the schematic is used as the basis of the PCB. The schematics provided represent the inter-component details as defined in Section 5.1. The schematic is separated into two circuits, the main and the handheld board. A 25 pin DVI connector is used to connect these two circuits via a 1m DVI cable. Power lines, digital and analog signals are shared between these two circuits.

Most integrated circuits (IC) suffer negative effects if noise or voltage ripple on the power supply are present. Decoupling capacitors reduce these electrical impairments by suppressing high-frequency noise in power supply signals. Larger electrolytic capacitors are required to suppress low-frequency noise. Ceramic capacitors connected parallel across IC and battery power supply pins suppress high-frequency noise. A low impedance ground path is preferred for these capacitors. The use of vias and short traces reduce series inductance. [84].

A large 22F electrolytic decoupling capacitor is placed between the battery's power terminals to prevent large dips in the supply voltage. Ceramic 2.7uF and 100nF capacitors are also placed in series (Figure 5.2.1). It is common to use various capacitors in a system as some capacitor values will be better than others at filtering out specific frequencies of noise. Electrolytic and ceramic capacitors are both used in the circuit for this reason. Decoupling capacitors around the ICs on the board act also as power reservoirs, where they can briefly supply power at the correct voltage if the power supply ripples. Therefore, all power regulators and select other circuits have ceramic capacitors in close proximity. Ripples occur when there are large sudden current draws from ICs such as the MCU [85].

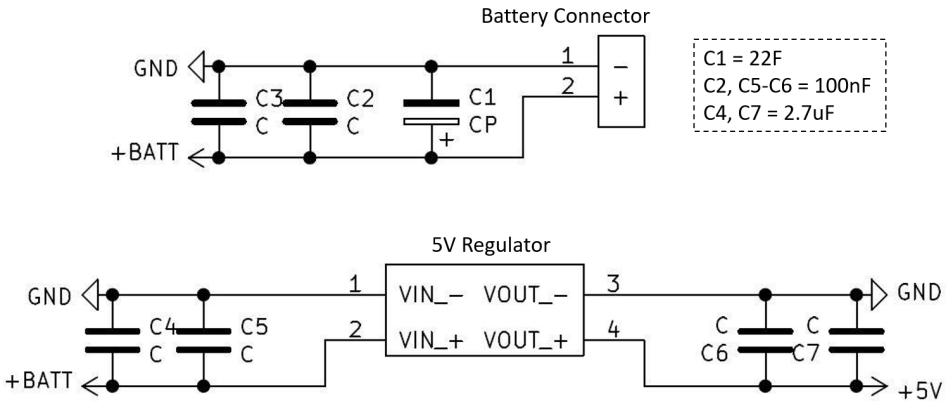

Figure 5.2.1: Decoupling capacitor placement

The schematic has been designed to be customisable after manufacture. As this is a prototype board a large amount of bug testing, alterations and additional features are likely to be necessary. To accommodate this, a row of headers has been included on either side of the Teensy, which are connected in series to the corresponding pin.

5.3 PCB Generation

Kicad 4.0.7 was also used for the design of the PCB. A two-layer PCB has been developed to support the electrical requirements of the exoskeleton.

Proper PCB design rules have been followed during the design of the PCB. Copper traces are used to route power and signal lines. Resistance was considered when deciding trace width as traces can induce voltage drops, power dissipation, and a temperature rise when current flows through it. Larger traces are used for tracks that have a larger current to avoid these issues. The standard trace size used was 0.25mm for all non-load carrying analog/digital signals. A larger trace width of 2.00mm was typically used for battery and power rail connections due to their higher load, with even larger trace widths were used when suitable. Trace length was kept short where possible so that signals take direct paths, reducing electronic magnetic interference (EMI). A polygon ground plane pour was used for the underside of the PCB. By using a ground plane the resistance of the return path of a signal is reduced. The decreased resistance reduces noise caused by fluctuations in return current, and it creates a uniform ground voltage. The polygon pour also helps avoid ground loops where the system is affected by a difference in ground potential at two circuits placed distally [86]. As noted in Section 5.2 decoupling capacitors are used for the power supply and at IC's. The capacitors are placed as near as possible to the power and ground pins of IC's to maximize decoupling efficiency, as placing capacitors farther away introduces stray inductance.

The circuit has been designed with a modular approach, every ICs placed on a set of headers, which can be removed and replaced if required. The removal of a part could be done to replace the part, and to speed up development by allowing the easy individual testing of components after the circuit has been developed. The PCB is a prototype board, if developed further for commercial or trial use, external factors such as vibrations would need to be considered and would likely result in permanently soldered parts and fixtures. In addition to removable ICs, an extra pair of motor connectors were mounted and routed to the Teensy for step/dir motors, this was done so that if the UART controlled motors were not suitable, replacement motors could be plugged in for continued testing. Figure 5.3.1 shows the outlines of the designed PCBs, where the red traces are top layer connections and green are

bottom layer. The ground polygon pour has been turned off for this graphic but covers the majority of the bottom plane .

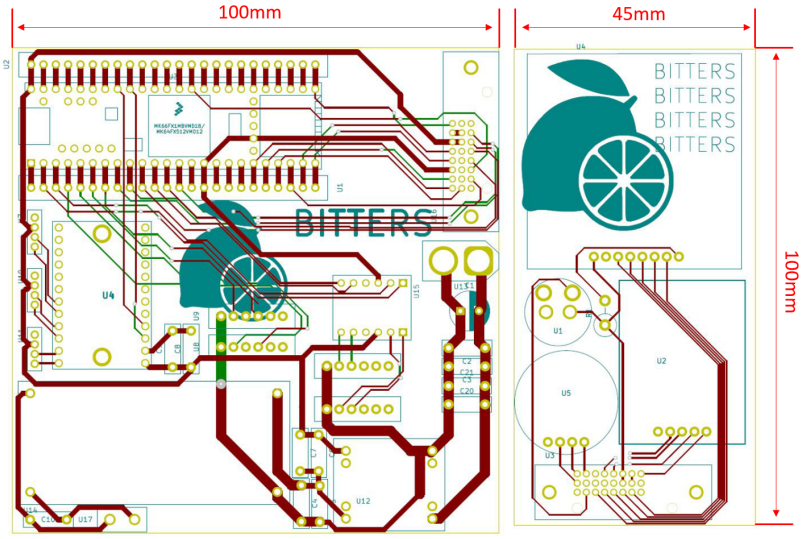

Figure 5.3.1: Routed main board PCB design

The printed and assembled models can be seen in Figure 5.3.2, key components have been labelled for reference. Some decoupling capacitors are under components and may not be visible in this image.

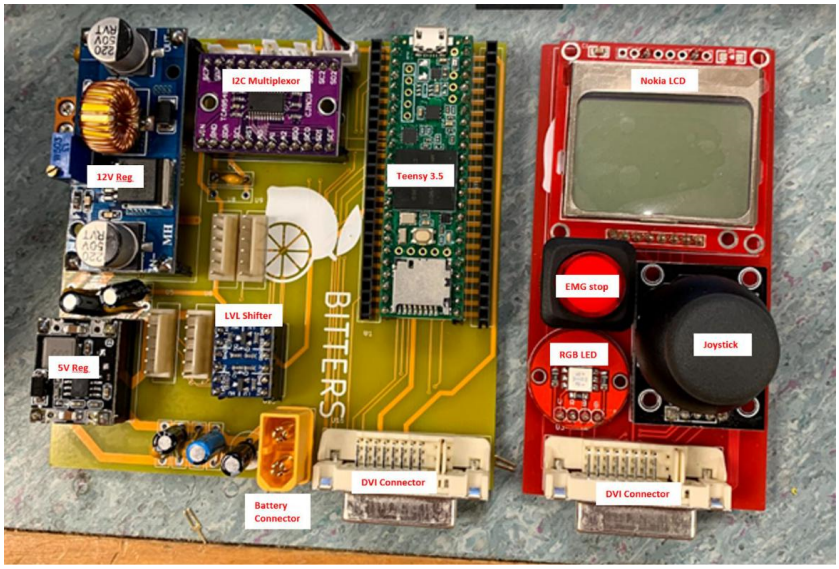

Figure 5.3.2: Populated PCB for exoskeleton

5.4 Power Supply

Power can be supplied at 5V through the Teensy USB serial port, or through the battery connector. The battery connector can either connect directly to the battery, which is a 14.8V 35C 4000mAh Li-Po (Giant Power), or to a bench-top power supply.

The main circuit at 14.8V pulls 0.034A when not connected to the motors and 0.128A connected to motors. The motors rotating at no load, individually pull a current of 0.8-1.5A (this differs from the datasheet as there is an increased load due to Bowden drive system and distally placed actuation), and a maximum current threshold of 7.5A (unlikely to be reached in this application). The External EMG board pulls 0.13A through the XL4015 12V regulator. The regulator has an efficiency of 96%, from Equation 5.4.1 it can be assumed that it will draw 0.11 A from the battery at 14.8V.

$$VoltageIn * CurrentInput * Efficiency = VoltageOut * CurrentOutput \tag{5.4.1}$$

The resulting power consumption of the exoskeleton is calculated with Equation 5.4.2, these are shown in Table 5.4.1

$$P = IV \tag{5.4.2}$$

Table 5.4.1: Exoskeleton energy consumption

State	Load	Current (mA)	Power (W)	Battery Life Estimate
Rest	No Load	238	3.5	16h 48m
Single Motor	No Load	1738	25.7	2h 18m
	Maximum Load	7738	114.5	0h 31m
Dual Motor	No Load	3238	47.9	1h 14m
	Maximum Load	15238	225.5	0h 15m

These values are for continuous current pull in the corresponding state. It is expected that in practice the exoskeleton will not be working at maximum load continuously (spikes to this current draw are possible) and will spend a large portion in the rest state or at lower current draws. Assuming that during a session that the exoskeleton

will be in its rest state for 70% and actuating for 30% of the time, for a single motor at maximum load, the exoskeleton will last 98 minutes. If both motors were actuating at maximum load the exoskeleton will last 51 minutes. This duration satisfies the portability requirements. If more power is required, simply specifying a larger battery or replacing the battery would give additional length to rehabilitation time. The battery is rated for 4000mAh at 35C, which equates to a safe discharge current of 140A using Equation 5.4.3.

$$(mAh/1000) * CRate = ContinuousDischargeAmperage \tag{5.4.3}$$

This is far above the maximum load of 15.24A. An RCX03-087 LiPo battery voltage audio indicator is used to alert the user when the battery is 2.7V below maximum charge and therefore needs recharging.

5.5 Summary of Electrical Design

The electrical implementation of the exoskeleton successfully supported the actuation and control of the system. A Teensy 3.5 MCU is used to read sensor feedback, implement control, and provide a user interface. The Teensy MCU was selected due to its size, low-cost, low power consumption, and open-source software platform.

The exoskeleton was powered by a 14.8V 4000mAh LiPo battery and has a maximum operating life of 51 to 90 minutes. 5V (MP1584) and 12V (XL4015) buck converters are used to supply power to the ICs on the PCBs. A 22F electrolytic decoupling capacitor is placed between the battery's power terminals to prevent large dips in the supply voltage. Ceramic 2.7uF and 100nF capacitors are also placed parallel in close proximity to the battery supply and all ICs to minimise voltage ripple and noise.

Sensory feedback was provided by potentiometers measuring joint angle, with IMUs mounted for redundant measurements. Potentiometer values were used to enable software safety stops. An interrupt-driven emergency stop button is included on the hand-held circuit for further safety precautions. User feedback is provided by a Nokia 54110 LCD screen and the RGB smart LED. The Display is used to navigate and control the system, where the LEDs provide a redundant indication of progress during exercises.

6 Software Design

Atom integrated development environment (IDE) was used to develop the software for the BITERS project. Arduino IDE was used to upload the project files to the device, with Teensyduino interfacing between the Teensy 3.5 and Arduino IDE. The Teensy was programmed in C++ with object orientated code used to define and use code-based objects and classes. The software is used to implement control strategies and control external peripherals. The software architecture is shown in Figure 6.0.1, this accurately represents the state machine of the exoskeleton. The Exoskeleton has two control modes, manual and autonomous.

Manual joystick mode. The joysticks (X, Y) values are scaled to suitable motor speed values for motor control. The joystick values of 0-1024 are mapped to a motor speed of 0-255, the speed of the motor increases linearly with joystick position. Both motors are controlled simultaneously, with the X and Y joystick axes acting as control inputs for actuated joints 3 and 5 motors respectively. A dead band of (X=200, Y=200) is set at the joysticks (X, Y) "zero" position when scaling, to reduce the effects of any noise of drifting of values. Proportional (P) control is used to control the motor's speed based on the speed of the actuated link as outlined in the subsequent sections. The speed of the links is derived from the current and previous potentiometer values. The direction and magnitude of the exoskeletons speed are mapped to the LCD display where its corresponding position is displayed as an interactive target.

Automatic EMG mode. Movement is incited based on the EMG signal from the user's muscle and is applied to autonomously assist the user. Details on the hardware and external circuit filtering of the EMG signal are found in Section 7. Further signal processing was required to make the EMG signal suitable for control. A five-element median filter is implemented to smooth the data for this purpose. The amplitude of the EMG data indicates the torque desired from the muscle, testing data in Section 7.4 is used to estimate the desired exoskeleton angle from this. The initial gradient of the EMG signal sets the desired motor speed. P control is used to adjust the motor's speed based on the error between the desired position and the current position. Potentiometer values from the actuated joints determine the current an-

gle, speed, and direction of movement used in control. Adduction/Abduction and flexion/extension can only be actuated exclusively, due to limitations in the EMG hardware.

Smooth ramp up/down time-based functions are used during actuation to reduce the instantaneous torque experienced, backlash, and over-current draw. Software stops are implemented based on pre-defined potentiometer positions.

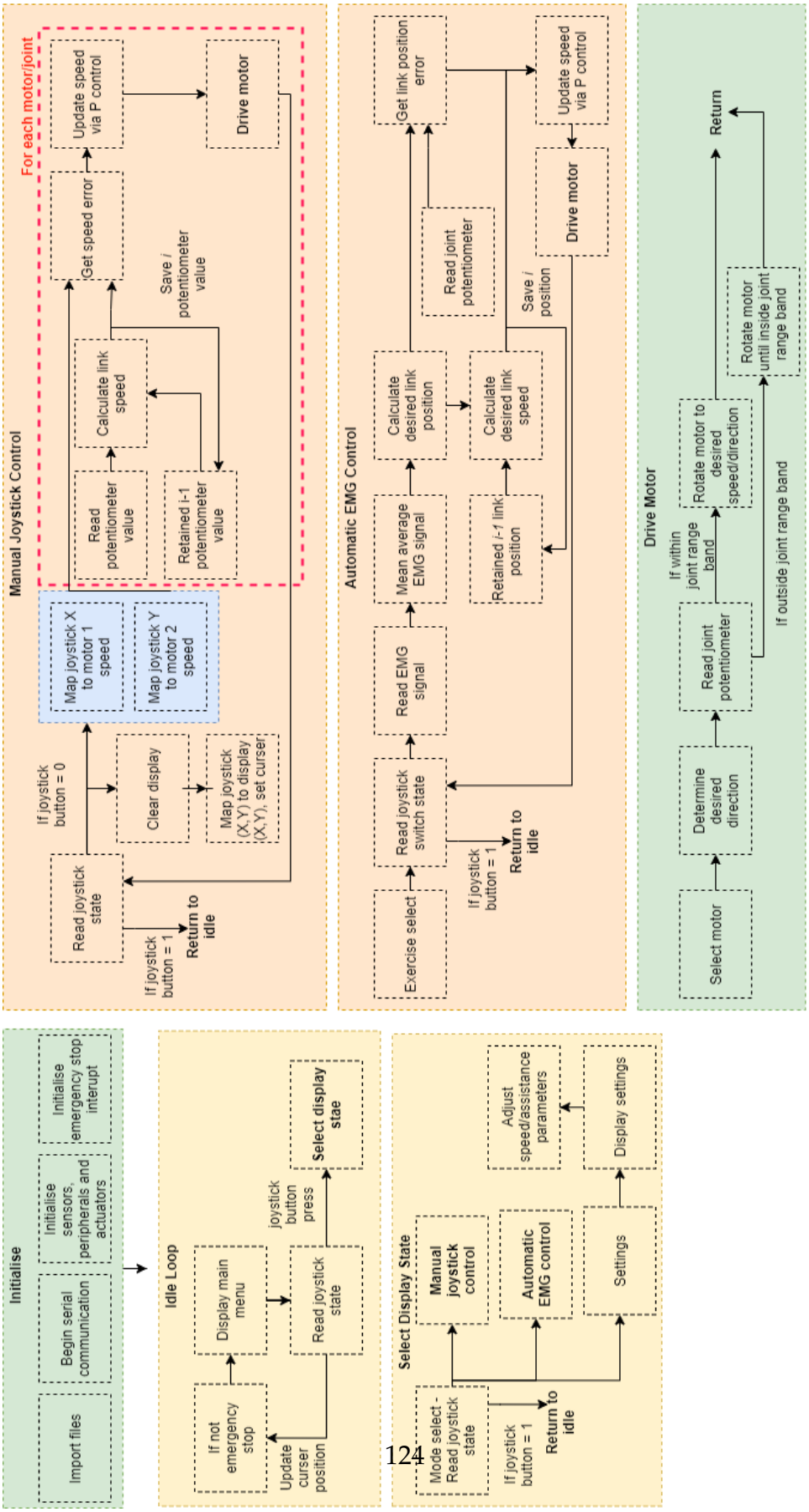

Figure 6.0.1: Software state diagram

6.1 Actuation Control

The Rhino RMCS-2201 provides high correction torque through a closed proportional-integral (PI) control loop using optical encoder feedback to determine the positional error (Figure 6.1.1).

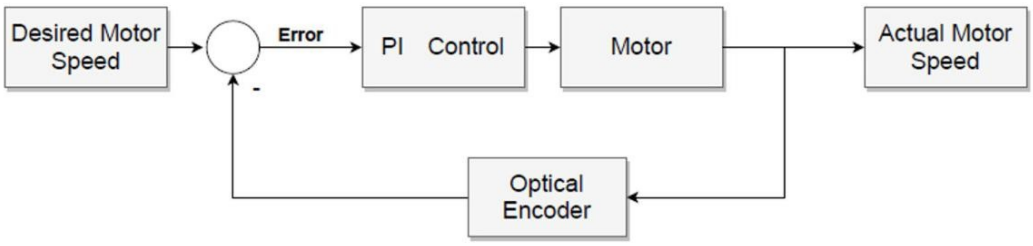

Figure 6.1.1: Motor PI control block diagram

The control is error based and uses the error between the measured state and the desired state with set gains to control the output. The proportional controller response is the product of the error (between the desired and current joint state) and the P gain constant K. P control works because of inherent damping in the system.

The control of both manual and autonomous actuation modes are similar, Figure 6.1.2 describes the actuation control architecture for these. For the EMG based system, the EMG signal indicates the torque (force) of the muscle, this can be used to estimate the desired link position (based on its amplitude) and the desired link speed (based on the gradient of its rise). The speed is mapped to the motor, which used PI control, to actuate the end effector. The error between the desired position and the link position (provided by the potentiometer) is used to alter the speed using P control. This control loop executes until the desired position has been reached. Assist-as-need like control is achieved, as assistance is provided based on the effort outputted by the user. Where the provided motor output is proportionally adjusted based on the EMG signal input.

For the manual joystick based system, the analog signal provides a desired joint speed (based on the displacement of the joystick from its center). The speed is mapped to the motor, which again uses PI control, to actuate the end effector. The error between the desired speed and the joint speed alters the motors desired speed dynamically using P control.

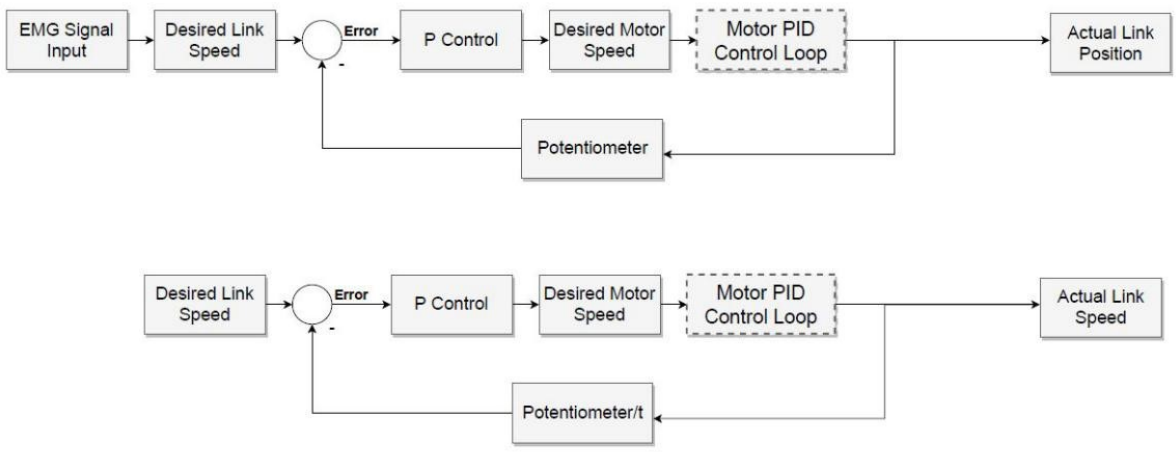

Figure 6.1.2: Automatic (top) and manual (bottom) control block diagrams

6.2 Summary of Software Design

The Software is implemented on a Teensy 3.5 MCU in object-orientated C++. The software is used to apply system control, which incorporates sensor data, user interface peripheral control, and motor control to safely and successfully actuate the exoskeleton.

The exoskeleton control system can be likened to an assist-as need controller, where proportionally adjusted assistance is provided based on the effort outputted by the user. Proportional control is used to adjust the motor speed for all actuation. Where the control system is error-based and uses the error between the measured state and the desired state with set gains to control the output. Potentiometers are used on the actuated joints to get the joints position and velocity for control error inputs. Manual actuation mode used the joystick as a sensory input, and maps the (X, Y) value to corresponding motor speed values. The P controller uses the error between the desired joint velocity and the velocity of the actuated joint to adjust the speed. Automatic EMG mode uses EMG values, which represent the desired torque output of the user's muscles, to estimate the desired active joint angle. The P controller uses the error between the desired joint position and the position of the actuated joint to adjust the speed. The relationship between movement, EMG signal, and desired

position, is derived in subsequent sections.

7 Electromyography (EMG)

7.1 System Hardware

Fortune et al. [87] developed an EMG circuit for applied exoskeleton use and development for stroke rehabilitation. This technology was developed in the same wider team as this exoskeleton research, L. McKenzie's EMG circuit was used for the EMG data acquisition and output. As defined previously, EMG is a bio-feedback based circuit whose signals amplitude directly correlates to the muscular activation energy.

The EMG board uses three surface electrodes, two of these are the positive and negative electrodes (cathode and anode) and the other is the right leg driver electrode, which is used to reduce the effect of electromagnetic interference (EMI) on the EMG signal. The foremost form of noise in the system is EMI, dominantly introduced by alternating current (AC) power line interference through connected external devices and capacitively coupled onto the body. The RLD circuit attenuates the EMI interference by applying the common mode voltage back into the system through the RLD electrode. The surface electrode provides a relative low impedance path between the body and amplifier common. The common mode voltage is inverted and amplified to achieve attenuation. The EMG signal uses low and high pass filters to remove unwanted frequencies from the signal, with respective cut-off frequencies of 20Hz and 459Hz (which is essentially for anti-aliasing). The low pass filter removes motion artifact noise between the electrodes/skin, while the high pass filter attempts to remove signals introduced by muscular tissue [87].

The sampling rate of the hardware is 1kHz, this is interrupt-driven. The CMRR is a minimum of 110 dB. The data from an EMG device is processed using a Teensy 4.0 microcontroller which allows data gathering by serial communication (Figure 7.1.1).

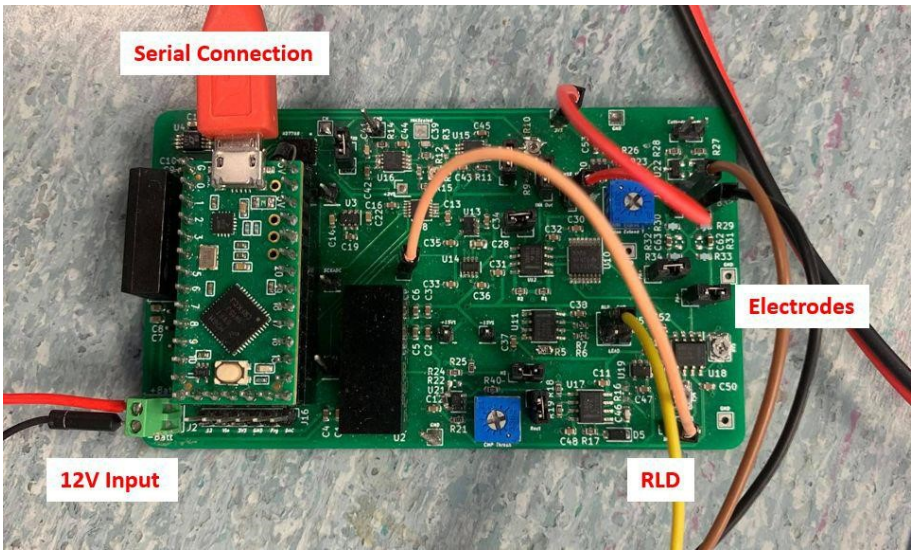

Figure 7.1.1: EMG hardware layout [87]

7.2 Applied EMG

The exoskeleton's 12V regulator provides power to the EMG board. The EMG signal is processed on the Teensy 4.0 board by applying a 100ms windowed RMS filter, as specified in Section 3.9. The signal is written to an analog pin on the Teensy 4.0 and read on an analog pin on the main circuit by the Teensy 3.5. A simple five value moving average filter is applied on the Teensy 3.5 to further smooth the data and remove the effects outliers, making it more suitable for control applications.

Ag/AgCl electrodes (VMVerity Medical Ltd) offer a stable connection to the skin. Spectra 360 electrode gel was applied to increase the traction of the electrodes and to reduce the impedance of the skin. The non-polarizable quality of the electrodes ensures a high signal to noise ratio (SNR), and reduced power line and body movement interference [88]. The surface electrodes were placed 20mm apart and parallel to the muscles fibre. The RLD electrode was placed slightly distally on a harder bone structure as can be seen in Figure 7.2.1, where it is placed on the AC joint when measuring AD EMG.

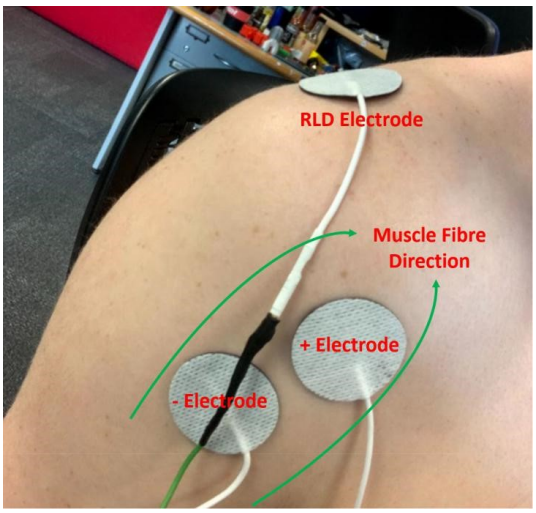

Figure 7.2.1: Placement of surface electrodes for the AD muscle

The Effects of the RLD circuit can be seen in Figure 7.2.2. The orange waveform is the EMG signal and the green waveform is the RMS of the EMG signal. It is clear that there is a large amount of external noise introduced into the system from EMI, particularly at 50Hz due to mains line-noise. The noise causes an increase in the

resulting resting RMS signal, which if applied to a controller system, would likely result in false muscle movements and inaccurate results in subsequent testing.

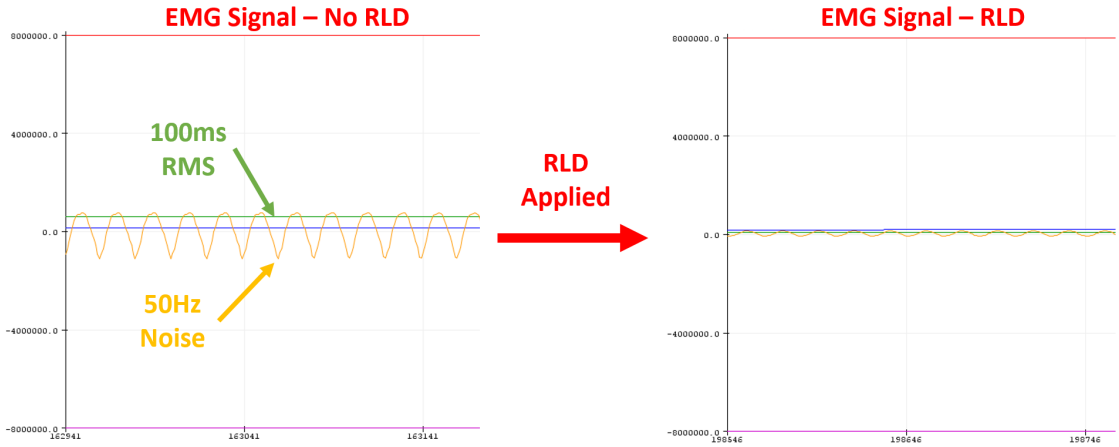

Figure 7.2.2: RLD noise reduction in EMG signal

The RMS window is applied to get the effective value of the raw EMG signal. Stabilising the signal, and ensuring a positive sign, making it suitable for control. The effects of the RMS window on the raw EMG signal can be seen Figure 7.2.3.

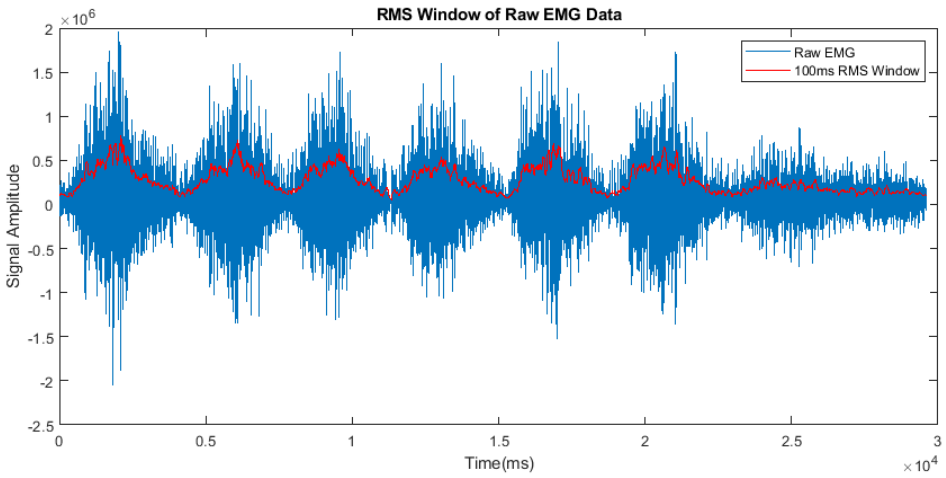

Figure 7.2.3: 100ms RMS filtering on raw EMG data

7.3 Experimental Muscle Testing Set

The aim of this experiment is to investigate EMG muscle activity, and activation patterns for varying loads during flexion/extension, abduction/adduction, and internal/external rotation, for muscles that contribute to shoulder actuation. The results of this will support the design and EMG based control strategy of the BITERS upper-limb exoskeleton. This study was approved by the Human Ethics Committee at the University of Canterbury (HEC 2020/75).

Subjects. All testing was completed with one 22 year old healthy male subject, with no known impairments which would affect the results of this study.

Muscle Set. To determine the characteristics of the muscle groups, the AD, MD, PD, UT, LT, SA, TM muscles were measured for all shoulder movements, as defined in Section 3.9 .

Movement Set. Data will be gathered for the following isolated movements: Flexion, extension, abduction, internal rotation, and external rotation.

7.3.1 Methodology

The subject was required to do ten of each of the defined movements, completed in the sitting position, with each movement lasting approximately 2 seconds. There is a 3 minute rest between each set to eliminate the effects of fatigue. Movements will be completed with a straight arm with the shoulder and forearm in the neutral position. A 1kg load is held in hand to incite muscle activity. For load analysis testing, three loads were used for shoulder flexion, these were 0kg, 1kg and 2kg. The subject held the loads in their hand and completed shoulder flexion with a straight arm with the shoulder and forearm in the neutral position.

Electrodes were placed parallel to the muscle fibers in the centre of the measured muscle, 20mm apart. An RLD electrode will be placed on the body on a skeletal

joint/bone close to the muscle of interest.

Equipment. EMG signals were recorded using the hardware as described in Section 7.1. Bipolar, disposable, self-adhesive pre-gelled Ag/AgCl 20mm surface electrodes were used to record the activity of the muscle set during activation.

Data Capture. Data is gathered by the Teensy 4.0 on the EMG hardware. Data was recorded through the MCUs serial port to the PCs USB port. The raw EMG data was captured in a 100ms root mean squared (RMS) window to smooth the output data. Arduino IDE serial port/plotter was used to capture the data.

Analysis. Data was exported to a CSV file and processed in MATLAB (v9.7). Data will be compared for each of the muscle groups with reference to the mean RMS EMG during activation, and analysed in the time domain to get an understanding of muscle activation patterns. Time normalised data was element-wise meaned across movements to produce the mean EMG signal amplitude at each point over the set of data. No further filtering was applied as to not mask the discrete signal fluctuations. It was decided that contrary to standard practice, the data would not be normalised to a high amplitude EMG signal when displayed, as it was preferred to keep the data in their raw states for ease of reference to future work using the same hardware.

7.3.2 Results

Mean RMS EMG Analysis. As seen in Figure 7.3.1, the UT has the highest resting signal amplitude of $170000\mu V$, where the mean at rest signal was $50000\mu V$ ($SD = 10000\mu V$) for the remainder of the muscles. Significant readings for flexion, extension, and adduction were recorded, with the UT flexion similar to AD. Negligible change was recorded for PM and LD for all muscle movements. LT, SA, and TM also recorded very low readings on average. The LT shows a relatively large EMG amplitude during shoulder abduction, the SA increasing for flexion and abduction, but minimal change for extension, and TM increasing with shoulder extension. Muscle response to internal/external rotation was minimal across all muscle groups, with

the AD showing the largest increase from zero position for internal rotation. The PD and MD show a larger response for external rotation. The AD was significantly more active during flexion/abduction than extension and rotation. As the AD can produce both shoulder flexion and abduction, it is likely to not only be producing a flexion torque but also contributing to canceling out unwanted shoulder adduction.

Significant EMG response for active flexion was seen in AD, MD, PD, UT, and SA. For extension, significant response was seen by the PD, UT muscles, and to a lesser degree the MD. For abduction, significant response was seen by the AD, MD, PD, UT, LT and SA muscles. A small response was seen for internal rotation by the MD and PD muscles and for external rotation the AD.

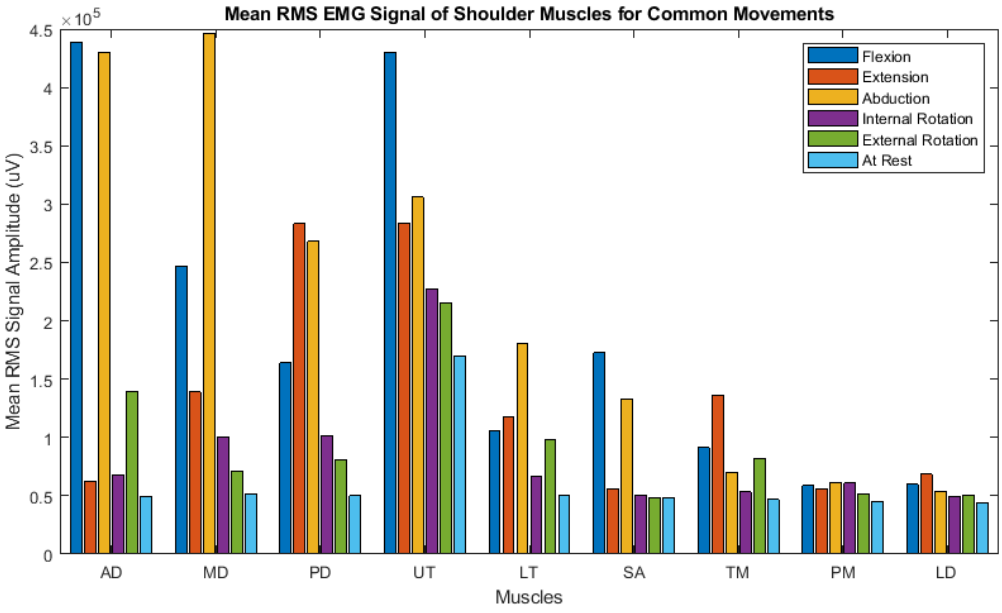

Figure 7.3.1: Mean RMS EMG signal amplitudes for common movements

Mean RMS EMG Load Analysis. The load testing showed that there is a systematic increase in activity level in all active muscles as load increased. For most muscle groups, the largest increase in amplitude occurs between no load and the 1kg applied load. However, the difference between 1kg and 2kg loads is often minimal or even zero for the PD. The AD shows a larger increase between the 1kg and 2kg loads than 0kg-1kg load. This increase could be an indication that the muscle is susceptible to the effects of varying loads. The trends seen for the AD could be because it is

the largest contributor to shoulder flexion, and therefore the majority of the load is applied to it, where the other muscles experience a more distributed load.

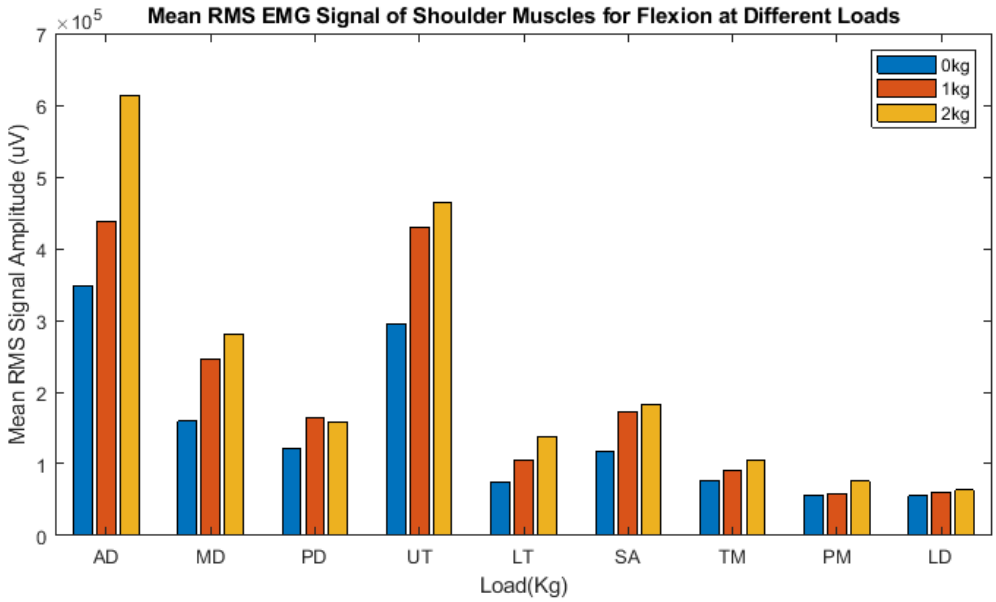

Figure 7.3.2: Mean EMG signal of shoulder muscles at varying loads

Muscle Activity Patterns The AD was chosen as it had the largest increase in mean signal amplitude with load, therefore the muscle recruitment patterns will be easily distinguishable. Figure 7.3.3 shows the muscle response for shoulder abduction with 0kg, 1kg and 2kg. The muscle activity patters show an increase of amplitude with load. The activation of the muscle with load (>1kg) occurs before flexion movement is recorded and much earlier than with no distal load, indicating that load is required to produce significant EMG activation before the movement has taken place. This pre-emptive signal could be used to recognise user intention before movement, or at a minimum allow for a "lag time" between sensing and control to produce real-time control with movement.

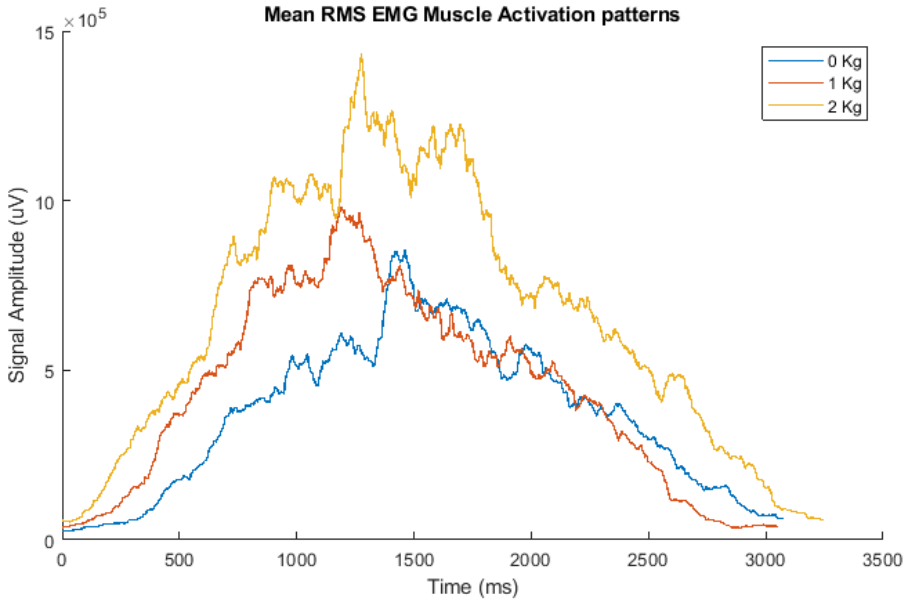

Figure 7.3.3: Muscle activity patterns of the PD at varying loads during shoulder flexion

7.3.3 Further Discussion

The PD and UT are the only two muscles that show significant mean RMS EMG signal response for all actuated movements, with a relatively low EMG response to internal/external rotation. As described in Section 4, BITERS has two active rotational DOFS, which enable shoulder adduction/abduction and flexion/extension. Where the remainder of the shoulders motion (internal/external rotation, elevation/depression, protraction/retraction) are passively supported. As movement in the internal/external rotational directions are not actively actuated, high response for rotation is not desired as it may introduce error into the control system.

Increasing muscle activity with load will have quite a large effect on the EMG based control system of the exoskeleton. Varying user weights, and applied distal loads depending on the exercise, will give false positional and speed parameters. It is unknown how differences in distal weight and differences in arm weight exclusively affect the EMGs amplitude with loads, with the arms mass inertia characteristics and unknown positional arguments (arm shape, weight distribution, angle, strength) being unknown parameters. Although active compensatory measures have not been

implemented to reduce the effects of these parameters (such as calibration procedures or adjustable variables for user weight or applied load), consideration has been given when selecting the muscle set for applied EMG. Muscles which have a diminishing increase of signal amplitude with increasing loads are suitable for control, as the effects of varying user mass on the signal will be reduced. Only the AD conforms to this requirement. This trend of signal amplitude with increasing load is approximated by Equation 7.3.1. Where A is the mean signal amplitude, the asymptotic value, b the half-life/rise time, and F the load. Where the mean RMS EMG amplitude trend shows a high initial gradient and diminishing return in signal amplitude with increased load.

$$A \approx a(1 - exp(-bF)) \tag{7.3.1}$$

In general, the muscle activation patterns across muscle sets are very similar, with load producing a steeper rising gradient. This increase of gradient is expected as it is to reach a higher EMG amplitude within the same time frame. The muscle patterns show a steep increase during abduction, with a more linear decrease during adduction, with this trend staying consistent over varying loads. This trend aligns with the findings of Wattanaprakornkul et al. which theorised that shoulder muscle recruitment patterns to produce flexion is established at low load levels and does not vary as load increases. So although an increasing load causes subsequent increasing EMG readings, the pattern of muscular stays the same just scaled to a higher signal. This pattern is important to be aware of for EMG controlled actuation, as variances in muscle energies make it difficult to model accurate position/speed control.

7.4 EMG Applied Control

For applied EMG the location of the measured muscle on the user must be considered. Electrodes must be placed at easy to reach locations. Therefore, muscles such as the LD and LT are not considered for further applications as they are on the back, making them difficult to reach and accurately place electrodes. In addition, muscle size is a contributing factor as a smaller muscle surface area makes it more difficult to achieve the correct application by the user. The distortion of the skin surface was found to be an issue for muscles such as the PM's. Large displacement of the electrodes during motion degrades the connectivity with the skin as the edges of the electrodes often detach if significant bi-directional movement of the skin surface occurs. As only flexion/extension and adduction/abduction are actuated, and internal/external rotation is free moving, any activation energy contributed by rotation is undesirable. Only energies that contribute to active joint movement are desirable for control. Therefore, muscles with relatively low EMG signals for rotation are considered.

The results from the load testing indicated that for the majority of muscles in the set, there was a systematic increase in signal amplitude with an increase of distal load. The only deviation from this trend is the PD, which only shows an increase between no-load and 1kg load. A 2kg applied load did not indicate significantly increased muscle activity. Review of the EMG activation patterns shows that the muscle activation patterns are developed at low loads, and their trends are consistent with increased loads. A significant response to muscle activation energies is desirable, with a low deviation in this response with varying loads. This low deviation will reduce the effects of disproportionate muscle masses between users on the EMG signal, and therefore control. Considering the load and mean amplitude test data described above, both PD and UT are suitable for EMG control.

PD was chosen for control due to its lack of activity for shoulder internal/external rotation and its high median activation characteristics across all movements. As only one set of input electrodes are configured, the exoskeleton can be configured to achieve autonomous isolated flexion, extension or adduction/abduction individually. If two sets of electrodes were available, different sets of muscle energies could be gathered in varying locations to determine precise intended angles and direc-

tions. As the EMG is used as a control signal, further signal processing was required as outlined in Section 6. The amplitude of the signal and the gradient of the rising signal was used to estimate position and speed.

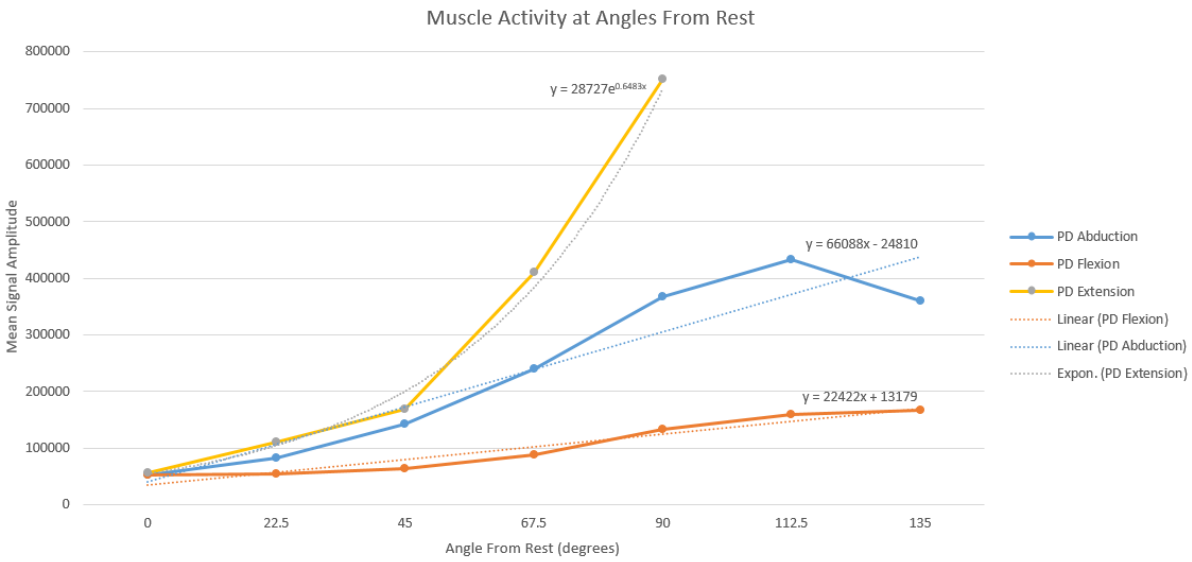

Figure 7.4.1: Muscle activity at angles from rest

Figure 7.4.1 shows the relationship between PD muscle energies and shoulder angle in flexion, extension, and abduction. Data was gathered sitting down with the angle positions written on a parallel wall. The arm was moved to each angle and the mean signal amplitude over 8 seconds was used to determine the muscle activation characteristic.

Extension was modelled as an exponential curve, where flexion and abduction are modelled with linear lines of fit. Motor control signal set-point is calculated using these equations. The abduction signal is significantly lower than recorded previously, this is likely due to large spikes in muscle activation energy as movement occurs, where data for this was gathered when the muscle in a static position, the moving averaging of the data decreases the magnitude of these spikes. For extension, the simple reason that previous data shows lower readings is that this testing set recorded the signal amplitude at much larger degrees of extension (135° vs 90°).

7.5 Summary of Electromyography

EMG muscle activation energy signals were determined using an external EMG board developed by L.McKenzie [87]. Ag/AgCl surface electrodes were used to interface between the hardware and users skin. The sampling rate of the hardware is 1kHz, this is interrupt-driven. The EMG signals filtered by a 100ms windowed RMS filter, as specified in Section 3.9. The exoskeleton's 12V regulator circuit provides power to the EMG board.

An EMG study was completed to determine the characteristics of the AD, MD, PD, UT, LT, SA, TM muscles during shoulder flexion/extension, adduction/abduction, internal/external rotation, and at rest. For all muscle sets, there was a systematic increase in EMG signal activity with increased applied load. It was also found that muscle activation patterns are developed at low loads, with signal trends remaining constant with increased load.

The UT and PD were determined to be suitable for exoskeleton control, with the PD selected due to its low EMG signal response to internal/external rotation, its low sensitivity to changes of load, and its high median activation characteristics across all actuated movements. These results supported the design and EMG based control strategy of the BITERS upper-limb exoskeleton.

8 Testing and Validation Against Design Requirements

This section compares the performance of the exoskeleton against the design requirements, further detail key design aspects, and discuss its limitations. The design requirements are defined in Section 3.15.

8.1 Passive Exoskeleton Performance

The kinematic model of the exoskeleton is modelled as a 5-DOF open-loop chain, which includes two passive revolute joints, two active revolute joints, and a prismatic joint. The exoskeleton did not restrict the motion of the shoulder. The specified ROM defined for the exoskeleton was based on research findings which considered the skeletal ROM and muscular constraints as described in Section 3.5. The minimum achievable ROM's specified are defined as such; 154° flexion, 74° extension, 163° abduction , 48° internal rotation and 87° external rotation. DH parameters were used to theoretically model the exoskeleton workspace, which verified the required ROM can be achieved. Following the manufacture and assembly of the passive exoskeleton, un-restrained movement within this workspace was achieved for a smaller range of motion than modelled. Manual actuation of the links in a 2D plane (singular direction motion) verified that flexion/extension and adduction/abduction ROM specifications were met. The passive second rotational joint of the kinematic GH joint DOFs allows free moving internal/external rotation. Although this is not actuated, the kinematic design and compliance in the system allows for 90° of rotation in either direction.

Displacement simulations were completed for the CAD model of the exoskeleton, with applied materials and forces used to accurately model the real use-case. These determined that the end effector would experience a displacement of 55.3mm to 121mm for 30N and 60N applied loads respectively. These loads were determined to be reasonable and realistic, to test the maximum limits of the exoskeleton. The displacements were mostly experienced in the downwards Y-axis, with a forward torsion experienced also. It was found that the force to displacement relationship at any singular point along the exoskeleton, is approximately linear. The displacement

decreases linearly from the actuated end effector towards the centre of the trunk. Similar displacement to the simulations was seen in the physical build of the exoskeleton, with a displacement of <10mm seen at the end effector for the maximum gravitational torque (10.37Nm).

The exoskeleton links were printed in Prusa-blend PC (10mm links with 50% infill) as PC is high strength and low weight. Flex in the material/links is a significant contributor to the exoskeletons displacement. This flex makes the system less rigid, more compliant, and less prone to breakage. However, this compliance introduced other issues in relation to the reduced reachable workspace and diminished efficiency of power transfer to the end effector. A higher density of PC filament would increase the rigidity of the system, further testing to determine the relation between fill density and flexion would confirm this.

8.2 Active Exoskeleton Performance

The active exoskeleton is the passive design with applied electrical actuation on two joints. Of the five DOF's in the modelled shoulder complex, two are active. DC motor actuation in series with Bowden cable transmission allows the bi-directional movement of revolute joints around the GH joint to allow abduction/adduction and flexion/extension. Bowden cable transmission is used as a means to actuate the joint while introducing elements of compliance into the system by having non-rigid actuation on the exoskeleton arm. In addition, Bowden cables allow motors to be placed distally to more appropriate load-bearing orientations. This weight re-distribution places the large majority of the weight of the exoskeleton over the subject's shoulders. The rigid perspex back-plate ensured that bending in the exoskeleton arm mount was eliminated, which is beneficial as displacement at the base of the exoskeleton significantly affects the orientation of the end effector. This rigidity also securely mounted the exoskeleton arm and motors, effectively isolating the user from actuated components and forces.

Potentiometers on the device's joints are used to determine the joint angles and velocity for feedback control. IMUs were fixed onto three positions on the exoskeleton to provide absolute positioning and redundant sensor readings, but were not func-

tionally used in this project.

3D printed components, reinforced with structural bolts, were printed to house the Bowden system, with Bowden wheels, joint/termination, cable mounts, and wheel shields were printed in PLA. Load applied to active joints, and gravitational torque acting on the system results in the displacement of surrounding members. The compliance causes the velocity profile of the exoskeleton to be slower. In addition, the compliance distorts the links, altering the exoskeleton profile, and resulting in changes of angle. Distortion in the structure of the exoskeleton due to compliance may reduce power transfer efficiency and cause deviation from the desired applied force direction.

The complete active exoskeleton is shown in Figure 8.2.1. The exoskeleton pictured, was a completely isolated functional unit, with no reliance on external software or power connections (operating on battery power). Manual joystick actuation is used as the control input for this test (EMG circuitry included but electrodes not attached). Further imagery of the final model can be found in Appendix G.

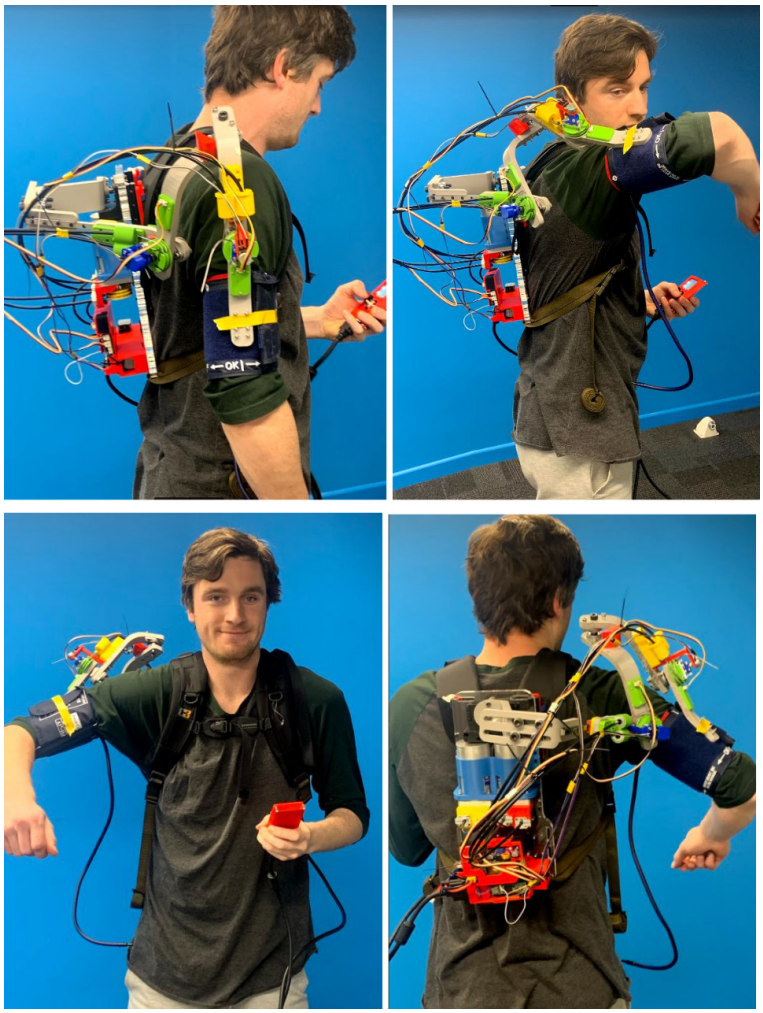

Figure 8.2.1: Physical build of BITERS exoskeleton
Top left: exoskeleton at rest, top right: exoskeleton at shoulder adduction/flexion, Bottom left: shoulder adduction (front on), bottom right: shoulder adduction/extension

The achieved active ROM of the exoskeleton was determined through motion tracking and workspace analysis. The measured ROM against the requirements is shown in Table 8.2.1. Flexion and internal/external rotation were verified to exceed the specified ROM. Adduction towards the body was achieved in the final exoskeleton design. However, this cannot be separated from other movements and quantified as its movement is innately paired with shoulder elevation. Extension is the only ROM requirement not met, this may due to a lack of data points in the testing set and pre-mature software limits. The resulting volume of the measured workspace was $0.00446m^3$, this satisfies the maximum workspace requirement of $0.5m^3$.

Table 8.2.1: Exoskeleton ROM comparison

ROM	Flexion	Extension	Abduction	Adduction	Internal Rotation	External Rotation
Specified	154°	74°	163°	5°	47.5°	86.5°
Achieved	157°	30°	177°	-°	90°	90°

8.3 Actuation Control

The exoskeleton control system can be likened to an assist-as need controller, where proportionally adjusted assistance is provided based on the effort outputted by the user. EMG muscle activation energy signals are recorded from the user by surface electrodes and hardware processed using an external EMG board [87]. The EMG values represent the desired torque output of the user's muscles, the amplitude of this can estimate the desired active joint angle, while the gradient of the signal can estimate the velocity. A simple P controller controls the motor speed. The implemented EMG-based control successfully detected muscle movement for each of the desired movements. The effects of the controller were verified visually and over a serial connection with the MCU. Fluctuations of RMS EMG signal when at the desired position, caused motor jitters and volatile movement of the motor. Further development is required to increase the accuracy and ensure the smooth motion of the assistive control, as defined in sections below.

8.4 Torque Profile

The Bowden system in series with the RMCS-2201 Rhino geared DC motors, successfully provided bi-directional actuation to the active joints. The force at the joints were measured using a SHUERLI HF500 digital force load gauge, which has a peak load of 5000N, 1N load diversion, and +-0.5% indication error [89]. The load gauge was mounted to the body of the exoskeleton in the direction of the active link trajectory. The active links were manually moved to 90° perpendicular to the load gauge, and a hook was used to pair the link to the gauge. Motor activation was controlled by the handheld joystick module and was set at a maximum motor speed of 25%. Readings were logged at 2Hz, with time starting from when the joystick is moved from rest. The test was executed until the failure of an element in the system or the recorded torque became constant, Figure 8.4.1 shows the results of this study.

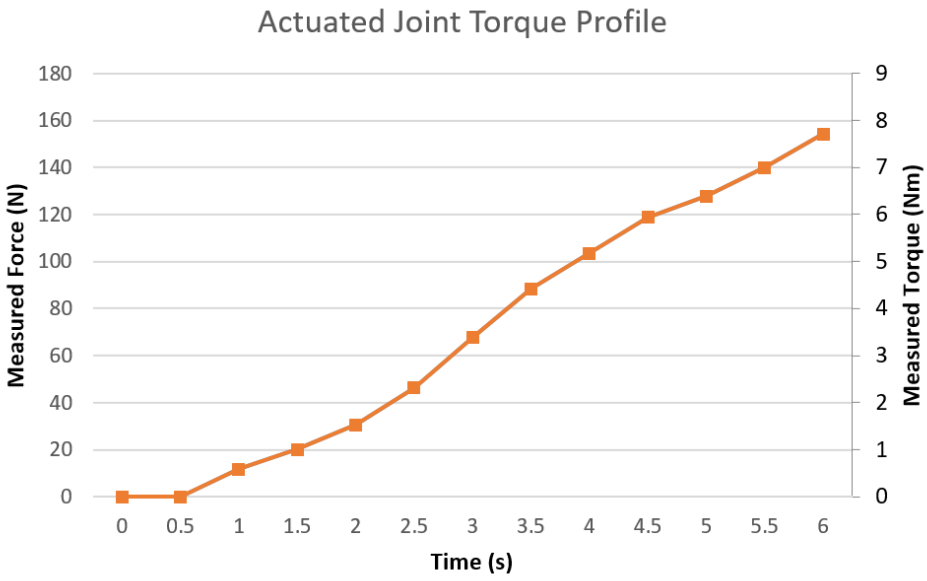

Figure 8.4.1: Plot of measured force/torque at actuated joints

The test was completed until the failure of an element in the system. The Bowden cable clamping hub mount failed. A weakness in the cable-motor holders wall thickness could not withstand the force and the cable was pulled through onto the motor wheel.

The force response of the actuated linkage has a relatively linear relationship, with a systematic increase of torque with time, to a peak of 7.71Nm. A time delay can be seen at the start of the testing set, the main contribution to this is looseness in the Bowden cable system. A delay in control to output motor actuation is a factor, however, this is negligible.

The peak recorded torque was lower than the rated torque of the motors (11.77 Nm). The lower torque is due to the gearing of the Bowden system, limited current supply, and motor not outputting rated torque. The testing set finished pre-maturely when the Bowden cable holding element in the system failed. The maximum applied torque could therefore not be achieved. To remedy this, the cable-motor holder internal wall thickness should be increased to 4mm and regular inspections of the clamping hubs screw tightness should be completed. The power supply used was set to 14.8V with a maximum 4A current output, where the DC motors are rated to 7.5A maximum current draw. Using the specified battery during use will result in a higher current draw being achieved if required. The Bowden cable system is not lossless, as friction along the internal length of the cable housing and in the pulley drive wheels adds losses to the system, this was minimised as outlined in Section 4.3.3. The total torque of the system could be increased by incorporating gear drive ratios.

The peak torque achieved was 7.71Nm at the actuated joints, which meets the requirements of the lower torque bracket (4.2Nm to 10.37Nm) as specified in Section 3.15. This applied torque was sufficient to actuate the arm against gravitational force, enabling assisted shoulder motion in flexion/extension and adduction/abduction. Testing indicated that shoulder actuation by the exoskeleton is achieved at much lover torques than this. Therefore, the exoskeleton meets the required specifications.

8.5 Further Discussion

8.5.1 Portability

Portability suggests that the device can be transferred from one place to another with relative ease. For a rehabilitation device, portability has many benefits in terms of rehabilitation environment restrictions, access to situational rehabilitation at home with ADLs, compliance, and user orientation adaptability. The exoskeleton will be reviewed against portability requirements.

Weight/Size: The exoskeleton is lightweight, with its arm unit weighing 500g and back unit weighing 3500g, for a total weight of 4kg. Larger loads are positioned distally on the backplate, whose force is distributed across the user's shoulders by padded yoke straps. It is worth noting that as the exoskeleton is for a single side, there is always going to be an imbalance of force. However, the inclusion of three different tightening straps minimises this by restricting the movement of the backplate, keeping it mounted in place. The motors were selected partially due to their low weight and size, with the Bowden cable system not adding any extraneous forces onto the body. The geometry of the links were optimised to increase the workspace of the exoskeletons end effector, while reducing the workspace of other joints/links, conforming movement around the human anatomy where possible. The resulting volume of the measured workspace was $0.00446m^3$, which is significantly lower than the required $0.5m^3$.

Power/Specialised Connections: The exoskeleton requires no external or specialised connections to operate. Although a DC power supply was used for testing, a 14.8V 4000mAh battery is specified to power the portable system, this was determined to last a suitable time for rehabilitation (30-90 minutes). All data gathering and control is implemented by a Teensy 3.5, and actuation by a DC motor Bowden cable system. None of these require any special connections (such as power supply, link to PC, air supply etc).

C Software: By using an embedded MCU, the reliance on any paid specialised software is eliminated. The MCU is programmed in C++ and edited in Atom (a free IDE), the micro USB port is extruded from the circuit board holder to allow open access to the control system so customisation of the open-source code can be done if desired.

Supervision requirements: Exoskeletons in reviewed literature required a supervisor/therapist operating the machine at all times, which limits the use of the machines to a hospital environment. This exoskeleton has been designed to be used independently, where self-tightening cuffs for the end effector attachment, mechanical flexion in linkages, and the body's low weight allow the unit to be easily applied without supervision. Mechanical and software stops ensure that the user does not experience any discomfort by exceeding their natural ROM, other safety measures are also in place.

8.5.2 Comfort and Safety

The system was designed to be compliant so that the user can move easily when wearing the exoskeleton. This acts as a safety measure and contributes to the comfort of the user, as the exoskeleton tolerates minor amounts of passive movement and fits the user easily.

Distally placed motors from the actuated joints help reduce weight and improve the comfort of the user. The weight/size of the exoskeleton is minimised in order to improve comfort. The dispersion of excess actuation torque onto the shoulders (which are structurally sound), and compliant exoskeleton-body attachment (cuffs), are also used to increase comfort for the user. Adjustable parameters are featured to align the exoskeletons to the skeletal frame of the user, aligning the GH joint centre with the three rotational DOF intersections. These adjustable parameters are featured in the form of; a lateral slider to increase/decrease the width of the device, multiple mounts for the linear sliding bearing, and various passive stop mounts to allow a varied ROM.

Passive physical stops to limit the ROM of all links, and software-enabled stops to

limit the joint angles for each actuated link of the exoskeleton were used. The joint velocities are also limited, and an interrupt-driven emergency stop toggle button is included on the handheld device as a safety measure.

8.6 Summary of Testing and Validation

A 5-DOF active upper-limb shoulder exoskeleton was developed, which did not restrict the motion of the shoulder, and provided sufficient torque to achieve controlled shoulder actuation. DC motor actuation in series with Bowden cable transmission, enables bi-directional movement of active revolute joints. Electrical, spring, and passive user force contribute to the successful actuation of the exoskeleton. The peak torque achieved was 7.71Nm at the actuated joints, meeting the requirements of the lower torque bracket (4.2Nm to 10.37Nm). This was sufficient to actuate the arm, enabling assisted shoulder motion for flexion/extension and adduction/abduction.

The ROM achieved by the exoskeleton was, 157° flexion, 30° extension and 177° abduction, with unrestrained internal/external passive motion. This satisfies most of the ROM requirements, With the exception being extension, which was 30° compared to the required 74°.

Portability requirements were met, with the exoskeleton being lightweight (4Kg) and having a small workspace volume of $0.00446m^3$. No external connections were required to control and power the exoskeleton. A 4000mAh battery provides power, and a Teensy 3.5 MCU provides control, both of which are mounted on the backplate of the exoskeleton. Sensory devices were used for control and safety feedback. Potentiometers were used to determine the position and velocity of the joints. IMUs were mounted for redundant measurements. The exoskeleton links were printed in PC, which is high strength and low weight. The displacement of the exoskeleton resulting from flex in the material, introduced a satisfactory level of compliance, which did not impede the functionality of the system.

The exoskeleton satisfied mostly all of the requirements defined in Section 3.15, with torque, compliance, portability, safety, and sensory requirements all being met. ROM requirements were all met, with the exception of extension.

9 Conclusion

This thesis detailed the research, design, construction, and testing of an upper-limb active shoulder exoskeleton for stroke rehabilitation. Research into the current state of rehabilitation practices showed that there are many approaches that can be adopted to assist rehabilitation efficiency and recovery time. Stroke rehabilitation robotics and exoskeletons were identified to have many benefits over traditional methods and other technology. This field has a range of approaches in terms of actuation, sensing, and control systems.

A kinematic model was developed to simplify the shoulder elements and discrete movements into key translations and rotations, whose links and DOFs will approximate the normal movement of the human subject allowing a full ROM. The Kinematic compatibility between the exoskeleton and the human model is essential to support the intricate motions of the shoulder complex, therefore sufficient DOFs were given to allow the alignment of critical joints/motions so its functionality mimics that of the shoulder while not over complicating the system. The kinematic model of the exoskeleton has been modelled as an open-loop chain encompassing from the centre of the torso out to the upper arm (Humerus). The GH joint allows the rotation of the humeral head and is approximated by three rotational joints which form a spherical assembly whose axes intercept with the centre of the humerus head. For the inner shoulder complex, The acromioclavicular sliding movement is modelled by a prismatic DOF while sternoclavicular elevation/depression is modelled by a rotational DOF connected to the centre of the torso. This joint allows a relative up/downwards movement from a distal rotational point. These DOFs accommodate for the translation of the GH joint and accommodates for any discrete shoulder complex movement.

The exoskeleton's mechanical design and build adopted an iterative cyclical development structure. CAD software was used to determine parameter values that result in a large ROM and adequate compliance to the human body. DH parameters were used to study the kinematics of the exoskeleton, with 60000 possible configurations of the exoskeleton analysed. Stress/displacement simulations were run on the complete exoskeleton assembly.This study indicated that between 55mm and 121mm of displacement could be expected at the end effector due to the flexion in the exoskele-

ton links. The 3D printed PC build of the exoskeleton arm provides high tensile strength while reducing weight, a 50% infill is used in these links to improve flexibility. All components were printed at a -45°/45° raster angle and in an orientation so that all applied loads act to the normal to the 3D printed fibres.

Motion tracking was used to verify the ROM of the exoskeleton by using reflective markers to distinguish points and rigid bodies on the exoskeleton and track their position in 3D space. The measured data and kinematic modelled data were plotted as a 3D convex hull. Flexion was measured to be 157°, extension 30°, and abduction 177°. The ROM measured from the motion tracking system was significantly lower of that of the kinematic model. The resulting volume of the modelled and measured workspaces were $0.0359m$ˆ3 and $0.00446m^3$ respectively. This satisfies the maximum workspace requirement of $0.5m^3$. The discrepancies in the volume are due to the size of the motion-tracked data set, mechanical flexion of the exoskeleton and unmodelled muscular constraints. Without muscular constraints, the kinematic model is able to reach physically unreachable, kinematically valid, exoskeleton configurations.

A Teensy 3.5 microcontroller is used to read sensor feedback, implement control, and provide a user interface. The exoskeleton was powered by a 14.8V 4000mAh battery and has an operating life of 45 to 90 minutes. Sensory feedback was provided by potentiometers measuring joint angle, with IMUs mounted for redundant measurements. DC motors (RMCS-2201, 11.7Nm) were chosen due to their exceptional torque to weight ratio, size, and minimal backlash. These were connected in series with a single wire Bowden cable transmission, allowing for the motors to be placed distally from the actuated joint and reducing any unwanted force (weight/motor torque) experienced by the user. The prismatic joint in the design of the exoskeleton was realized by a passive linear bearing, with a compression spring (6Nmm) to provide a restorative force. Torque measurements indicated that the actuated joints can provide up to 7.8Nm of torque. However, this was limited by failing components and maximum current draw. The applied torque was sufficient to actuate and hold the arm against gravitational torque, enabling assisted shoulder motion in flexion/extension and adduction/abduction. Testing indicated that shoulder actuation was achieved at much lower torques than this.

The exoskeleton control system can be likened to an assist-as need controller, where

proportionally adjusted assistance is provided based on the effort outputted by the user. EMG muscle activation energy signals are gathered via surface electrodes and hardware processed using an external EMG board. The amplitude of the EMG data is used to indicate the desired active joint angle while the gradient of the EMG rising signal is used to determine the motor speed. An EMG study was completed to determine the characteristics of the AD, MD, PD, UT, LT, SA, TM muscles during shoulder flexion/extension, adduction/abduction, internal/external rotation and at rest, the results of which were used to determine which were suitable for EMG control. The UT and PD were determined to be suitable for control, with the PD selected due to its lack of activity for shoulder internal/external rotation and its high median activation characteristics across all movements.

BITERS successfully modelled the human shoulder motion and allowed for the active actuation of the shoulder with DC motor actuation and Bowden cable transmission. Both manual control and EMG based control were implemented by software-based assist-as-need P control. Validation of the exoskeletons ROM was successfully performed through the use of CAD simulation, kinematic workspace analysis, and 3D motion tracking technology.

10 Further Developments

Assist-as-need like control was implemented in principle. Further development of the signal processing and control architecture is required to provide a more "true" assist-as-need control. P position control is used for assistive control. However, the controller could be improved by using force output/input rather than desired trajectory as control inputs. This proportional model assumed that EMG signal amplitude can be used to estimate the desired position and speed of the user, from a measure of subjects effort. The mathematical relationships which model these relationships will alter with electrode placement and between users. The inclusion of output actuation torque and a measure of the subject effort/force will allow more advantageous assist-as-need control. Additionally, EMG based frequency spectrum testing should be conducted and applied to give a measure of subject fatigue. A second set of electrodes on the EMG hardware, would enable simultaneous fully autonomous movement in flexion/extension and adduction/abduction.

SEAs could be introduced into the Bowden drive system to achieve a greater level of system compliance and smoother bi-directional movement. The distortion of an SEA on the actuator can be used to estimate the torque applied to the system for control and safety measures, which could applied to assist-as-need control. Self-tightening, spring tension, or additional load sensing would improve the Bowden cable system. The inclusion of gear ratios on the Bowden wheels, or a higher torque motor, would increase the achievable torque. The application of pneumatic air to the restraining cuff should be investigated for potential benefits to the user.

Further investigation into the relationship between link flexion, applied force, and printing density would be beneficial towards estimating the ultimate exoskeleton flex. User feedback on variable compliance in the system would provide an applied insight into the required flex.

IMUs were mounted on the exoskeleton. The purpose of these IMUs was to provide an absolute position of the exoskeleton in 3D space, as tilt, height, speed, displacement and more could be determined software based signal processing and triangulation. These would also be used as a redundant sensor for joint rotation. Hardware, electronics and software were developed for the IMUs, but these were not imple-

mented on the final design. The LCD screen could be utilised for further user interaction with more complex visual-based tasks. Interactive visual tasks have shown to increase patient interaction during rehabilitation [27].

References

[1] "The social and economic costs of stroke in New Zealand - NZIER report to the Stroke Foundation," *Stroke Foundation*, 2018.

[2] G. Miss.B.M.Gund, "Stroke: A Brain Attack," *IOSR J. Pharm. IOSRPHR*, vol. 03, no. 08, pp. 01–23,, 2013.

[3] *Stroke (Brain attack*. Mayfield Clinic, Apr. 2019.

[4] C. Lang, M. Bland, R. Bailey, S. Schaefer, and R. Birkenmeier, "Assessment of upper extremity impairment, function, and activity after stroke: foundations for clinical decision making," *J. Hand Ther*, vol. 26, no. 2, pp. 104–115,, Apr. 2013.

[5] C. English, H. McLennan, K. Thoirs, A. Coates, and J. Bernhardt, "Loss of Skeletal Muscle Mass after Stroke: a Systematic Review," *Int. J. Stroke*, vol. 5, no. 5, pp. 395–402,, Oct. 2010.

[6] C. Hafer-Macko, "Skeletal muscle changes after hemiparetic stroke and potential beneficial effects of exercise intervention strategies," *J. Rehabil. Res. Dev*, vol. 45, no. 2, pp. 261–272,, Dec. 2008.

[7] S. Kessner, U. Bingel, and G. Thomalla, "Somatosensory deficits after stroke: a scoping review," *Top. Stroke Rehabil*, vol. 23, no. 2, pp. 136–146,, Feb. 2016.

[8] L. Carey, T. Matyas, and C. Baum, "Effects of Somatosensory Impairment on Participation After Stroke," *Am. J. Occup. Ther*, vol. 72, no. 3, pp. 7 203 205 100 1,, Apr. 2018.

[9] S. Hatem, "Rehabilitation of Motor Function after Stroke: A Multiple Systematic Review Focused on Techniques to Stimulate Upper Extremity Recovery," *Front. Hum. Neurosci*, vol. 10, Sep. 2016.

[10] "Hemiplegic Shoulder Subluxation," *Physiopedia*.

[11] M. E. Mlinac and M. C. Feng, "Assessment of Activities of Daily Living, Self-Care, and Independence," *Archives of Clinical Neuropsy-*

chology, vol. 31, no. 6, pp. 506–516, Sep. 2016. [Online]. Available: https://academic.oup.com/acn/article-lookup/doi/10.1093/arclin/acw049

[12] P. F. Edemekong, D. L. Bomgaars, S. Sukumaran, and S. B. Levy, "Activities of Daily Living (ADLs)," p. 9.

[13] D. H. Gates, L. S. Walters, J. Cowley, J. M. Wilken, and L. Resnik, "Range of Motion Requirements for Upper-Limb Activities of Daily Living," *American Journal of Occupational Therapy*, vol. 70, no. 1, p. 7001350010p1, Dec. 2015. [Online]. Available: http://ajot.aota.org/article.aspx?doi=10.5014/ajot.2016.015487

[14] N. Bayona, J. Bitensky, K. Salter, and R. Teasell, "The Role of Task-Specific Training in Rehabilitation Therapies," *Top. Stroke Rehabil*, vol. 12, no. 3, pp. 58–65,, Jul. 2005.

[15] R. Riener, T. Nef, and G. Colombo, "Robot-aided neurorehabilitation of the upper extremities," *Med. Biol. Eng. Comput*, vol. 43, no. 1, pp. 2–10,, Feb. 2005.

[16] M. Dimyan and L. Cohen, "Neuroplasticity in the context of motor rehabilitation after stroke," *Nat. Rev. Neurol*, vol. 7, no. 2, pp. 76–85,, Feb. 2011.

[17] S. SAVAfi and S. AKKUfi, "Impact of Delayed Initiation to Stroke Rehabilitation on Functional Outcomes and Medical Complications," *Stroke Rehabil*, p. 5.

[18] L. Sheffler and J. Chae, "Neuromuscular electrical stimulation in neurorehabilitation," *Muscle Nerve*, vol. 35, no. 5, pp. 562–590,, May 2007.

[19] K. Allen and C. Goodman, "Using Electrical Stimulation," *Sydney Local Health District and Royal Rehabilitation Centre*, 2014.

[20] A. S. Gorgey, C. D. Black, C. P. Elder, and G. A. Dudley, "Effects of Electrical Stimulation Parameters on Fatigue in Skeletal Muscle," *Journal of Orthopaedic & Sports Physical Therapy*, vol. 39, no. 9, pp. 684–692, Sep. 2009. [Online]. Available: http://www.jospt.org/doi/10.2519/jospt.2009.3045

[21] S. Shim and J. Jung, "Effects of bilateral training on motor function, amount of activity and activity intensity measured with an accelerometer of patients with stroke," *J. Phys. Ther. Sci*, vol. 27, no. 3, pp. 751–754,, 2015.

[22] P. Langhorne, J. Bernhardt, and G. Kwakkel, "Stroke rehabilitation," *The Lancet*, vol. 377, no. 9778, pp. 1693–1702,, May 2011.

[23] C. Wu, C. Yang, M. Chen, K. Lin, and L. Wu, "Unilateral versus bilateral robot-assisted rehabilitation on arm-trunk control and functions post stroke: a randomized controlled trial," *J. NeuroEngineering Rehabil*, vol. 10, no. 1, pp. 35,, 2013.

[24] M. Stoykov, G. Lewis, and D. Corcos, "Comparison of Bilateral and Unilateral Training for Upper Extremity Hemiparesis in Stroke," *Neurorehabil. Neural Repair*, vol. 23, no. 9, pp. 945–953,, Nov. 2009.

[25] Z. Guerra, A. Lucchetti, and G. Lucchetti, "Motor Imagery Training After Stroke: A Systematic Review and Meta-analysis of Randomized Controlled Trials," *J. Neurol. Phys. Ther*, vol. 41, no. 4, pp. 205–214,, Oct. 2017.

[26] N. Sharma, V. Pomeroy, and J.-C. Baron, "Motor Imagery: A Backdoor to the Motor System After Stroke?" *Stroke*, vol. 37, no. 7, pp. 1941–1952,, Jul. 2006.

[27] K. Laver, B. Lange, S. George, J. Deutsch, G. Saposnik, and M. Crotty, "Virtual reality for stroke rehabilitation," *Cochrane Database Syst. Rev*, Nov. 2017.

[28] D. Corbetta, F. Imeri, and R. Gatti, "Rehabilitation that incorporates virtual reality is more effective than standard rehabilitation for improving walking speed, balance and mobility after stroke: a systematic review," *Journal of Physiotherapy*, vol. 61, no. 3, pp. 117–124, Jul. 2015. [Online]. Available: https://linkinghub.elsevier.com/retrieve/pii/S1836955315000569

[29] H. Thieme, "Mirror therapy for improving motor function after stroke," *Cochrane Database Syst. Rev*, Jul. 2018.

[30] A. Pollock, S. E. Farmer, M. C. Brady, P. Langhorne, G. E. Mead, J. Mehrholz, and F. van Wijck, "Interventions for improving upper limb function after stroke," *Cochrane Database of Systematic Reviews*, Nov. 2014. [Online]. Available: http://doi.wiley.com/10.1002/14651858.CD010820.pub2

[31] A. Prochazka, V. Mushahwar, and D. McCreery, "Neural prostheses," *Journal of Physiology*, vol. 533, pp. 99–107, Sep. 2001.

[32] *Human Physiology/The Muscular System*. N/A.

[33] J. Li, Z. Zhang, C. Tao, and R. Ji, "A number synthesis method of the self-adapting upper-limb rehabilitation exoskeletons," *Int. J. Adv. Robot. Syst*, vol. 14, no. 3, pp. 172 988 141 771 079,, May 2017.

[34] T. O. . P. V. Library, "Anatomical Movements Related to Upper Extremity Prosthetics." [Online]. Available: http://www.oandplibrary.org/reference/uclamanual/UCLA-02.pdf

[35] R. R. Inawat, "Kinematic Analysis of the Glenohumeral Joint: A Comparison of Post-Operative Rotator Cuff Repair Patients and Controls," p. 114.

[36] P. Lindberg, C. Schmitz, H. Forssberg, M. Engardt, and J. Borg, "Effects of passive-active movement training on upper limb motor function and cortical activation in chronic patients with stroke: a pilot study," *Journal of Rehabilitation Medicine*, vol. 36, no. 3, pp. 117–123, May 2004. [Online]. Available: https://medicaljournals.se/jrm/content/abstract/10.1080/16501970410023434

[37] P. L. Cheng and M. Pearcy, "A three-dimensional definition for the flexion/extension and abduction/adduction angles," *Biological Engineering*, vol. 37, p. 5, 1999.

[38] H. M. Vermeulen, "Measurement of three dimensional shoulder movement patterns with an electromagnetic tracking device in patients with a frozen shoulder," *Annals of the Rheumatic Diseases*, vol. 61, no. 2, pp. 115–120, Feb. 2002. [Online]. Available: http://ard.bmj.com/cgi/doi/10.1136/ard.61.2.115

[39] J. Dougherty, S. Walmsley, and P. G. Osmotherly, "Passive Range of Movement of the Shoulder: A Standardized Method for Measurement and Assessment of Intrarater Reliability," *Journal of Manipulative and Physiological Therapeutics*, vol. 38, no. 3, pp. 218–224, Mar. 2015. [Online]. Available: https://linkinghub.elsevier.com/retrieve/pii/S0161475414002711

[40] N. McLauren, "Glenohumeral joint," Sep. 2020. [Online]. Available: https://www.kenhub.com/en/library/anatomy/the-shoulder-joint

[41] C. J. Barnes, S. J. Van Steyn, and R. A. Fischer, "The effects of age, sex, and shoulder dominance on range of motion of the shoulder," *Journal of Shoulder*

and Elbow Surgery, vol. 10, no. 3, pp. 242–246, May 2001. [Online]. Available: https://linkinghub.elsevier.com/retrieve/pii/S1058274601224070

[42] I. A. Murray and G. R. Johnson, "A study of the external forces and moments at the shoulder and elbow while performing every day tasks," *Clinical Biomechanics*, vol. 19, no. 6, pp. 586–594, Jul. 2004. [Online]. Available: https://linkinghub.elsevier.com/retrieve/pii/S0268003304000531

[43] physiopedia, "Acromioclavicular Joint." [Online]. Available: https://www.physio-pedia.com

[44] K.-S. Lee, J.-H. Park, J. Beom, and H.-S. Park, "Design and Evaluation of Passive Shoulder Joint Tracking Module for Upper-Limb Rehabilitation Robots," *Frontiers in Neurorobotics*, vol. 12, p. 38, Jul. 2018. [Online]. Available: https://www.frontiersin.org/article/10.3389/fnbot.2018.00038/full

[45] P. de Leva, "Adjustments to Zatsiorsky-Seluyanov's segment inertia parameters," *J. Biomech*, vol. 29, no. 9, pp. 1223–1230, 1996. [Online]. Available: http://bipop.inrialpes.fr/software/private/deleva.pdf

[46] R. Krishnan, N. Björsell, E. M. Gutierrez-Farewik, and C. Smith, "A survey of human shoulder functional kinematic representations," *Medical & Biological Engineering & Computing*, vol. 57, no. 2, pp. 339–367, Feb. 2019. [Online]. Available: http://link.springer.com/10.1007/s11517-018-1903-3

[47] P. Cordo, L. Carlton, L. Bevan, M. Carlton, and G. K. Kerr, "Proprioceptive coordination of movement sequences: role of velocity and position information," *Journal of Neurophysiology*, vol. 71, no. 5, pp. 1848–1861, 1994, _eprint: https://doi.org/10.1152/jn.1994.71.5.1848. [Online]. Available: https://doi.org/10.1152/jn.1994.71.5.1848

[48] J. Yang, X. Feng, J. H. Kim, and S. Rajulu, "Review of biomechanical models for human shoulder complex," *International Journal of Human Factors Modelling and Simulation*, vol. 1, no. 3, p. 271, 2010. [Online]. Available: http://www.inderscience.com/link.php?id=36791

[49] J. Lenarcic and A. Umek, "Simple model of human arm reachable workspace," *IEEE Transactions on Systems, Man, and Cybernetics*, vol. 24, no. 8, pp. 1239–1246, Aug. 1994. [Online]. Available: http://ieeexplore.ieee.org/document/299704/

[50] J. Yang, K. Abdel-Malek, and K. Nebel, "Reach Envelope of a 9-Degree-of Freedom Model of the Upper Extremity," *International Journal of Robotics and Automation*, vol. 20, no. 4, 2005. [Online]. Available: http://www.actapress.com/PaperInfo.aspx?paperId=22192

[51] J. Yang, "SWEPT VOLUMES: THEORY AND IMPLEMENTATIONS," p. 172.

[52] J. Li, C. Zhang, M. Dong, and Q. Cao, "A Kinematic Model of the Shoulder Complex Obtained from a Wearable Detection System," *Applied Sciences*, vol. 10, no. 11, p. 3696, May 2020. [Online]. Available: https://www.mdpi.com/2076-3417/10/11/3696

[53] J. Lenarcic and M. Stanisic, "A humanoid shoulder complex and the humeral pointing kinematics," *IEEE Transactions on Robotics and Automation*, vol. 19, no. 3, pp. 499–506, Jun. 2003. [Online]. Available: http://ieeexplore.ieee.org/document/1206810/

[54] S. T. Tumer and A. E. Engin, "Three-Dimensional Kinematic Modelling of the Human Shoulder Complex—Part II: Mathematical Modelling and Solution Via Optimization," *Journal of Biomechanical Engineering*, vol. 111, no. 2, pp. 113–121, May 1989. [Online]. Available: https://asmedigitalcollection.asme.org/biomechanical/article/111/2/113/396812/ThreeDime
Kinematic-Modelling-of-the-Human

[55] R. Suhaimi, "Analysis of EMG-based muscles activity for stroke rehabilitation," in *2014 2nd International Conference on Electronic Design (ICED), Penang*, Malaysia, 2014, pp. 167–170.

[56] J. Cram and G. Kasman, *THE BASICS OF SURFACE ELECTROMYOGRAPHY*.

[57] O. Alizadehkhaiyat, D. H. Hawkes, G. J. Kemp, and S. P. Frostick, "ELECTROMYOGRAPHIC ANALYSIS OF SHOULDER GIRDLE MUSCLES DURING COMMON INTERNAL ROTATION EXERCISES," p. 10.

[58] B. S Rajaratnam, "A Comparison of EMG Signals from Surface and Fine-Wire Electrodes During Shoulder Abduction," *International Journal of Physical Medicine & Rehabilitation*, vol. 02, no. 04, 2014. [Online].

Available: https://www.omicsonline.org/open-access/a-comparison-of-emg-signals-from-surface-and-finewire-electrodes-during-shoulder-abduction-2329-9096.1000206.php?aid=28555

[59] D. Wattanaprakornkul, M. Halaki, C. Boettcher, I. Cathers, and K. A. Ginn, "A comprehensive analysis of muscle recruitment patterns during shoulder flexion: An electromyographic study," *Clinical Anatomy*, vol. 24, no. 5, pp. 619–626, Jul. 2011. [Online]. Available: http://doi.wiley.com/10.1002/ca.21123

[60] S. Wolf, A. Butler, J. Alberts, and M. Kim, "Contemporary linkages between EMG, kinetics and stroke rehabilitation," *J. Electromyogr. Kinesiol*, vol. 15, no. 3, pp. 229–239,, Jun. 2005.

[61] T. Bosch, J. van Eck, K. Knitel, and M. de Looze, "The effects of a passive exoskeleton on muscle activity, discomfort and endurance time in forward bending work," *Applied Ergonomics*, vol. 54, pp. 212–217, May 2016. [Online]. Available: https://linkinghub.elsevier.com/retrieve/pii/S0003687015301241

[62] H. Najam, B. Bal, and R. Ünal, "MATERIAL SELECTION FOR KNEE EXOSKELETON FRAME," p. 8, 2018.

[63] J. Cantrell, S. Rohde, D. Damiani, R. Gurnani, L. DiSandro, J. Anton, A. Young, A. Jerez, D. Steinbach, C. Kroese, and P. Ifju, "Experimental Characterization of the Mechanical Properties of 3D-Printed ABS and Polycarbonate Parts," p. 19.

[64] N. G. Tanikella, B. Wittbrodt, and J. M. Pearce, "Tensile strength of commercial polymer materials for fused filament fabrication 3D printing," *Additive Manufacturing*, vol. 15, pp. 40–47, May 2017. [Online]. Available: https://linkinghub.elsevier.com/retrieve/pii/S2214860416300859

[65] L. Cappello, Dinh Khanh Binh, Shih-Cheng Yen, and L. Masia, "Design and preliminary characterization of a soft wearable exoskeleton for upper limb," in *2016 6th IEEE International Conference on Biomedical Robotics and Biomechatronics (BioRob)*. Singapore, Singapore: IEEE, Jun. 2016, pp. 623–630. [Online]. Available: http://ieeexplore.ieee.org/document/7523695/

[66] B. K. Dinh, M. Xiloyannis, L. Cappello, C. W. Antuvan, S.-C. Yen, and L. Masia, "Adaptive backlash compensation in upper limb soft wearable exoskeletons,"

Robotics and Autonomous Systems, vol. 92, pp. 173–186, Jun. 2017. [Online]. Available: https://linkinghub.elsevier.com/retrieve/pii/S0921889016303591

[67] B. K. Dinh, M. Xiloyannis, C. W. Antuvan, L. Cappello, and L. Masia, "Hierarchical Cascade Controller for Assistance Modulation in a Soft Wearable Arm Exoskeleton," *IEEE Robotics and Automation Letters*, vol. 2, no. 3, pp. 1786–1793, Jul. 2017. [Online]. Available: http://ieeexplore.ieee.org/document/7855728/

[68] U. Jeong and K.-J. Cho, "Feedforward friction compensation of Bowden-cable transmission via loop routing," in *2015 IEEE/RSJ International Conference on Intelligent Robots and Systems (IROS)*. Hamburg, Germany: IEEE, Sep. 2015, pp. 5948–5953. [Online]. Available: http://ieeexplore.ieee.org/document/7354223/

[69] C. O'Neill, N. Phipps, L. Cappello, S. Paganoni, and C. Walsh, "A soft wearable robot for the shoulder: Design, characterization, and preliminary testing," in *2017 International Conference on Rehabilitation Robotics (ICORR*, London, 2017, pp. 1672–1678.

[70] J. Lu, K. Haninger, W. Chen, S. Gowda, M. Tomizuka, and J. Carmena, "Design of a Passive Upper Limb Exoskeleton for Macaque Monkeys," *J. Dyn. Syst. Meas. Control*, vol. 138, no. 11, pp. 111 011,, Jul. 2016.

[71] R. Soltani-Zarrin, A. Zeiaee, A. Eib, R. Langari, and R. Tafreshi, *CLEVERarm: A Novel Exoskeleton for Rehabilitation of Upper Limb Impairments*.

[72] A. Zeiaee, R. Soltani-Zarrin, R. Langari, and R. Tafreshi, "Design and kinematic analysis of a novel upper limb exoskeleton for rehabilitation of stroke patients," in *2017 International Conference on Rehabilitation Robotics (ICORR*, London, 2017, pp. 759–764.

[73] J. Perry, J. Rosen, and S. Burns, "Upper-Limb Powered Exoskeleton Design," *IEEEASME Trans. Mechatron*, vol. 12, no. 4, pp. 408–417,, Aug. 2007.

[74] B. Kim and A. D. Deshpande, "An upper-body rehabilitation exoskeleton Harmony with an anatomical shoulder mechanism: Design, modeling, control, and performance evaluation," *The International Journal of Robotics Research*, vol. 36, no. 4, pp. 414–435, Apr. 2017. [Online]. Available: http://journals.sagepub.com/doi/10.1177/0278364917706743

[75] H.-C. Hsieh, D.-F. Chen, L. Chien, and C.-C. Lan, "Design of a Parallel Actuated Exoskeleton for Adaptive and Safe Robotic Shoulder Rehabilitation," *IEEE/ASME Transactions on Mechatronics*, vol. 22, no. 5, pp. 2034–2045, Oct. 2017. [Online]. Available: http://ieeexplore.ieee.org/document/7954711/

[76] T. Nef, M. Mihelj, and R. Riener, "ARMin: a robot for patient-cooperative arm therapy," *Medical & Biological Engineering & Computing*, vol. 45, no. 9, pp. 887–900, Sep. 2007. [Online]. Available: http://link.springer.com/10.1007/s11517-007-0226-6

[77] T. Nef, M. Guidali, and R. Riener, "ARMin III – arm therapy exoskeleton with an ergonomic shoulder actuation," *Applied Bionics and Biomechanics*, vol. 6, no. 2, pp. 127–142, Jul. 2009. [Online]. Available: http://content.iospress.com/doi/10.1080/11762320902840179

[78] G. Andrikopoulos, G. Nikolakopoulos, and S. Manesis, "A Survey on applications of Pneumatic Artificial Muscles," in *2011 19th Mediterranean Conference on Control & Automation (MED)*. Corfu, Greece: IEEE, Jun. 2011, pp. 1439–1446. [Online]. Available: http://ieeexplore.ieee.org/document/5982983/

[79] M. N. Castro, J. Rasmussen, M. S. Andersen, and S. Bai, "A compact 3-DOF shoulder mechanism constructed with scissors linkages for exoskeleton applications," *Mechanism and Machine Theory*, vol. 132, pp. 264–278, Feb. 2019. [Online]. Available: https://linkinghub.elsevier.com/retrieve/pii/S0094114X18313430

[80] "Technical Data Sheet: Prusament PC Blend by Prusa Polymers." [Online]. Available: https://shop.prusa3d.com

[81] "Deflection of Beams." [Online]. Available: https://notendur.hi.is/ mvg1/09-01ChapGere.pdf

[82] R. M. Controls, "RMCS220x DCServo Driver Manual." [Online]. Available: https://robokits.download/downloads/RMCS220x

[83] D. Systems, "Introduction to Motion Studies: Degrees of Freedom." [Online]. Available: http://help.solidworks.com/2018/english/solidworks/motionstudies

[84] "Decoupling Techniques," 2019. [Online]. Available: https://www.analog.com/media/en/training-seminars/tutorials/MT-101.pdf

[85] J. Blom, "Capacitors." [Online]. Available: https://learn.sparkfun.com/tutorials/capacitors/application-examples

[86] R. Keim, "PCB Layout Tips and Tricks," Nov. 2018. [Online]. Available: https://www.allaboutcircuits.com/technical-articles/pcb-layout-tips-and-tricks-use-a-ground-plane-whenever-possible

[87] B. C. Fortune, A. Stewart, E. Hansenne, L. McKenzie, L. Chatfield, and C. G. Pretty, "Design and testing of a low-cost electromyogram that uses a right leg driver circuit," in *2017 24th International Conference on Mechatronics and Machine Vision in Practice (M2VIP)*. Auckland: IEEE, Nov. 2017, pp. 1–6. [Online]. Available: http://ieeexplore.ieee.org/document/8211490/

[88] M. G. a and T. Vieira, "Surface electromyography: Why, when and how to use it," *Sci. Inf. Syst. Netw. Sci. J*, vol. 4, pp. 17–28,, 2011.

[89] "DIGITAL FORCE GAUGE MANUAL." [Online]. Available: http://doc.diytrade.com/docdvr/1280161/25623445/1335232495.pdf

11 Appendix

A 3D Rendering

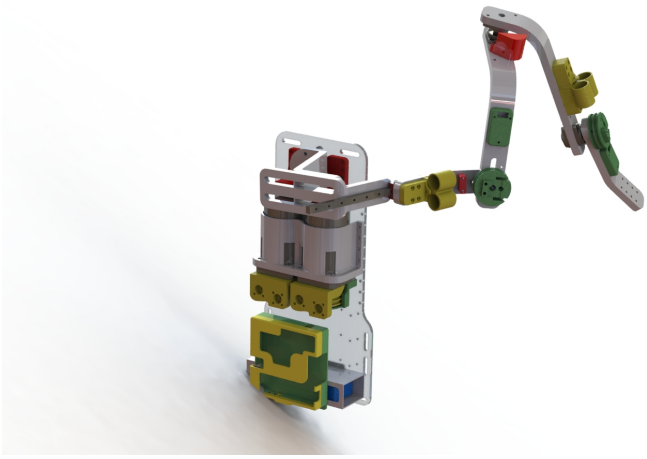

Figure A.0.1: Final CAD render of BITERS: back view

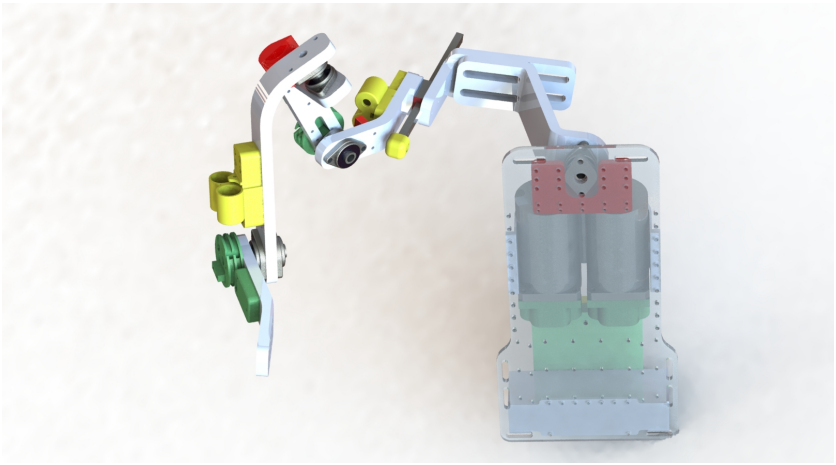

Figure A.0.2: Final CAD render of BITERS: front view

B DH Coordinates

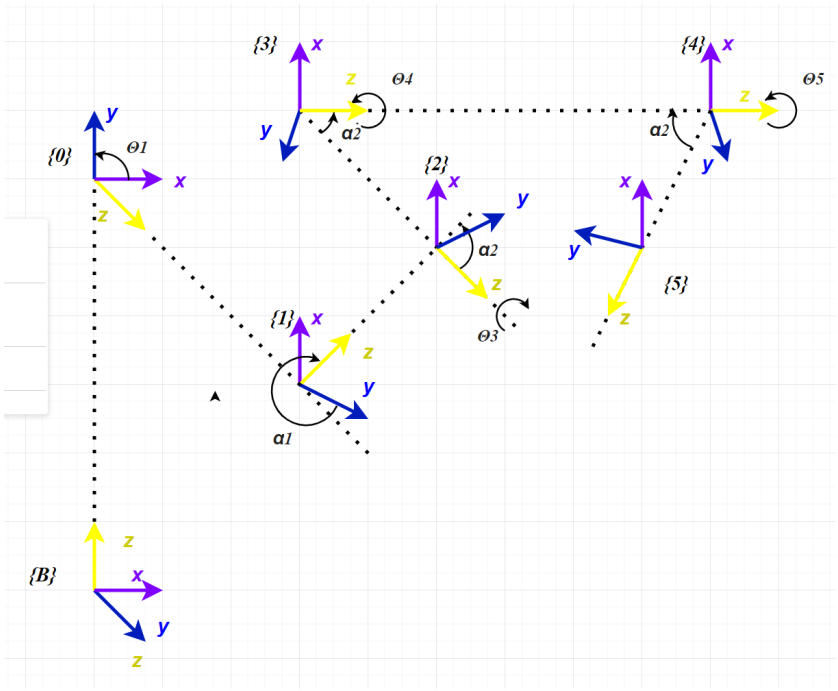

Figure B.0.1: DH coordinate axes in free space

C Modelled Workspace

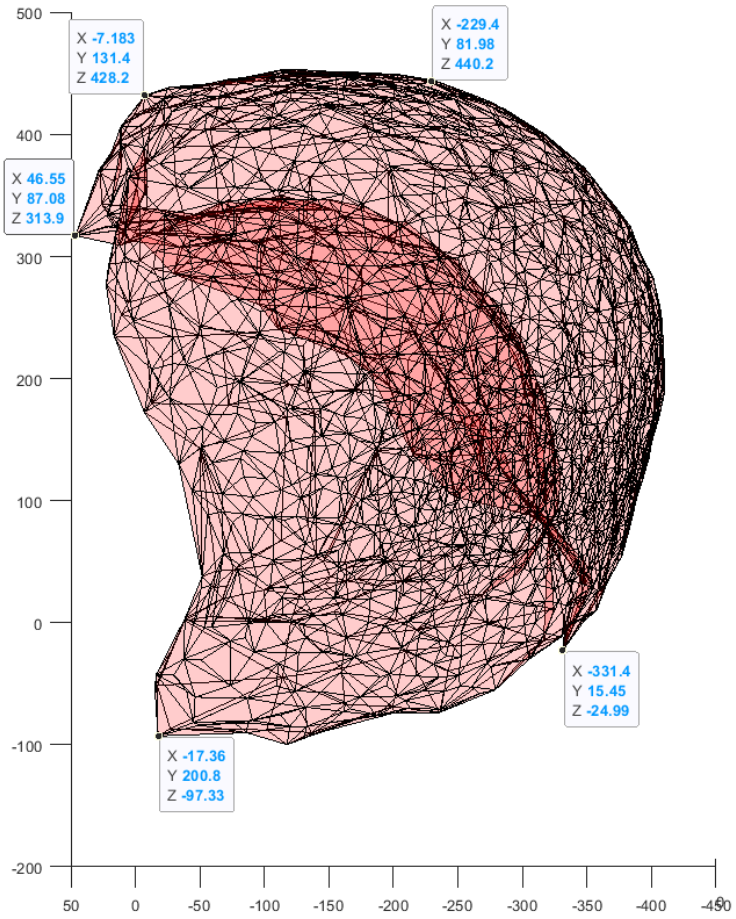

Figure C.0.1: Top view of modelled exoskeleton workspace

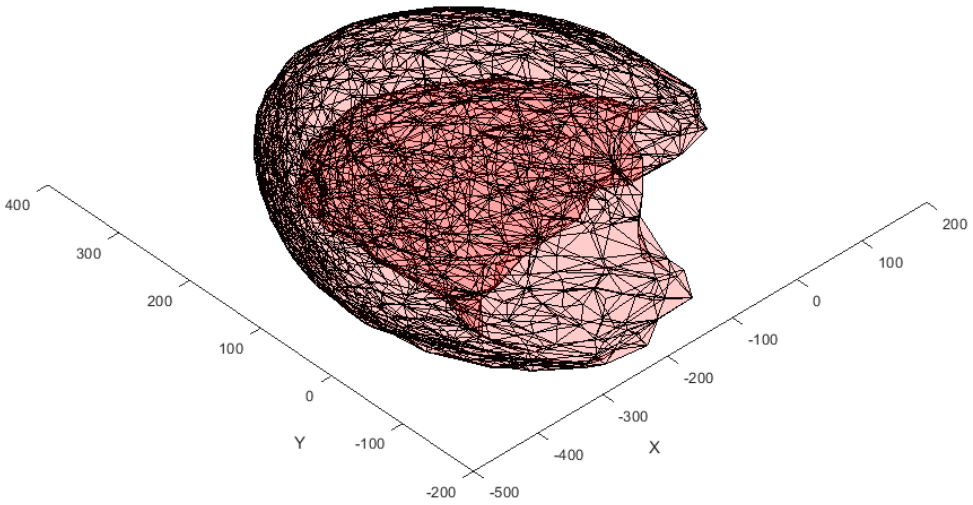

Figure C.0.2: modelled parameter model workspace convex hull

D Node positioning

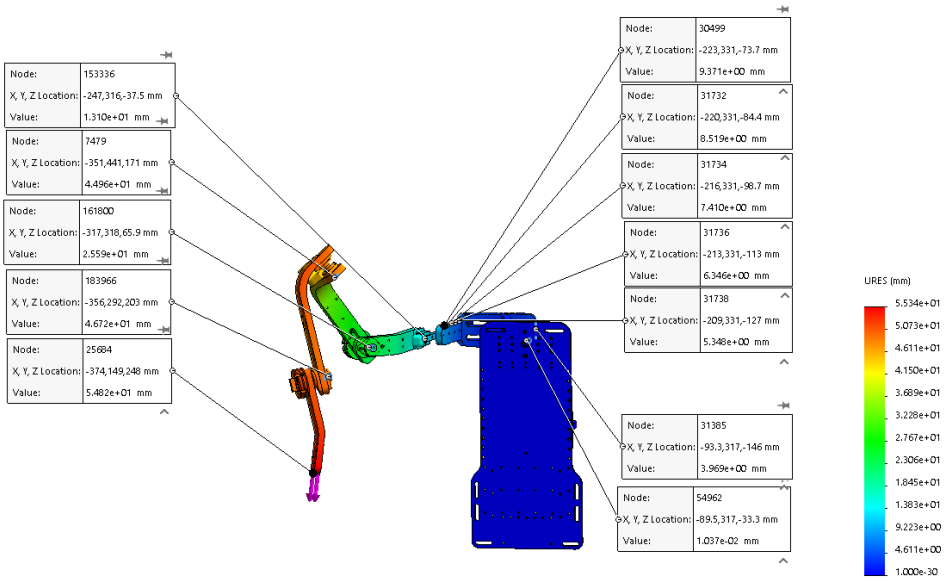

Figure D.0.1: Node positioning for 30N and 60N displacement simulations

E Additional Figures from Optitrack analysis

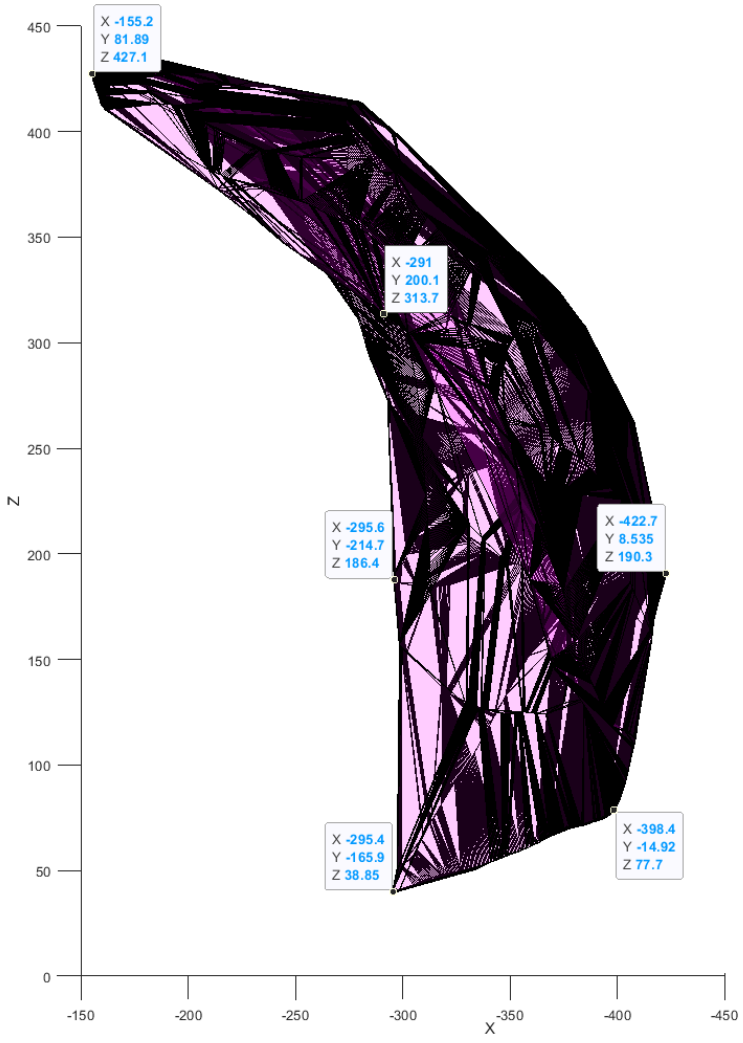

Figure E.0.1: Measured exoskeleton workspace - top view

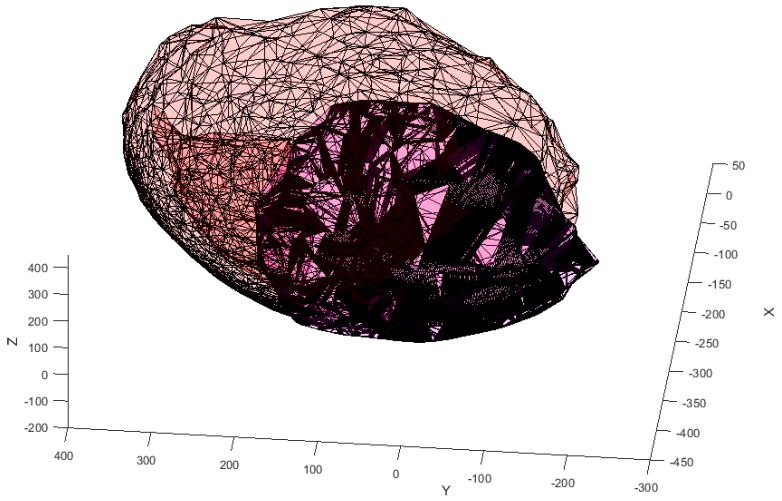

Figure E.0.2: Measured and modelled work-space comparison - 3D view

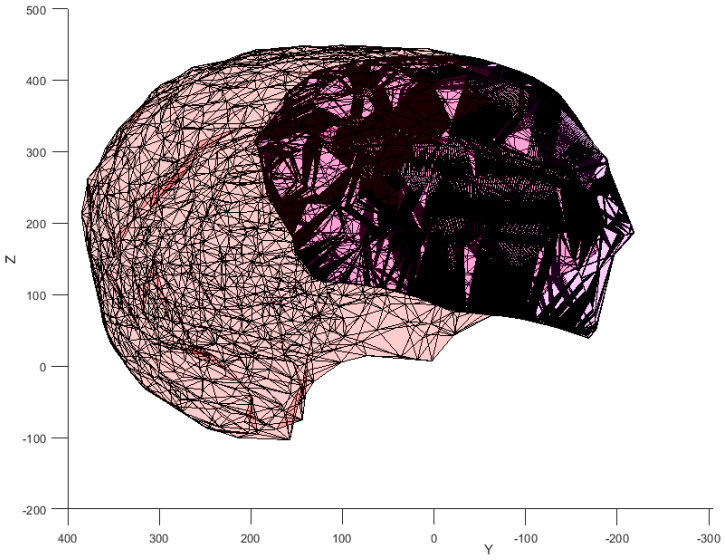

Figure E.0.3: Measured and modelled work-space comparison - side view

F Electrical Schematics

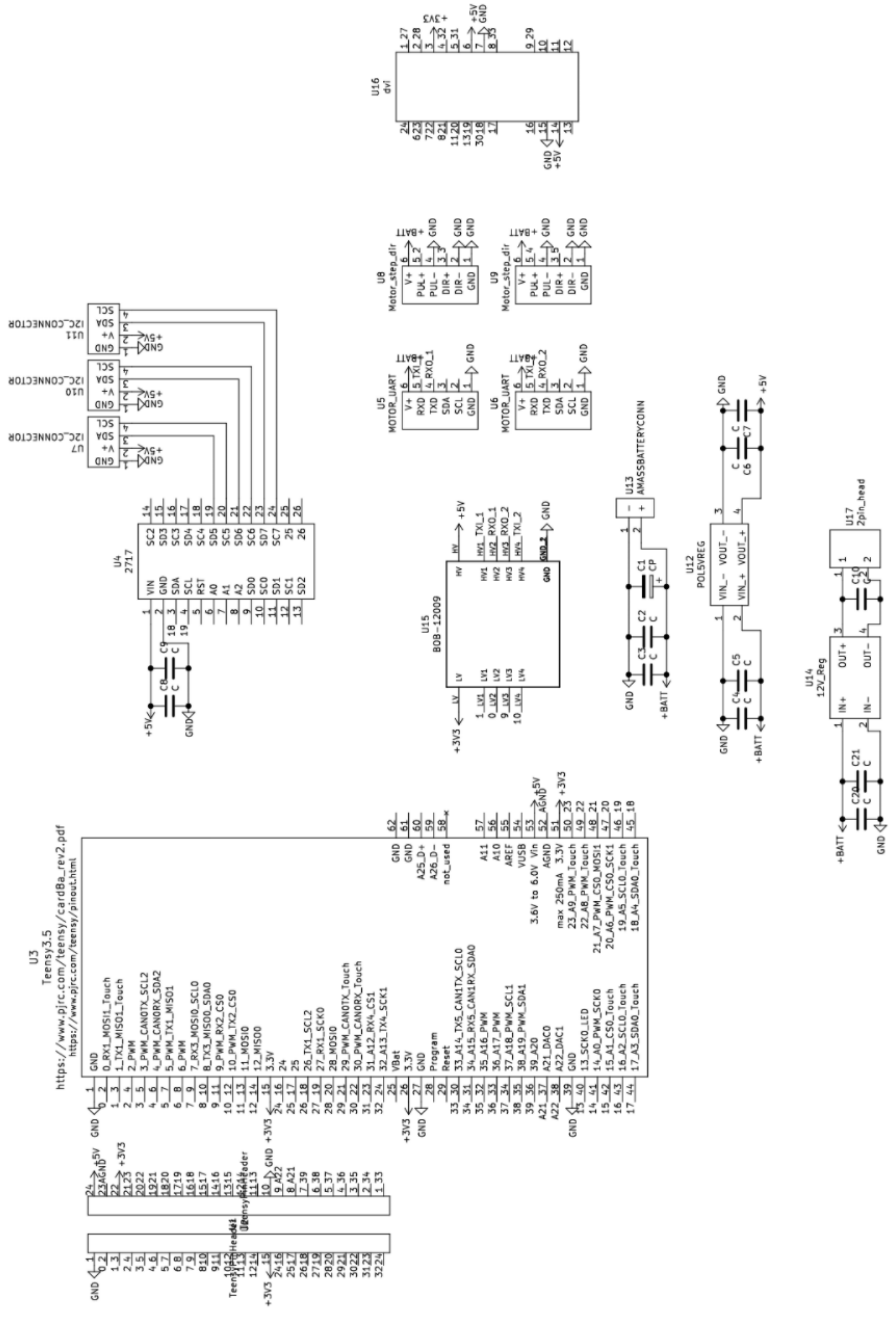

Figure F.0.1: Main circuit schematic

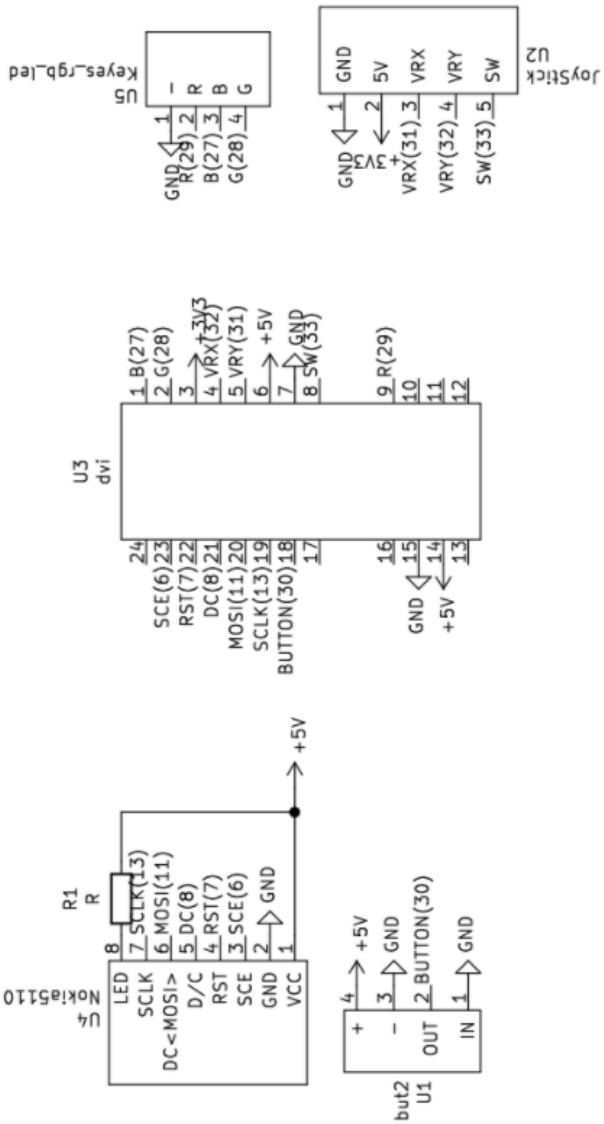

Figure F.0.2: Hand circuit schematic

G Additional Figures of Exoskeleton

Figure G.0.1: Mounted exoskeleton returning to rest from flexion: no load

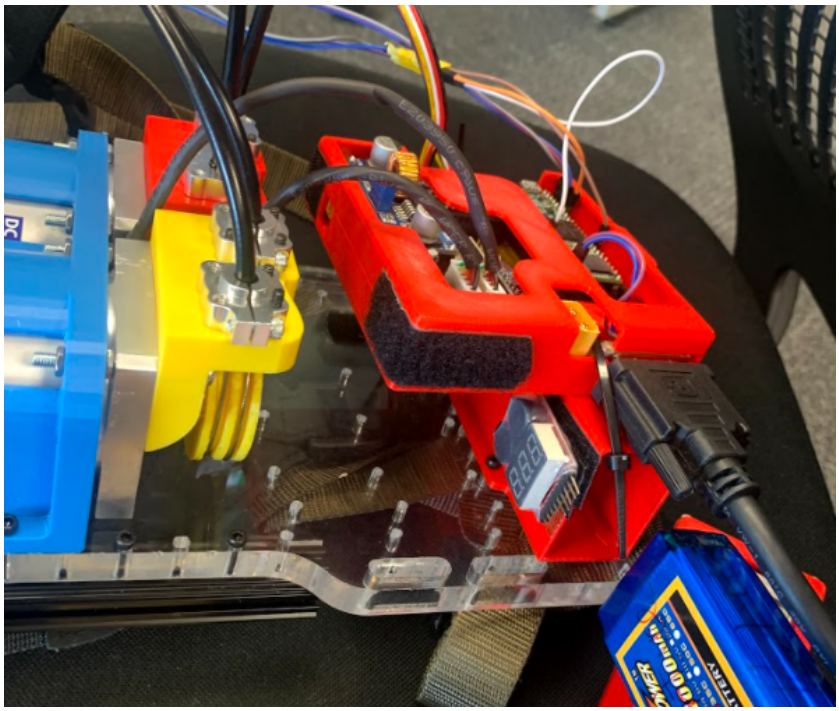

Figure G.0.2: View of electronics housings